



Università degli Studi di Napoli Federico II
SCUOLA POLITECNICA E DELLE SCIENZE DI BASE

DIPARTIMENTO DI INGEGNERIA INDUSTRIALE
Corso di Laurea in Ingegneria Aerospaziale

Tesi di Laurea Magistrale
in
Ingegneria Aerospaziale ed Astronautica

**Development of a Java Framework for
Parametric Aircraft Design**

The Performance Analysis Module

Candidato:
Vittorio Trifari
Matricola M53/411

Relatori:
Prof. Fabrizio Nicolosi
Prof. Agostino De Marco

Abstract

This thesis has the main purpose of providing a comprehensive overview about the development, in Java, of a software dedicated to the preliminary design of an aircraft, focusing on the performance analysis module.

The point of view from which this subject will be observed expects first to define methodologies and theoretical aspects necessary for the examined performance calculation for then to show, in more detail, the implementation of these latter within the software; this will be seen both from the point of view of the developer, through a detailed explanation of the architecture of the different calculation modules, both of a potential **user developer**, by showing some commented examples of use supplied with graphical and numerical results suitable, among other things, also to the validation of calculations performed.

Sommario

Questo lavoro di tesi ha lo scopo principale di fornire una panoramica esaustiva circa lo sviluppo, in ambiente Java, di un software dedicato al progetto preliminare di un aeromobile, concentrandosi sull'aspetto dell'analisi delle performance.

Il punto di vista con il quale verrà affrontato questo argomento prevede dapprima di inquadrare le metodologie e gli aspetti teorici necessari per la stima delle performance in esame per poi mostrare, più nel dettaglio, l'implementazione di questi ultimi all'interno del software; ciò sia dal punto di vista dello sviluppatore, attraverso la spiegazione dettagliata dell'architettura dei vari moduli di calcolo, sia dal punto di vista di un potenziale utente, tramite alcuni esempi d'uso commentati e corredati di risultati grafici e numerici atti, tra l'altro, anche alla validazione dei calcoli svolti.

CONTENTS

1 Software overview	5
1.1 Main purposes	5
1.2 Input file structure	5
1.3 The Core Package	5
1.4 Aircraft model creation	5
1.5 The Graphical User Interface	5
2 Payload-Range	6
2.1 Theoretical background	6
2.2 Java class architecture	10
2.3 Case study: ATR-72 and B747-100B	13
3 Specific Range and Cruise Grid	25
3.1 Theoretical background	25
3.2 Java class architecture	29
3.3 Case study: ATR-72 and B747-100B	32
4 High lift devices effects	41
4.1 Theoretical background	42
4.1.1 ΔC_{l0} and ΔC_{L0} calculation	45
4.1.2 $\Delta C_{l\max}$ and $\Delta C_{L\max}$ calculation for trailing edge and leading edge devices	48
4.1.3 $C_{l\alpha,\text{flap}}$ and $C_{L\alpha,\text{flap}}$ calculation	53
4.1.4 $\Delta\alpha_{\text{stall}}$ calculation for trailing edge and leading edge devices	53
4.1.5 Further effects calculations	54
4.2 Java class architecture	58
4.3 Case study: ATR-72 and B747-100B	61
5 Take-off performance	68
5.1 Theoretical background	68
5.1.1 All Operative Engines (AOE) take-off run	69
5.1.2 One Inoperative Engine (OEI) take-off run and balanced field length	74
5.2 Java class architecture	75

5.3 Case study: ATR-72	75
----------------------------------	----

Appendices

A HDF database creation and reading	77
A.1 Creation of a database using MATLAB	77
A.2 Reading data from an HDF database in JPAD	80
Bibliography	82
Glossary	84
Acronyms	86
List of symbols	87

Chapter **1**

SOFTWARE OVERVIEW

- 1.1 Main purposes**
- 1.2 Input file structure**
- 1.3 The Core Package**
- 1.4 Aircraft model creation**
- 1.5 The Graphical User Interface**

Chapter 2

Payload-Range

The Payload-Range diagram is a very important resource in aircrafts design because it allows to illustrate an aircraft operational limits by showing the trade-off relationship between the payload that can be carried and the range that can be flown; moreover, in synergy with the **Direct Operative Cost (D.O.C.)** diagram, it's very useful to the future aircraft customers to have an idea of expected profits derived by their investment. Payload-Range is also a key feature of the design requirements so it's possible to state that its relevance is felt through all the preliminary design phase.

2.1 Theoretical background

To better understand the theoretical background behind this diagram, the first step is to focus the attention upon the link between the range and the fuel consumption, which is influenced by aircraft weight through Breguet formulas. It's possible to imagine, at first, an aircraft in which payload and fuel weights can be managed at will, so that, in this completely flexible aircraft, the more the required range is, the less is the payload in order to carry more fuel at a specified maximum take-off weight; this leads to the diagram in figure 3.1. Because the payload is carried in the fuselage while the fuel is carried in wing tanks, the more the payload, the more the weight in the fuselage; this means that wings are incrementally more bending loaded so that a heavier structure is required. However, in this way the operating empty weight grows up limiting the payload the aircraft can carry, at that maximum take-off and fuel weights, for that range; the consequence of this is that, in particular for long range missions, the payload is too low, providing low profits. In order to avoid this situation it's possible to decide, preventively, the maximum payload weight the aircraft can carry in fuselage so that the maximum bending load for wings and, in consequence their structural weight, is set; this particular weight is named **Maximum Zero Fuel Weight (MZFW)**.

As a result of this, the previous diagram changes in the one reported in figure 3.2 which starts with the maximum zero fuel weight and keep it constant until the maximum take-off weight is

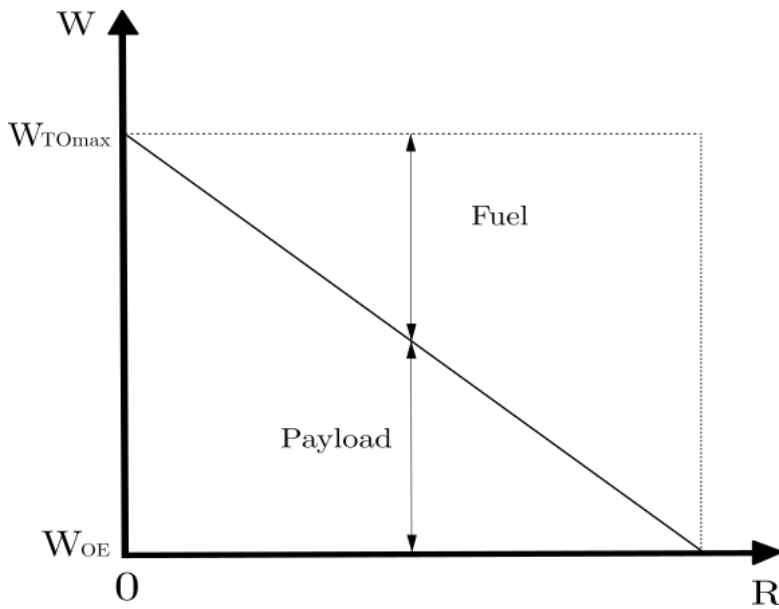


Figure 2.1 Payload-Range for a completely flexible aircraft

reached. From this point on, the far the aircraft have to go, the more the fuel it needs, but, since the maximum take-off weight is set, the only way to increase fuel weight is to reduce the payload; this condition is represented by the second segment of the diagram and, along this, the aircraft weight is always equal to the maximum take-off weight. With further increase of the required range for the aircraft, the fuel tanks maximum capacity will be reached prevent to store more fuel; the only solution at this problem is to put the additional fuel into the fuselage, reducing, consequently, the payload weight in order to respect the maximum zero fuel weight limitation. Along this last segment the payload weight decreases more rapidly with increasing range reaching, ideally, the value of zero at which the flight mission is useless; moreover the aircraft weight is not equal to the maximum take-off weight anymore but to a lower one.

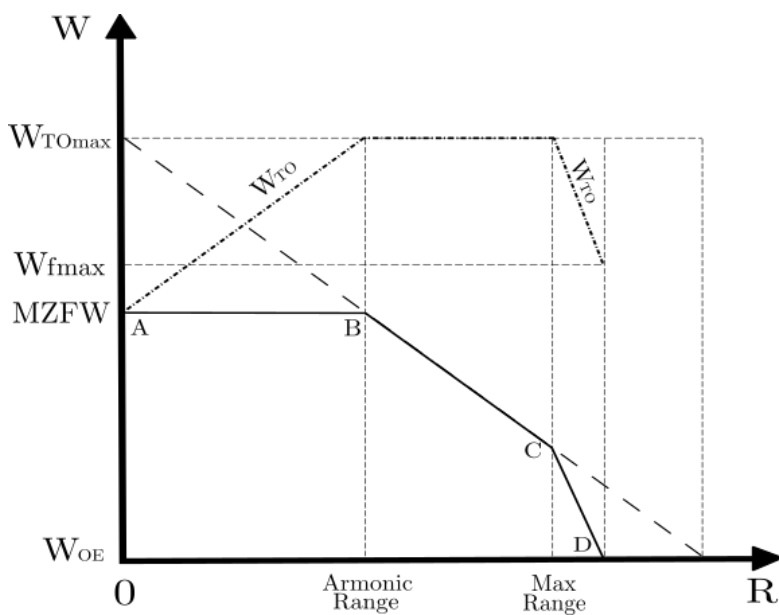


Figure 2.2 Payload-Range with MZFW limitation

Now that the theory behind the Payload-Range is explained, it's interesting to see how to build up the diagram. For this purpose at least the preliminary weight estimation has to be done in order to know the value of the following weights.

- W_{TO}
- W_{OE}
- $W_{Payload}$

Furthermore four fundamental couples of payload and range values have to be defined:

- Point A, in which the payload is the maximum allowed and the range is zero.
- Point B, in which the maximum range, with maximum take-off weight and maximum payload, is reached. This range value is called Armoinc Range.
- Point C, in which the fuel tanks full capacity is reached with a payload lower than the maximum one and still the maximum take-off weight.
- Point D, in which the take-off weight decreases because of the reduction of payload to zero in order to store more fuel in the fuselage.

Since point A is very simple to obtain, it's more interesting to analyze how to calculate points B, C and D coordinates. For point B it's necessary to focus the attention upon Breguet formulas in order to calculate the maximum range the aircraft can fly at maximum take-off weight with maximum payload; these are different for jet or propeller aircraft and can be written as follow, with R in km, Specific Fuel Consumption (SFC) in $\frac{\text{lb}}{\text{hp}\cdot\text{h}}$ and Jet Specific Fuel Consumption (SFCJ) in $\frac{\text{lb}}{\text{lb}\cdot\text{h}}$.

$$R = 603.5 \cdot \left(\frac{\eta_p}{SFC} \right)_{cruise} \cdot \left(\frac{L}{D} \right)_{cruise} \cdot \ln \left(\frac{W_i}{W_f} \right) \quad \text{if propeller engine driven} \quad (2.1a)$$

$$R = \left(\frac{V}{SFCJ} \right)_{cruise} \cdot \left(\frac{L}{D} \right)_{cruise} \cdot \ln \left(\frac{W_i}{W_f} \right) \quad \text{if jet engine driven} \quad (2.1b)$$

Knowing the specific fuel consumption, the aerodynamic and propeller efficiency, or speed for jet aircraft, in cruise condition, the only unknown left for calculate the range is the weight ratio. In order to calculate this it's necessary to start by evaluating the amount of fuel the airplane can take on board, at maximum take-off weight and maximum payload, with the following formula.

$$W_{TO,max} = W_{OE} + W_{payload,max} + W_{fuel} \quad (2.2)$$

Once the used fuel weight is known, it's possible to use the fuel fraction method from the weight estimation design phase in order to find the total weight ratio across the entire aircraft mission.

$$W_{fuel} = (1 - M_{ff}) \cdot W_{TO} \quad (2.3)$$

M_{ff} is the fuel fraction of the entire mission profile given by the following expression.

$$M_{ff} = \frac{W_1}{W_{TO}} \cdot \frac{W_2}{W_1} \cdot \frac{W_3}{W_2} \cdot \frac{W_4}{W_3} \cdot \frac{W_5}{W_4} \cdot \frac{W_6}{W_5} \cdot \frac{W_7}{W_6} \cdot \frac{W_8}{W_7} \cdot \frac{W_9}{W_8} \cdot \frac{W_{10}}{W_9} \cdot \frac{W_{final}}{W_{10}} \quad (2.4)$$

From this point on, it's necessary to have a table, like the one of table 3.1, in which all weight ratios can be found statistically except for cruise, alternate cruise and loiter phases; these three unknown ratios are those that build up the Breguet weight ratio required by the range formula.

Airplane type	Start, Warm-up	Taxi	Take-off	Brief descent	Brief climb	Landing, Taxi and Shutdown
Homebuilt	0,998	0,998	0,998	0,995	0,995	0,995
Single Engine	0,995	0,997	0,998	0,992	0,993	0,993
Twin Engine	0,992	0,996	0,996	0,990	0,992	0,992
Agricultural	0,996	0,995	0,996	0,998	0,999	0,998
Business Jets	0,990	0,995	0,995	0,980	0,990	0,992
Regional TBP's	0,990	0,995	0,995	0,985	0,985	0,995
Transport Jets	0,990	0,990	0,995	0,980	0,990	0,992
Mil. Trainers	0,990	0,990	0,990	0,980	0,990	0,995
Fighters	0,990	0,990	0,990	0,960-0,900	0,990	0,995
Mil.Patrol,Bmb and Trspt	0,990	0,990	0,995	0,980	0,990	0,992
Flying boats,Amph. and Floats	0,992	0,990	0,996	0,985	0,990	0,990
Supersonic Cruise	0,990	0,995	0,995	0,920-0,870	0,985	0,992

Table 2.1 Suggested fuel fractions

For the evaluation of point C, similar steps have to be followed with the difference that, in this case, the fuel is the maximum that the wing tanks can store and the payload is the unknown of the (2.5).

$$W_{TO,max} = W_{OE} + W_{payload} + W_{fuel,max} \quad (2.5)$$

From this equation it's possible to calculate point C ordinate, while for the range abscissa the same procedure used for point B range has to be followed with the difference that now it's necessary to use the fuel weight relative to the maximum fuel tank capacity which is known from the wing fuel tank design. Finally for point D, the payload is set at zero so that is

possible to evaluate the WTO, relative to maximum fuel weight with no passengers, from the following equation.

$$W_{TO} = W_{OE} + W_{fuel,max} \quad (2.6)$$

This new take-off weight generates a lower M_{ff} , from fuel fraction equation, which leads to a bigger weight ratio to be used in Breguet formulas with the result of a bigger range.

2.2 Java class architecture

In this paragraph the implementation in the JPAD software of the Payload-Range diagram, through the `PayloadRangeCalc` Java class, is presented. The idea has been to create a dedicated Java class which is demanded of the calculation of the four couple of range and payload values presented before; moreover it has to confront the user chosen Mach number condition with the best range one and to parametrize the analysis at different maximum take-off weight in order to help users making design decisions about different version of the same aircraft. The class core consists of the following three principal methods which have to evaluate points B, C and D coordinates using the procedure explained before.

- `calcRangeAtMaxPayload`
- `calcRangeAtMaxFuel`
- `calcRangeAtZeroPayload`

Each of these requires in input the table 3.2 data, a database which collects all data from table 3.1, named *FuelFractions.h5*, and an engine database, for turboprop or turbofan, in which all specific fuel consumption values, at given Mach number and altitude, are stored. From this point on, the evaluation of (2.2), (2.5) and (2.6), for each method, and of (2.3), for all of them, is performed in order to set up the following calculations and to obtain the unknown value of the payload in point C case; after that the fuel fractions database is read in order to obtain all known data necessary to calculate the required weight ratio to be used in (2.1a) or (2.1b) depending on the aircraft engine type. It's important to highlight that the database reading process is made up so that it can recognize all different kind of aircraft from table 3.1 and read the related line values.

Since each method has to compare the chosen Mach number condition with the best range one, the boolean variable presented before is used in order to distinguish between different application cases; in this way, when the user specify the aircraft engine type and the boolean variable, the method reads the specific fuel consumption value, at given Mach number and altitude, from the related engine database and performs the calculation of the lift and drag wing coefficients which are then used to obtain the aerodynamic efficiency value. At this point is possible to calculate the range that represents point B, C or D abscissa. It should be noted that, in case of a true value of the boolean variable, the evaluation of the lift and drag wing coefficients, as well as the best range Mach number that replaces the user chosen one, is performed by calculating the parabolic drag polar characteristic points and choosing those that maximizes the range (point E for the turboprop and point A for the turbofan); whereas for a

maxTakeOffMass	Maximum take-off mass
sweepHalfChordEquivalent	Equivalent wing sweep angle at half chord
surface	Wing surface
cd0	Wing c_{D0}
oswald	Wing oswald factor
cl	The current lift coefficient in cruise configuration
ar	Wing aspect ratio
tcMax	Mean maximum thickness of the wing
byPassRatio	Engine by-pass ratio (when needed)
eta	Propeller efficiency (when needed)
altitude	Cruise altitude
currentMach	The actual Mach number during cruise
isBestRange	A boolean variable that is true if the evaluation of the best range condition is performed, otherwise it's false

Table 2.2 Input data

false value of the boolean variable, the lift coefficient is calculated by using the current flight condition angle of attack into the linear part of the wing lift curve, while the drag coefficient is evaluated from the aircraft total drag polar taking also into account potential wave drag sources.

Now that all points coordinates are known, the two following methods are demanded to build up abscissas and ordinates values arrays to be used in plotting the diagram.

- `createRangeArray`
- `createPayloadArray`

Range Array	Payload Array
0,0	Maximum payload, in number of passengers
<code>calcRangeAtMaxPayload</code> output	Maximum payload, in number of passengers
<code>calcRangeAtMaxFuel</code> output	Payload calculated in <code>calcRangeAtMaxFuel</code>
<code>calcRangeAtZeroPayload</code> output	0,0

Table 2.3 Payload and range array components

They use the Java **List** interface to generate an ordered collection of values which are then populated with the following values.

Finally the two arrays are used as input, together with another one from the best range condition analysis, for the last method, named `createPayloadRangeCharts_Mach`, that has to plot

the diagram; this uses the JFreeChart Java library[10] to generate a Portable Network Graphics (png) output image into the output folder of the software and is also able to create a TikZ version of the diagram to be used in L^AT_EX. As said before, this class finds another purpose in parameterizing the diagram in different maximum take-off weight conditions. To do that, the three core methods are used again inside a new one, named `createPayloadRangeMatrices`, which implements a recursive calculation of the three points coordinates at different maximum take-off mass conditions generated by decreasing the original mass by 5% until it reaches a total decrease of 20%. This new method requires the same input data reported in table 3.2 except for the maximum take-off mass which is generated inside the method itself. The output matrices are then used in a plotting method, equivalent to previous one but named `createPayloadRangeCharts_MaxTakeOffMass`, which generates the .png and .tikz output images by receiving as input two matrices and not two arrays as before.

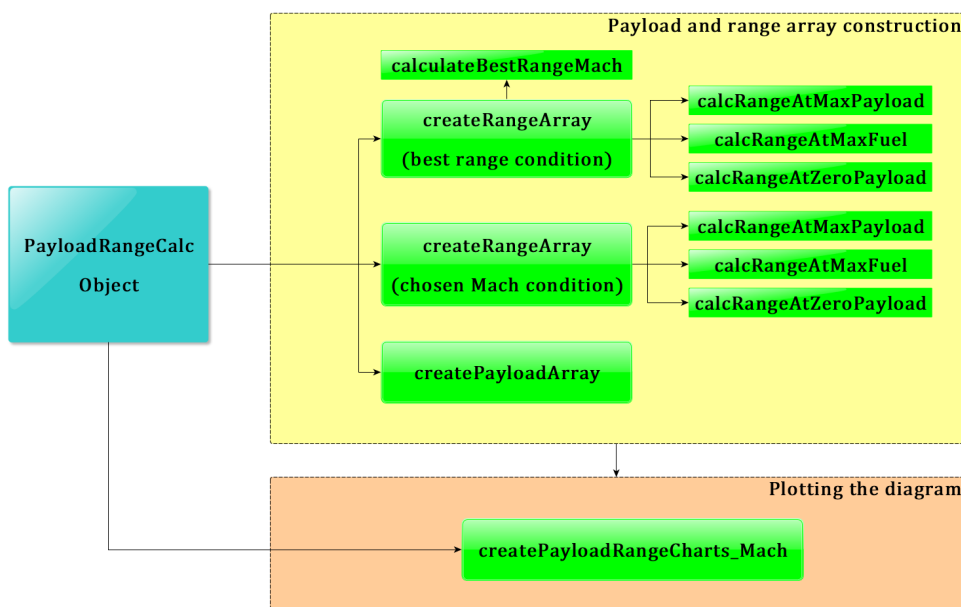


Figure 2.3 Payload-Range java class flowchart for best range and chosen Mach conditions comparison

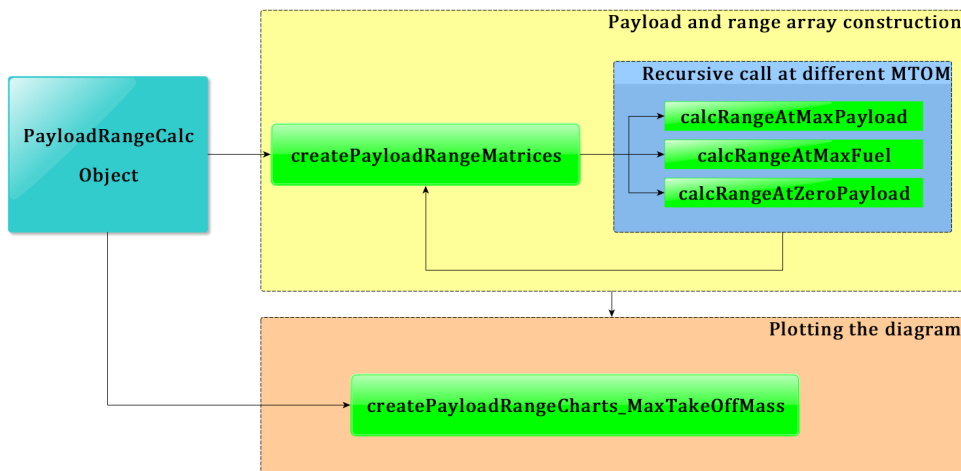


Figure 2.4 Payload-Range java class flowchart for maximum take-off mass parameterization

2.3 Case study: ATR-72 and B747-100B

With the purpose of validating calculations presented before, two case studies have been taken into account; the first one is on the ATR-72 and the second one on the B747-100B.

The ATR-72, made by the French-Italian aircraft manufacturer ATR, is a stretched variant of the original ATR-42 that entered in service in 1989; it's powered by two turboprop engine and it's used typically as a regional airliner. The main purpose of its design was to increase the seating capacity throughout the stretching of the fuselage by 4.5m, an increased wingspan, more powerful engines and an increased fuel capacity by approximately 10%.

The Boeing 747 is a wide-body commercial jet airliner and cargo aircraft, often referred to by its original nickname, Jumbo Jet, or Queen of the Skies. Its distinctive hump upper deck along the forward part of the aircraft makes it among the world's most recognizable aircraft, and it was the first wide-body produced. Manufactured by Boeing's Commercial Airplane unit in the United States, the original version of the 747 had two and a half times greater capacity than the Boeing 707, one of the common large commercial aircraft of the 1960s. The four-engine 747 uses a double deck configuration for part of its length and it's available in passenger and other versions. Boeing designed the 747's hump-like upper deck to serve as a first class lounge or extra seating, and to allow the aircraft to be easily converted to a cargo carrier by removing seats and installing a front cargo door. The 747-100B model was developed from the 747-100SR, using its stronger airframe and landing gear design; the type had an increased fuel capacity of 182000 L, allowing for a 5000 nautical mile range with a typical 452 passengers payload, and an increased maximum take-off weight of 340000 kg was offered; unlike the original 747-100, the 747-100B was offered with Pratt & Whitney JT9D-7A, General Electric CF6-50, or Rolls-Royce RB211-524 turbofan engines.

The two presented tests share the same architecture so that a general guideline can be followed; this strategy has been designed with the purpose of making a general procedure in order to simplify user's work.

For more clarity, listings of the two test types are reported, as an exemplificative practice, only in the case of the ATR-72 turboprop aircraft. First of all it's necessary to set up all default folders in order to make them achievable from any location inside the software; this is done with the static method `initWorkingDirectoryTree` of the `MyConfiguration` class located in `JPADConfigs` package. In this way, every time the user wants to point at a specific folder, like the input or output directory, it's necessary only to call the `static method getDir`, also from `MyConfiguration` class, which reads the folder name, from a dedicated `Enumeration`, and associate it with the related directory from a `Map` named `mapPaths`. The second step is to read the engine and the fuel fractions databases with the related java class reader; this particular class type uses the super class `DatabaseReader`, which implements the use of `MyHDFReader` class, to access an .h5 dataset values. For more information about how to build and use a **Hierarchical Data Format (HDF)** database, see appendix A.

```
1 public class PayloadRange_Test_TP{
```

```

2 //-----
3 // MAIN:
4 public static void main(String[] args) throws
5     HDF5LibraryException, NullPointerException{
6     System.out.println("-----");
7     System.out.println("PayloadRangeCalc_Test :: main");
8     System.out.println("-----");
9 //-----
10 // Assign all default folders
11 MyConfiguration.initWorkingDirectoryTree();
12 //-----
13 // Setup database(s)
14 String databaseFolderPath = MyConfiguration.getDir(FoldersEnum.DATABASE_DIR);
15 String aerodynamicDatabaseFileName = "Aerodynamic_Database_Ultimate.h5";
16 String fuelFractionDatabaseFileName = "FuelFractions.h5";
17 AerodynamicDatabaseReader aeroDatabaseReader = new AerodynamicDatabaseReader(
18     databaseFolderPath,
19     aerodynamicDatabaseFileName
20 );
21 FuelFractionDatabaseReader fuelFractionReader = new FuelFractionDatabaseReader(
22     databaseFolderPath,
23     fuelFractionDatabaseFileName
24 );

```

Listing 2.1 Excerpt of the ATR-72 Payload-Range test - preliminary steps

Now that all required resources are set up, following steps are to create the aircraft model, assign its operating conditions and perform all necessary analysis like the aerodynamic one. This is done throughout the use of the following three fundamental classes, which modes of operation are explained in the flowchart of figure 3.5.

- Aircraft class
- OperatingConditions class
- ACAnalysisManager class

```

1 //-----
2 // Operating Condition / Aircraft / AnalysisManager
3 // (geometry calculations)
4 OperatingConditions theCondition = new OperatingConditions();
5
6 Aircraft aircraft = Aircraft.createDefaultAircraft("ATR-72");
7
8 aircraft.get_theAerodynamics().set_aerodynamicDatabaseReader(aeroDatabaseReader);
9 aircraft.get_theFuelTank().setFuelFractionDatabase(fuelFractionReader);
10 aircraft.set_name("ATR-72");
11 aircraft.get_wing().set_theCurrentAirfoil(new MyAirfoil(
12     aircraft.get_wing(),
13     0.5)
14 );
15 ACAnalysisManager theAnalysis = new ACAnalysisManager(theCondition);

```

```

16     theAnalysis.updateGeometry(aircraft);
17
18     //-----
19     // Set the CoG(Bypass the Balance analysis allowing
20     // to perform Aerodynamic analysis only)
21     CenterOfGravity cgMTOM = new CenterOfGravity();
22
23     // x_cg in body-ref.-frame
24     cgMTOM.set_xBRF(Amount.valueOf(12.0, SI.METER));
25     cgMTOM.set_yBRF(Amount.valueOf(0.0, SI.METER));
26     cgMTOM.set_zBRF(Amount.valueOf(2.3, SI.METER));
27
28     aircraft.get_theBalance().set_cgMTOM(cgMTOM);
29     aircraft.get_HTail().calculateArms(aircraft);
30     aircraft.get_VTail().calculateArms(aircraft);
31
32     theAnalysis.doAnalysis(aircraft, AnalysisTypeEnum.AERODYNAMIC);

```

Listing 2.2 Excerpt of the ATR-72 Payload-Range test - Aircraft, OperatingConditions and ACAnalysisManager setup

All data required by the `PayloadRangeCalc` class are now ready to be used and it's possible to create an instance of this class accessing, in this way, to all its methods, which have been explained in the previous paragraph.

```

1     //-----
2     // Creating the Calculator Object
3     PayloadRangeCalc test = new PayloadRangeCalc(
4         theCondition,
5         aircraft,
6         AirplaneType.TURBOPROP_REGIONAL
7     );

```

Listing 2.3 Excerpt of the ATR-72 Payload-Range test - Payload-Range class instance creation

The first check that is implemented has the purpose of inspect whether or not the chosen cruise Mach number is bigger than the crest critical one; in this case a warning message is launched in order to inform the user of the situation. The method demanded of this is `checkCriticalMach` which accepts in input a given Mach number, compares it with the one calculated with Kroo method [6], starting from the cruise lift coefficient, and return a boolean variable that is true only if the chosen Mach number is bigger than the crest critical one indeed.

```

1     // -----CRITICAL MACH NUMBER CHECK-----
2     boolean check = test.checkCriticalMach(theCondition.get_machCurrent() );
3
4     if (check)
5         System.out.println("\n\n-----"
6             +"\nCurrent Mach lower then critical Mach number"
7             +"\nCurrent Mach = " + theCondition.get_machCurrent()
8             +"Critical Mach = " + test.getCriticalMach()

```

```

9      +"\\n\\n\\t CHECK PASSED -> PROCEDING TO CALCULATION "
10     +"\\n\\n"
11     +"-----");
12 else{
13     System.out.println("\\n\\n-----"
14     +"\\nCurrent Mach bigger then critical Mach number"
15     +"\\nCurrent Mach = " + theCondition.get_machCurrent()
16     +"\\nCritical Mach = " + test.getCriticalMach()
17     +"\\n\\n\\t CHECK NOT PASSED -> WARNING!!! "
18     +"\\n\\n"
19     +"-----");
20 }

```

Listing 2.4 Excerpt of the ATR-72 Payload-Range test - critical Mach number check

```

1 -----
2 Current Mach is lower then critical Mach number.
3 Current Mach = 0.43
4 Critical Mach = 0.6659791543529567
5
6     CHECK PASSED --> PROCEDING TO CALCULATION
7 -----

```

Listing 2.5 Excerpt of the ATR-72 Payload-Range test results - critical Mach number check

```

1 -----
2 Current Mach is lower then critical Mach number.
3 Current Mach = 0.84
4 Critical Mach = 0.8490814607347361
5
6     CHECK PASSED --> PROCEDING TO CALCULATION
7 -----

```

Listing 2.6 Excerpt of the B747-100B Payload-Range test results - critical Mach number check

At this point, if the user wants to compare the chosen Mach number condition with the best range one, all that it's needed is to invoke the `createRangeArray` method, for both the operative conditions, and the `createPayloadArray` one; after that the diagram is generated from the method `createPayloadRangeCharts_Mach`.

```

1 // -----BEST RANGE CASE-----
2 System.out.println();
3 System.out.println("-----BEST RANGE CASE-----");
4 List<Amount<Length>> vRange_BR = test
5         .createRangeArray(
6             test.getMaxTakeOffMass(),
7             test.getSweepHalfChordEquivalent(),
8             test.getSurface(),
9             test.getCd0(),
10            test.getOswald()),

```

```

11         aircraft.get_theAerodynamics().getcLE(),
12         test.getAr(),
13         test.getTcMax(),
14         test.setByPassRatio(0.0),
15         test.getEta(),
16         test.getAltitude(),
17         test.calculateBestRangeMach(
18             EngineTypeEnum.TURBOPROP,
19             test.getSurface(),
20             test.getAr(),
21             test.getOswald(),
22             test.getCd0(),
23             test.getAltitude(),
24             true);
25 // -----USER CURRENT MACH-----
26 System.out.println();
27 System.out.println("-----CURRENT MACH CASE-----");
28 List<Amount<Length>> vRange_CM = test
29     .createRangeArray(
30         test.getMaxTakeOffMass(),
31         test.getSweepHalfChordEquivalent(),
32         test.getSurface(),
33         test.getCd0(),
34         test.getOswald(),
35         test.getCl(),
36         test.getAr(),
37         test.getTcMax(),
38         test.setByPassRatio(0.0),
39         test.getEta(),
40         test.getAltitude(),
41         test.getCurrentMach(),
42         false);
43 // -----PLOTTING-----
44 // Mach parameterization:
45 List<Double> vPayload = test.createPayloadArray();
46 test.createPayloadRangeCharts_Mach(
47     vRange_BR,
48     vRange_CM,
49     vPayload,
50     test.calculateBestRangeMach(
51         EngineTypeEnum.TURBOPROP,
52         test.getSurface(),
53         test.getAr(),
54         test.getOswald(),
55         test.getCd0(),
56         test.getAltitude(),
57         test.getCurrentMach());
58 }
59 }
```

Listing 2.7 Excerpt of the ATR-72 Payload-Range test - Payload-Range diagram evaluation and plot

Otherwise, if it's the maximum take-off mass parameterization the wanted analysis, the required call is for `createPayloadRangeMatrices` method followed by the plotting method `createPayloadRangeCharts_MaxTakeOffMass`.

```

1   // -----MTOM PARAMETERIZATION-----
2   test.createPayloadRangeMatrices(
3       test.getSweepHalfChordEquivalent(),
4       test.getSurface(),
5       test.getCd0(),
6       test.getOswald(),
7       test.getCl(),
8       test.getAr(),
9       test.getTcMax(),
10      test.setByPassRatio(0.0),
11      test.getEta(),
12      test.getAltitude(),
13      test.getCurrentMach(),
14      false
15  );
16 // -----PLOTTING-----
17 // MTOM parameterization:
18 test.createPayloadRangeCharts_MaxTakeOffMass(
19     test.getRangeMatrix(),
20     test.getPayloadMatrix()
21 );
22 }
23 }
```

Listing 2.8 Excerpt of the ATR-72 Payload-Range test - maximum take-off mass parameterization

In conclusion, following pages shows a summary of input data used for each analyzed aircraft, together with their related results in terms of Payload-Range diagrams for both the chosen Mach number and best range comparison and max take-off mass parameterization.

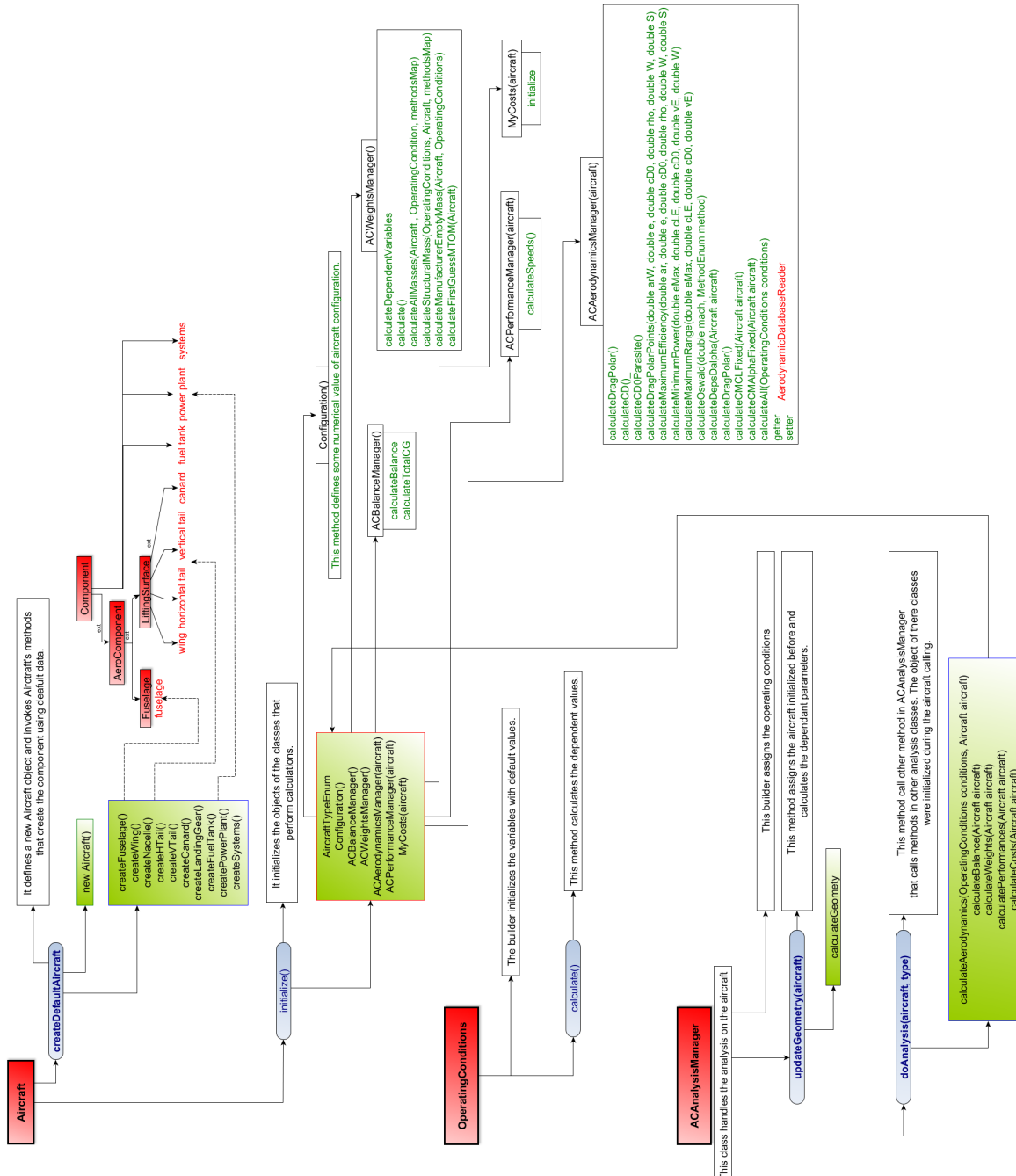


Figure 2.5 Aircraft, OperatingConditions and ACAnalysisManager flowchart

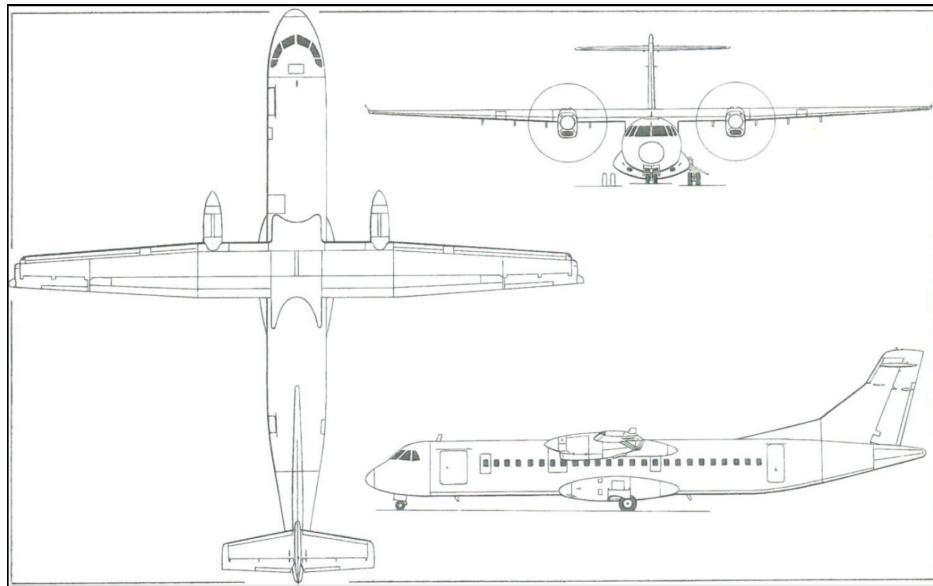


Figure 2.6 ATR-72 views – Jane's All the World's Aircraft 2004-2005

Variables	Description	Values
altitude	Cruise altitude	6000 m
machCurrent	The user chosen Mach number	0,43
surface	Wing surface	61 m ²
taperRatioEquivalent	Taper ratio of the equivalent wing	0,545
maxTakeOffMass	maximum take-off mass	23063,579 kg
operatingEmptyMass	operating empty mass	12935,579 kg
maxFuelMass	maximum fuel mass	5000,000 kg
nPassMax	maximum number of passengers	72
sweepLEEEquivalent	Equivalent wing leading edge sweep angle	3,142 °
oswald	Wing oswald factor	0,7585
byPassRatio	Engine bypass ratio	0,0
eta	propeller efficiency	0,85
tcMax	Mean maximum thickness of the wing	0,1675
cl	The cruise lift coefficient	0,45
ar	Wing aspect ratio	12
cd0	Wing parasite drag coefficient	0,0317

Table 2.4 ATR-72 input data

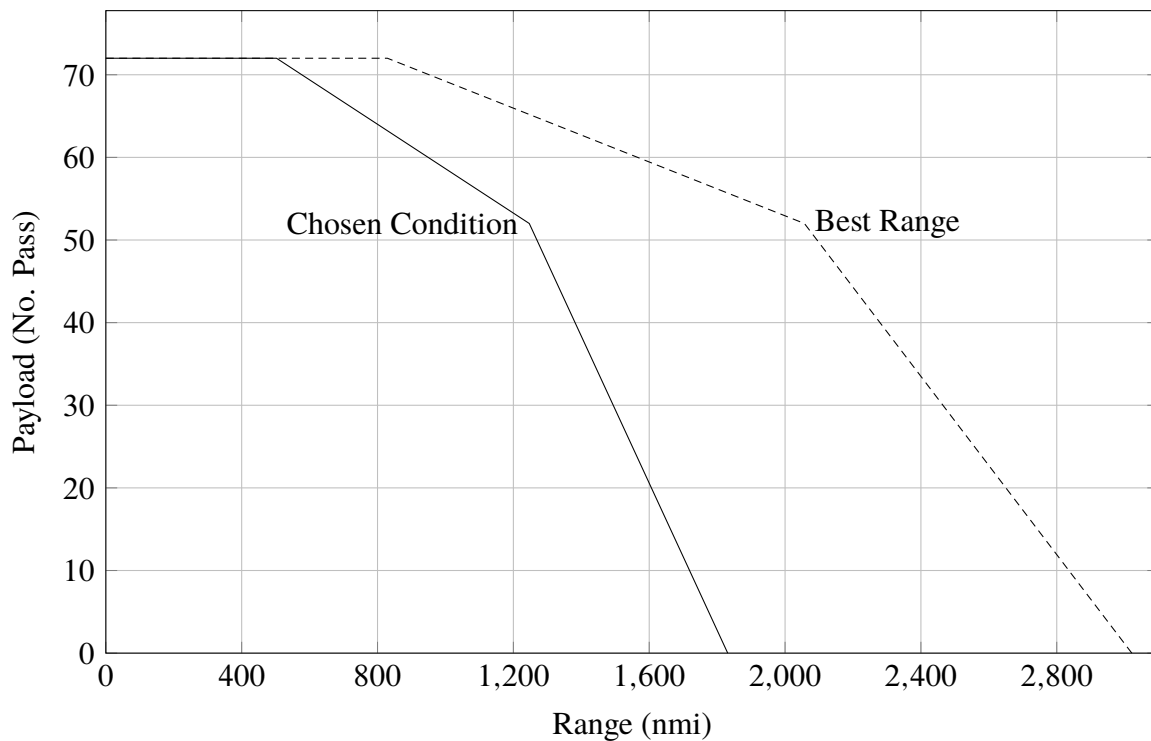


Figure 2.7 ATR-72 Payload-Range - Chosen Mach number and best range comparison

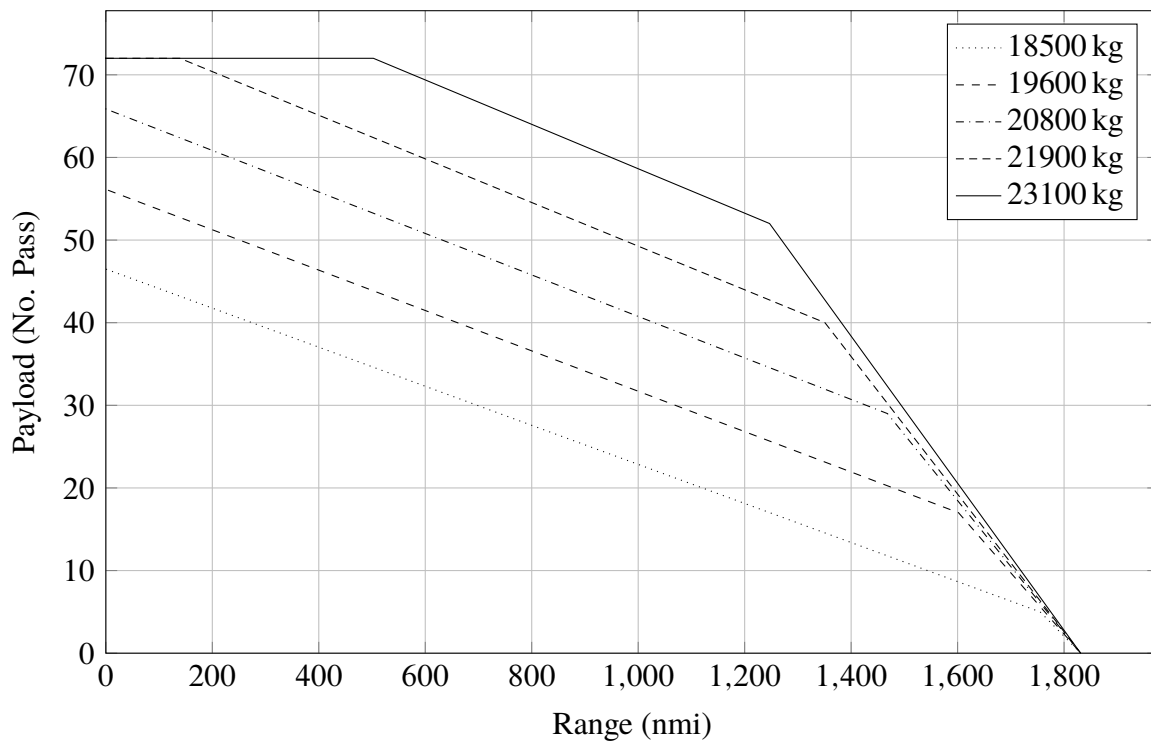


Figure 2.8 ATR-72 Payload-Range - Maximum take-off mass parameterization

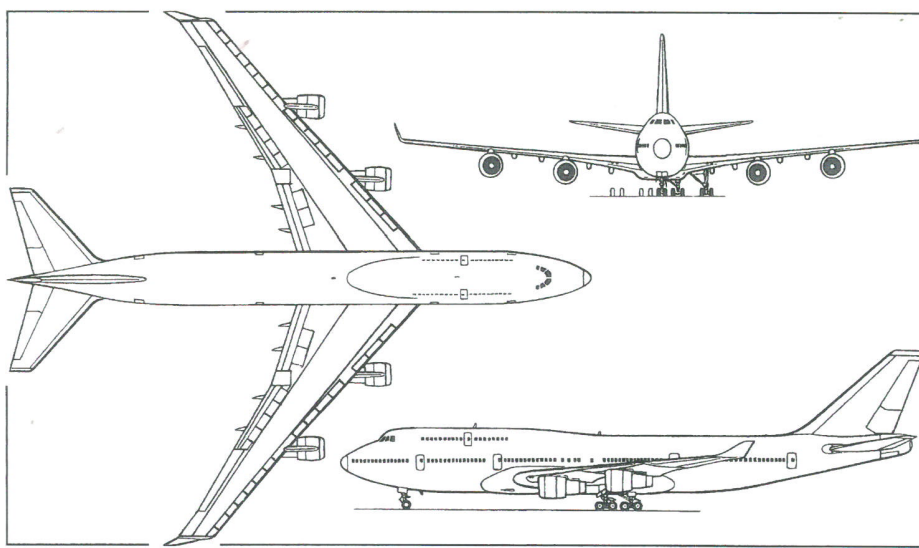


Figure 2.9 B747-100B views – Jane's All the World's Aircraft 2004-2005

Variables	Description	Values
altitude	Cruise altitude	11000 m
machCurrent	The user chosen Mach number	0,83
surface	Wing surface	511 m ²
taperRatioEquivalent	Taper ratio of the equivalent wing	0,284
maxTakeOffMass	maximum take-off mass	354991,506 kg
operatingEmptyMass	operating empty mass	153131,986 kg
maxFuelMass	maximum fuel mass	147409,520 kg
nPassMax	maximum number of passengers	550
sweepLEEEquivalent	Equivalent wing leading edge sweep angle	38,429 °
oswald	Wing oswald factor	0,6277
byPassRatio	Engine bypass ratio	5,0
eta	propeller efficiency	0,0
tcMax	Mean maximum thickness of the wing	0,1292
cl	The cruise lift coefficient	0,45
ar	Wing aspect ratio	6,9
cd0	Wing parasite drag coefficient	0,0182

Table 2.5 B747-100B input data

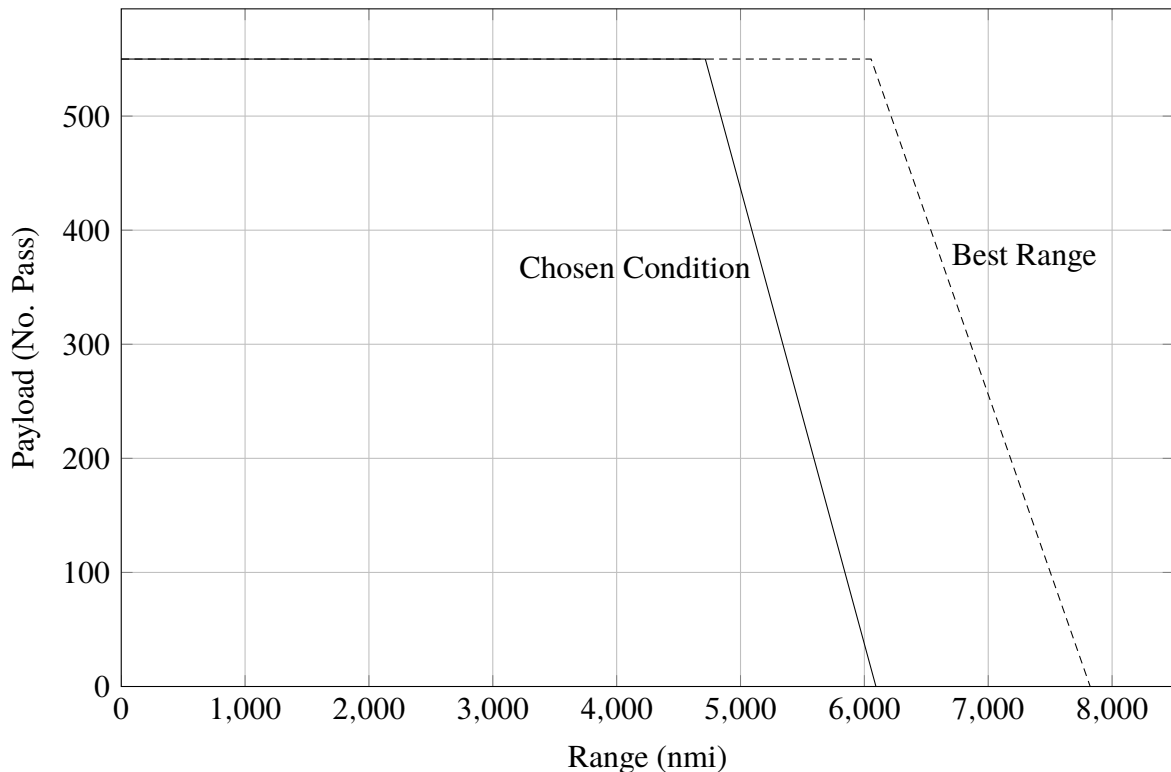


Figure 2.10 B747-100B Payload-Range - Chosen Mach number and best range comparison

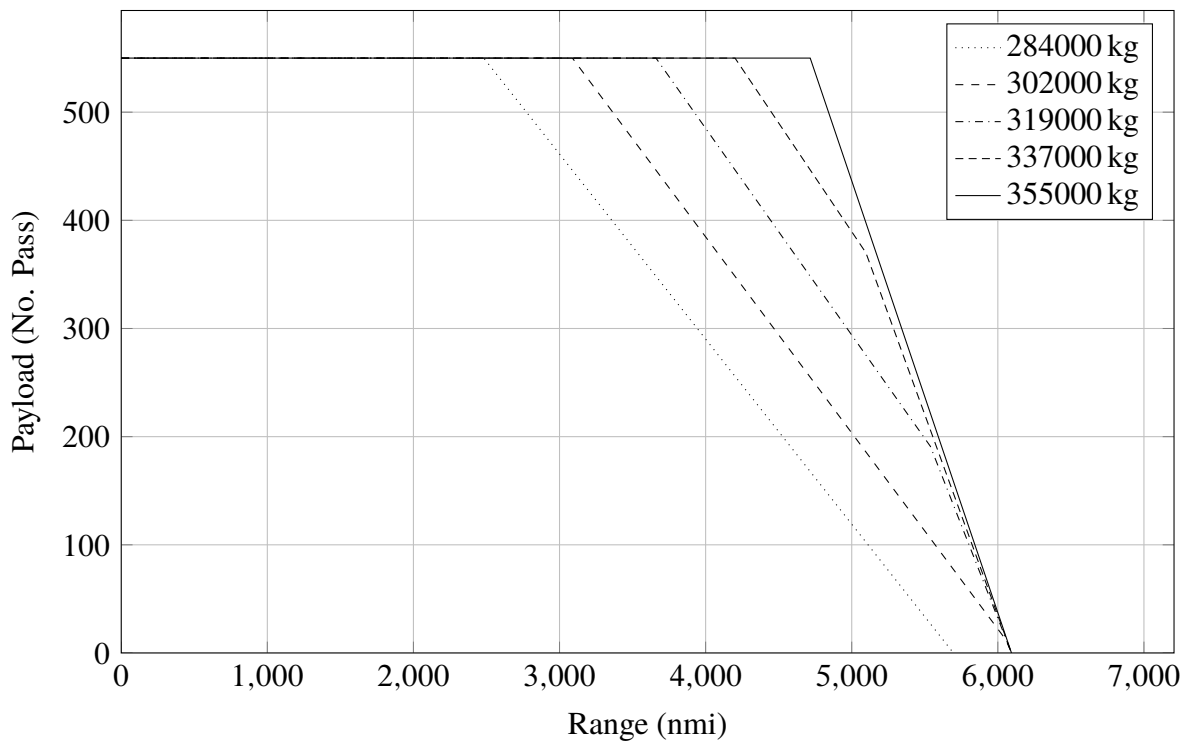


Figure 2.11 B747-100B Payload-Range - Maximum take-off mass parameterization

Variables	Values	Variables	Values
Range (point A)	0 nmi	Range (point A)	0 nmi
Payload (point A)	72 passengers	Payload (point A)	550 passengers
Range (point B)	502.587 nmi	Range (point B)	4714.449 nmi
Payload (point B)	72 passengers	Payload (point B)	550 passengers
Range (point C)	1246.827 nmi	Range (point C)	4715.799 nmi
Payload (point C)	52 passengers	Payload (point C)	550 passengers
Range (point D)	1831.171 nmi	Range (point D)	6093.423 nmi
Payload (point D)	0 passengers	Payload (point D)	0 passengers
C_L	0.421	C_L	0.385
C_D	0.0388	C_D	0.0296
Efficiency	10.853	Efficiency	13.00518
SFC	0.424	SFC	0.626

Table 2.6 Review of ATR-72 (left) and B747-100B (right) results at chosen Mach number conditions

Chapter 3

SPECIFIC RANGE AND CRUISE GRID

In this chapter an analysis of the specific range is performed with the aim of obtain useful information about cruise performance. In particular, starting from generalized performance evaluation and interfacing them with the fuel consumption, the final objective will be to define the specific range as function of Mach number, obtaining the so called *cruise grid chart* which is a very important tool for pilots because it allows to choose the correct speed, during cruising phase, in order to follow some mission objectives like minimum fuel consumption or a fast cruise.

3.1 Theoretical background

The first step that has to be done in order to obtain the *cruise grid chart* is to define generalized performance in terms of thrust and drag. The *generalized* attribute given to these quantities stands for the fact that they are independents from altitude and this result is reached through the parameter δ which represents a ratio between the total pressure at compressor inlet and the standard pressure at sea level.

Regarding the thrust, the generalized version can be obtained by dividing it by δ as shown below.

$$\frac{T}{\delta} = \frac{T_f}{\delta} - M \cdot a_0 \cdot \frac{\sqrt{\theta \cdot m_a}}{\delta} \quad (3.1)$$

where

- T , is the net thrust
- T_f , is the gross thrust
- M , is the mach number
- a_0 , is the sound speed at sea level

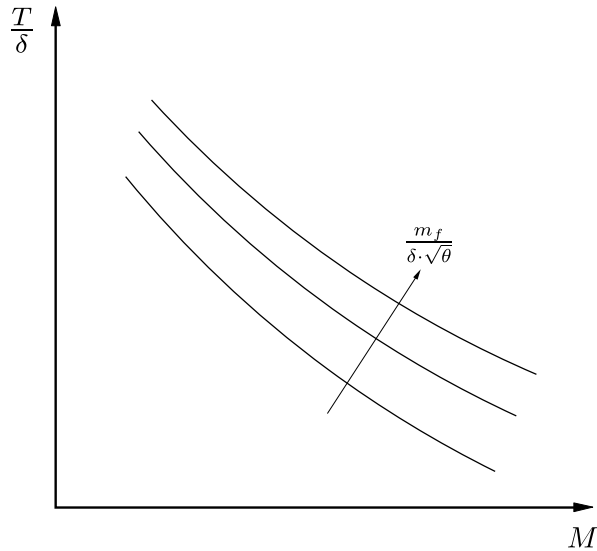


Figure 3.1 Qualitative trend of the generalized thrust v.s. Mach number parameterized in generalized fuel flow rate

- $\frac{\sqrt{\theta} \cdot m_a}{\delta}$, is the generalized air flow rate which is function of the generalized fuel flow rate given by $\frac{m_f}{\delta \cdot \sqrt{\theta}}$

In this way that the generalized thrust results as a function of Mach number and generalized fuel flow rate.

$$\frac{T}{\delta} = \frac{T_f}{\delta} \cdot f \left(\frac{m_f}{\delta \cdot \sqrt{\theta}} \right) \quad (3.2)$$

As shown in figure 3.1 the generalized thrust decreases with Mach number, at given fuel flow rate, and grows with the latter, at given Mach number. This because if the Mach number grows at fixed fuel flow rate, the air flow rate grows reducing the thrust; otherwise, if fuel flow rate grows at fixed Mach number, air flow rate is lower giving more thrust. With this function it's possible to correlate generalized thrust to hourly fuel consumption which is a main keypoint in building the cruise grid chart of an endurance based aircraft such as **Unmanned Aerial Vehicles (UAV)**. Since transport aircrafts rely more on range performance, it's necessary to obtain the same relationship between generalized thrust and fuel consumption referred to the generalized specific range indicated with $\delta \bar{s}$.

Dividing the generalized fuel flow rate, which is dimensionally equal to $\frac{\text{kg}}{\text{s}}$, by a velocity, the result has a dimension of $\frac{\text{m}}{\text{kg}}$ that represents the reciprocal of the specific range. In this way it's possible to state the following relation.

$$\frac{m_f}{\delta \cdot \sqrt{\theta}} = \frac{M \cdot a_0}{\delta \bar{s}} \quad (3.3)$$

As expected from the relation (3.3) the thrust has a trend which is the inverse of the previous parameterization. In fact now, for a given Mach number, if the pilot wants to go farther he has to decrease the thrust in order to reduce the fuel consumption; otherwise, at a given distance to reach, the pilot has to increase the thrust in order to make the Mach number grow.

Since the thrust has always to be compared with the drag in order to evaluate if the aircraft can

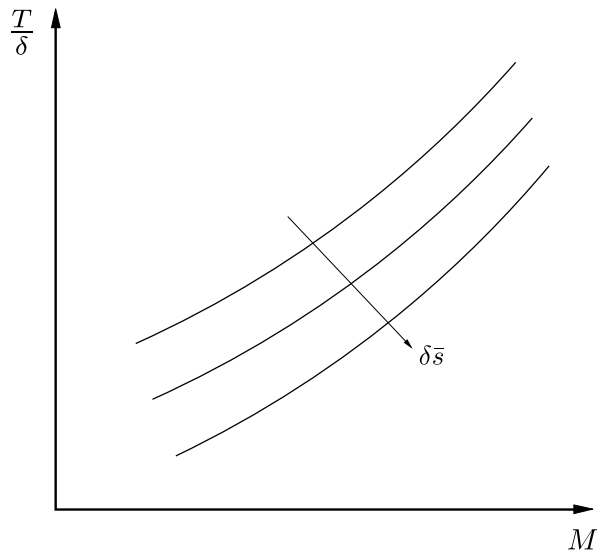


Figure 3.2 Qualitative trend of the generalized thrust v.s. Mach number parameterized in generalized specific range

fly in a specific cruise condition without loosing speed and altitude, it's necessary to obtain a generalized drag trend as well. This is very similar to the drag trend, as can be seen from figure 3.3, and it depends from aircraft weight as well; but, since these have to be generalized quantities, the weight is a generalized weight too.

By the overlap of figure 3.2 and figure 3.3 charts, it's easy to note that the best Mach number, for a given generalized weight, is located at the intersection of the two curves as reported in figure 3.4. In fact, in order to obtain a bigger specific range at fixed weight, the generalized drag would be higher than the generalized thrust; otherwise, if the pilot wants to fly faster at given weight, he has to increase thrust so that the specific range will decrease due to the increasing fuel consumption. Since during the cruise phase the aircraft weight decreases continuously, the pilot has to gain altitude in order to leave the generalized weight unchanged; this explains why during cruise the aircraft continues to climb.

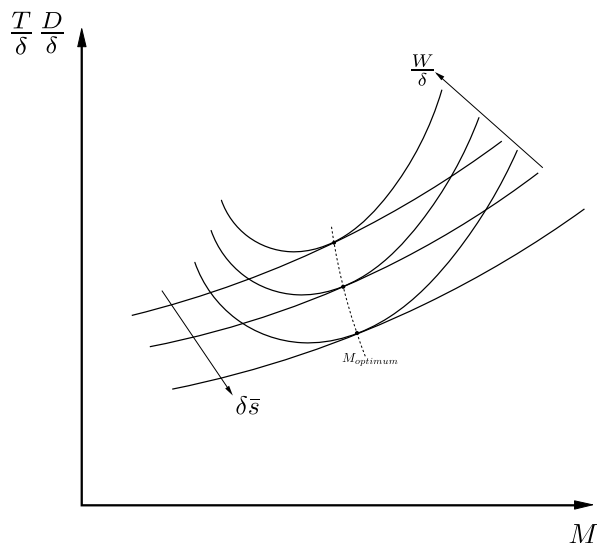


Figure 3.3 Qualitative trend of the generalized drag v.s. Mach number parameterized in generalized weight

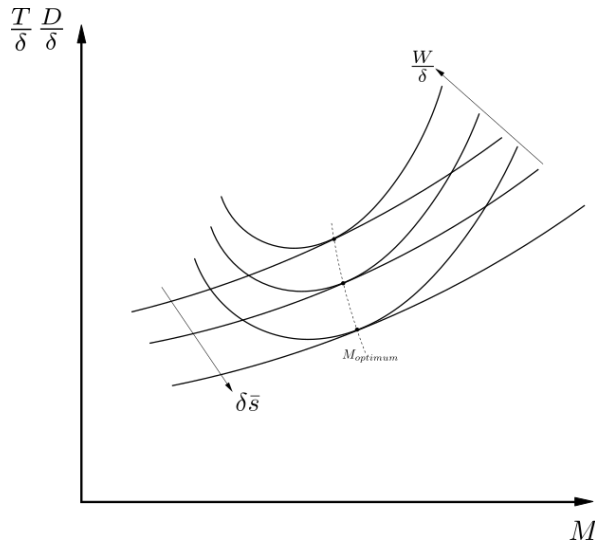


Figure 3.4 Comparison between generalized drag and generalized thrust as functions of Mach number

The specific range can also be connected to Breguet formulas (2.1) as it can be obtained by dividng the **Autonomy Factor (A.F.)** by the aircraft weight; in particular the autonomy factor, groups three main aircraft efficiency and can be written as follow.

$$A.F. = \frac{\eta_p}{SFC} \cdot \left(\frac{L}{D} \right) \quad \text{if propeller engine driven} \quad (3.4a)$$

$$A.F. = \frac{V}{SFCJ} \cdot \left(\frac{L}{D} \right) \quad \text{if jet engine driven} \quad (3.4b)$$

where

- η_p , is propeller efficiency
- SFC , is related to propulsive efficiency
- $\left(\frac{L}{D} \right)$, is the aerodynamic efficiency

At given generalized weight and generalized specific range, the optimum Mach is known as explained before and so the autonomy factor can be calculated by multiply $\frac{W}{\delta}$ and $\delta s̄$. Repeating this operation for different generalized weight conditions, allows to define the autonomy factor trend as function of the generalized weight in which each point of the chart is related to an optimum Mach number for the specific range. As can be seen from figure 3.5 the autonomy factor has a maximum at a specific generalized weight which is the one that the pilot should maintain during the cruise phase. If the altitude is fixed, and so δ is constant, the chart in figure 3.5 can be seen as function of Mach number for a given aircraft weight; at this point, knowing that the autonomy factor leads to the specific range if divided by the aircraft weight, it's possible to define the specific range trend as funcion of the Mach number parameterized in aircraft weight.

The chart, so obtained, in figure 3.6 is the one upon which the cruise grid is defined; on the latter, in fact, four lines are drawn each of which is related to a precise mission objecive. It's important to highlight that, on long distances, the maximum distance line is not often followed

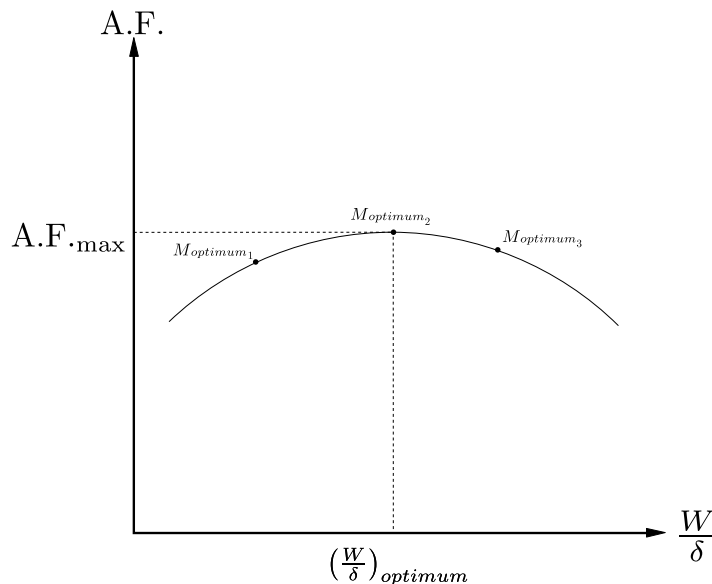


Figure 3.5 Autonomy factor trend as function of the generalized weight

during the cruise because it is tied to a low speed which adversely affects the total flight time increasing the D.O.C.; in order to avoid this condition, pilots prefer to follow the long range line which has only 1% of penalty on the specific range but, at the same time, allows to fly at significantly higher speed with benefits on flight time and, as a result, on the D.O.C.

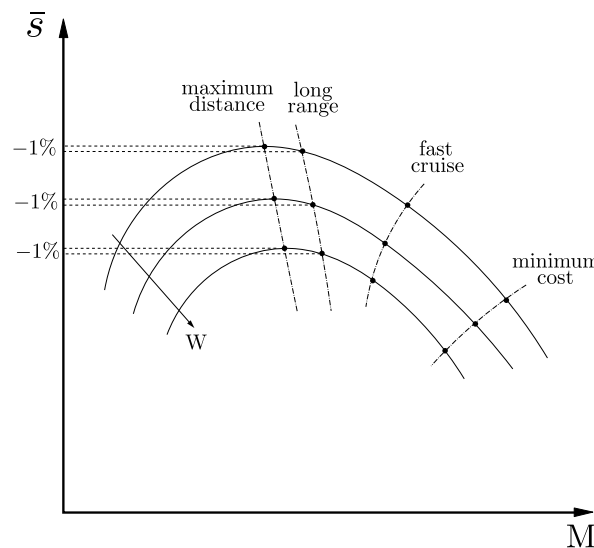


Figure 3.6 Specific range as function of the Mach number parameterized in aircraft weight

3.2 Java class architecture

After having introduced the theory behind the cruise grid chart, a presentation of the related Java class inside JPAD is shown. Using the same philosophy of the previous chapter, a dedicated class, named `SpecificRangeCalc`, has been implemented inside which a series of static methods provide the needed calculation tools. Generally speaking, the guideline followed in creating this class is to assign an array of Mach numbers, starting from the one relative to the minimum cruising speed and ending with the maximum cruising speed at that altitude and

weight, and then evaluate the *SFC*, from engine database, for each Mach number; from here the *A.F.* is built after the evaluation of the aerodynamic efficiency for each value of the same Mach array. Finally the specific range is calculated, in $\frac{\text{nmi}}{\text{lbs}}$, dividing the *A.F.* by the aircraft max take off mass.

The first **static method** presented is `calculateEfficiencyVsMach`. It allows to evaluate the aerodynamic efficiency value for each Mach number of a given array through the evaluation of the C_L and the relative C_D from the aircraft total drag polar; in particular the two aerodynamic coefficients are calculated by calling other two static methods which come from two classes of the aerodynamic calculator package of `JPADCore` named, respectively, `LiftCalc` and `DragCalc`. The static `LiftCalc` method, named `calculateLiftCoeff`, performs the C_L calculation using the following formula, valid in cruise phase.

$$C_L = \frac{2W}{\rho SV^2} \quad (3.5)$$

where V , is the **True AirSpeed (TAS)** derived from the actual Mach number of the array at that the given altitude. On the other hand, the static `DragCalc` method, named `calculateCDTotal`, performs the C_D calculation using the total drag polar expression.

$$C_D = C_{D0} + \frac{C_L^2}{\pi ARe} + C_{D\text{wave}} \quad (3.6)$$

In particular the $C_{D\text{wave}}$ is calculated as presented in [12].

The second **static method** implemented is `calculateSfcVsMach`, which accepts as input data reported in table 3.2 allows to evaluate the *SFC* of a turboprop aircraft, or the *SFCJ* of a turbofan aircraft, for each Mach number of the given array by reading data from the related engine database.

Finally, the two previous method leads to the last one named `calculateSpecificRangeVsMach` which allows to calculate the *A.F.* and, from it, the specific range by implementing the (3.4a) or

<code>maxTakeOffMass</code>	Maximum take-off mass
<code>sweepHalfChordEquivalent</code>	Equivalent wing sweep angle at half chord
<code>surface</code>	Wing surface
<code>cd0</code>	Wing c_{D0}
<code>oswald</code>	Wing oswald factor
<code>mach</code>	An array of Mach numbers
<code>ar</code>	Wing aspect ratio
<code>tcMax</code>	Mean maximum thickness of the wing
<code>altitude</code>	Cruise altitude
<code>airfoilType</code>	The wing airfoil type from the related <code>AirfoilType</code> enumeration

Table 3.1 `calculateEfficiencyVsMach` input data

mach	An array of Mach numbers
altitude	Cruise altitude
bpr	Engine By-Pass ratio
engineType	The engine type from the related <code>EngineType</code> enumeration

Table 3.2 `calculateSfcVsMach` input data

the (3.4b) depending on the given engine type. To do this, it's necessary to give as input the Mach numbers array, the aerodynamic efficiency array calculated with `calculateEfficiencyVsMach` and the *SFC* array calculated with `calculateSfcVsMach` as shown in table 3.3.

The class is completed by other four static methods demanded of plotting the results; in particular, using the same approach shown in the previous chapter, a .png and a .tikz output images are created for each of the *SFC*, the aerodynamic efficiency and the specific range. It's important to highlight that the first of these plotting methods, which is named `createSpecificRangeChart` and is demanded of plotting the cruise grid chart, has implemented, inside it, the evaluation of the maximum range condition as well as the long range one; this by calculating all maximum points and, from them, all points at -1% of penalty obtained through the evaluation of the bigger of the two intersction points that the line at -1% of penalty defines on each specific range curve. The fourth method is, insetad, used for plotting the intersection between the required and available thrust, giving as input a speed array, the altitude and two List of custom Map named `DragMap` and `ThustMap`; these are two classes used to store all data related to drag and thrust curves like the aircraft weight, the current altitude, the speed array on which the drag or thrust are evaluated and, finally, the drag or thrust array itself.

In conclusion a flowchart of the described class is shown in figure 3.7 in order to simplify its understanding.

maxTakeOffMass	Maximum take-off mass
mach	An array of Mach numbers
efficiency	An array of aerodynamic efficiency values
sfc	An array of SFC values
bpr	Engine By-Pass ratio
altitude	Cruise altitude
eta	Propeller efficiency (set to zero in case of turbofan)
engineType	The engine type from the related <code>EngineType</code> enumeration

Table 3.3 `calculateSpecificRangeVsMach` input data

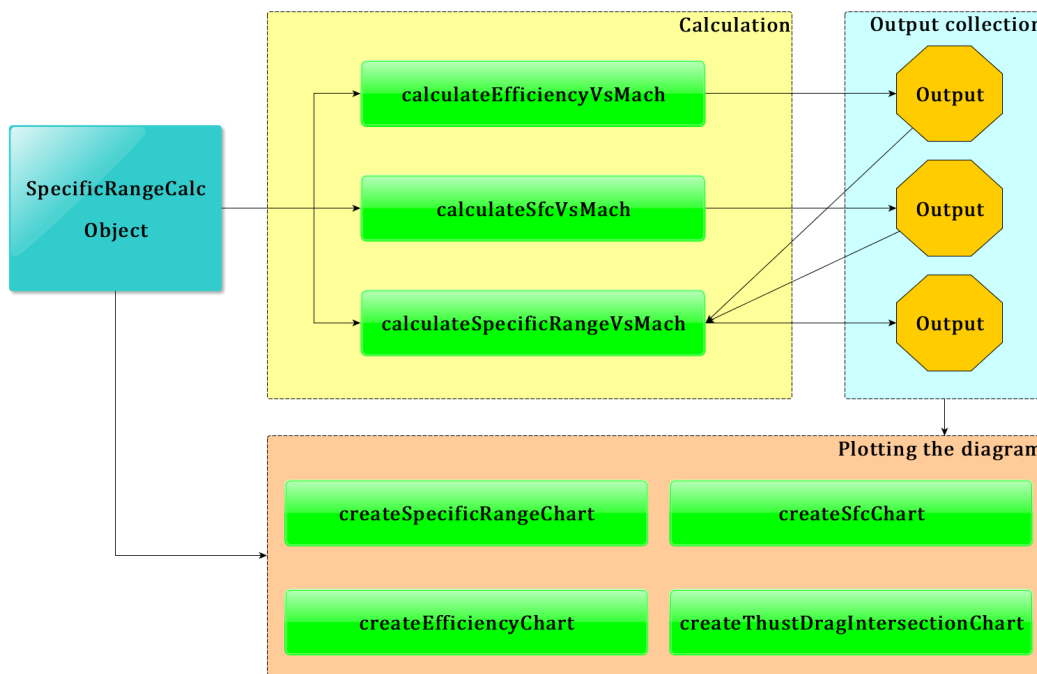


Figure 3.7 SpecificRangeCalc class flowchart

3.3 Case study: ATR-72 and B747-100B

In order to validate all the theoretical concepts explained in the previous paragraphs, as well as to give to the reader a useful example of how to handle this class usage, the following pages shows two application of the class methods made upon the two default aircraft described in paragraph 1.4.

Once all preliminary steps have been completed, as explained in paragraph 1.4, it's possible to start the test of this class. First of all, since the cruise grid chart is parameterized in aircraft weight, an array of aircraft masses has to be created; in particular, in this test, a variation of mass of -10% has been implemented, starting from the aircraft maximum take-off mass until it reaches the 60% of the latter. The second step is to define the independent variable, which is the Mach number, and in particular it's necessary to identify the upper and lower limitations of its array; this can be done by evaluating the required thrust, which is equal to the drag during cruise, and comparing it with the available thrust supplied by the power plant. By the intersections of the latter, the two required speeds can be derived; otherwise, if the minimum speed intersection can't be found, the cruising stalling speed, at that weight and altitude condition and for a specified $C_{L_{max}}$, replaces the missing intersection abscissa. In terms of code, the last step can be carried out using the static method, of the `JPADCore` class `PerformanceCalcUtils`, named `calculateDragThrustIntersection`; the latter requires as input the following data:

- An array of altitudes
- An array of speeds
- An array of weights

```

1   double[] maxTakeOffMassArray = new double[5];
2   for (int i=0; i<5; i++)
3       maxTakeOffMassArray[i] = aircraft.get_weights().get_MTOM()
4           .plus(aircraft.get_weights().get MLM())
5           .divide(2)
6           .getEstimatedValue()
7           *(1-0.1*(4-i));
8
9   double[] weight = new double[maxTakeOffMassArray.length];
10  for(int i=0; i<weight.length; i++)
11      weight[i] = maxTakeOffMassArray[i]*AtmosphereCalc.g0.getEstimatedValue();

```

Listing 3.1 Mass variation in Specific Range test - B747-100B

- An array of throttle settings
- An array of flight conditions chosen from the `EngineOperatingConditionEnum` enumeration
- The engine by-pass ratio, set to zero in case of propeller aircraft
- The wing surface
- Wing $C_{L_{max}}$ in clean configuration
- A List of custom data map named `DragMap`
- A List of custom data map named `ThrustMap`

The last two input are two collections of maps designed to store all data necessary to manage curves of drag, or thrust, as function of speed; in particular, in the reported example, the drag and thrust arrays passed to each of them are calculated using the static method of the JPADCore classes `DragCalc` and `ThrustCalc` named, respectively, `calculateDragVsSpeed` and `calculateThrustVsSpeed`. The first one implements the classic formula of drag as function of speed and of the C_D calculated with the (3.6), while the second one recognizes the engine type and reads the thrust value from the related external database.

```

1  // Drag Thrust Intersection
2  double[] speed = MyArrayUtils.linspace(
3      SpeedCalc.calculateTAS(
4          0.05,
5          theCondition.get_altitude().getEstimatedValue()
6          ), // start
7      SpeedCalc.calculateTAS(
8          1.0,
9          theCondition.get_altitude().getEstimatedValue()
10         ), // ending
11         250 // points
12     );
13
14 List<DragMap> listDrag = new ArrayList<DragMap>();
15 for(int i=0; i<maxTakeOffMassArray.length; i++)
16     listDrag.add(

```

```

17     new DragMap(
18         weight[i],
19         theCondition.get_altitude().getEstimatedValue(),
20         DragCalc.calculateDragVsSpeed(
21             weight[i],
22             theCondition.get_altitude().getEstimatedValue(),
23             aircraft.get_wing().get_surface().getEstimatedValue(),
24             aircraft.get_theAerodynamics().get_cD0(),
25             aircraft.get_wing().get_aspectRatio(),
26             aircraft.get_theAerodynamics().get_owald(),
27             speed,
28             aircraft.get_wing().get_sweepHalfChordEq().getEstimatedValue(),
29             aircraft.get_wing().get_maxThicknessMean(),
30             AirfoilTypeEnum.MODERN_SUPERCRITICAL
31         ),
32         speed
33     )
34 );
35
36 List<ThrustMap> listThrust = new ArrayList<ThrustMap>();
37 for(int i=0; i<maxTakeOffMassArray.length; i++)
38     listThrust.add(
39         new ThrustMap(
40             theCondition.get_altitude().getEstimatedValue(),
41             1.0, // phi
42             ThrustCalc.calculateThrustVsSpeed(
43                 aircraft.get_powerPlant()
44                     .get_engineList().get(0).get_t0().getEstimatedValue(),
45                     1.0, // phi
46                     theCondition.get_altitude().getEstimatedValue(),
47                     EngineOperatingConditionEnum.CRUISE,
48                     EngineTypeEnum.TURBOFAN,
49                     aircraft.get_powerPlant().get_engineList().get(0).get_bpr(),
50                     aircraft.get_powerPlant().get_engineNumber(),
51                     speed
52             ),
53             speed,
54             aircraft.get_powerPlant().get_engineList().get(0).get_bpr(),
55             EngineOperatingConditionEnum.CRUISE
56         )
57     );
58
59 List<DragThrustIntersectionMap> intersectionList = PerformanceCalcUtils
60     .calculateDragThrustIntersection(
61         new double[] {theCondition.get_altitude().getEstimatedValue()},
62         speed,
63         weight,
64         new double[] {1.0},
65         new EngineOperatingConditionEnum[]
66             {EngineOperatingConditionEnum.CRUISE},
67         aircraft.get_powerPlant().get_engineList().get(0).get_bpr(),
68         aircraft.get_wing().get_surface().getEstimatedValue(),
69         cLmax,
```

```

70         listDrag,
71         listThrust
72     );
73 // Definition of a Mach array for each maxTakeOffMass
74 List<Double[]> machList = new ArrayList<Double[]>();
75 for(int i=0; i<maxTakeOffMassArray.length; i++)
76     machList.add(MyArrayUtils.linspaceDouble(
77         intersectionList.get(i).getMinMach(), // start
78         intersectionList.get(i).getMaxMach(), // ending
79         250)); // points

```

Listing 3.2 Intersection of drag and thrust curves in Specific Range test - B747-100B

At this point all static methods of the `SpecificRangeCalc` class are called in order to follow the flowchart steps of figure 3.7 with the purpose of calculating and plotting the cruise grid points.

```

1 // Calculation of the SFC for each Mach array
2 List<Double[]> sfcList = new ArrayList<Double[]>();
3 for(int i=0; i<maxTakeOffMassArray.length; i++)
4     sfcList.add(SpecificRangeCalc.calculateSfcVsMach(
5         machList.get(i),
6         theCondition.get_altitude().getEstimatedValue(),
7         aircraft.get_powerPlant().get_engineList().get(0).get_bpr(),
8         EngineTypeEnum.TURBOFAN
9     ));
10 // Calculation of the Efficiency for each Mach array
11 List<Double[]> efficiencyList = new ArrayList<Double[]>();
12 for(int i=0; i<maxTakeOffMassArray.length; i++)
13     efficiencyList.add(SpecificRangeCalc.calculateEfficiencyVsMach(
14         Amount.valueOf(maxTakeOffMassArray[i], SI.KILOGRAM),
15         machList.get(i),
16         aircraft.get_wing().get_surface().getEstimatedValue(),
17         theCondition.get_altitude().getEstimatedValue(),
18         aircraft.get_wing().get_aspectRatio(),
19         aircraft.get_theAerodynamics().get_oswald(),
20         aircraft.get_theAerodynamics().get_cD0(),
21         aircraft.get_wing().get_maxThicknessMean(),
22         aircraft.get_wing().get_sweepHalfChordEq(),
23         AirfoilTypeEnum.MODERN_SUPERCRITICAL));
24 // Calculation of the Specific range:
25 List<Double[]> specificRange = new ArrayList<Double[]>();
26 for (int i=0; i<maxTakeOffMassArray.length; i++)
27     specificRange.add(SpecificRangeCalc.calculateSpecificRangeVsMach(
28         Amount.valueOf(maxTakeOffMassArray[i], SI.KILOGRAM),
29         machList.get(i),
30         sfcList.get(i),
31         efficiencyList.get(i),
32         theCondition.get_altitude().getEstimatedValue(),
33         aircraft.get_powerPlant().get_engineList().get(0).get_bpr(),
34         0.85,
35         EngineTypeEnum.TURBOFAN));
36

```

```

37 // PLOTTING:
38 // building legend
39 List<String> legend = new ArrayList<String>();
40 for(int i=0; i<maxTakeOffMassArray.length; i++)
41     legend.add("MTOM = " + maxTakeOffMassArray[i] + " kg ");
42
43 SpecificRangeCalc.createSpecificRangeChart(specificRange, machList, legend);
44 SpecificRangeCalc.createSfcChart(sfcList, machList, legend,
45     EngineTypeEnum.TURBOFAN);
45 SpecificRangeCalc.createEfficiencyChart( efficiencyList, machList, legend);
46 SpecificRangeCalc.createThrustDragIntersectionChart(
47     theCondition.get_altitude().getEstimatedValue(),
48     maxTakeOffMassArray,
49     listDrag,
50     listThrust,
51     speed
52 );
53 }
54 // END OF THE TEST

```

Listing 3.3 Intersection of drag and thrust curves in Specific Range test - B747-100B

In conclusion, the following images shows the cruise grid, and all the evaluated quantities, calculated with this class and referred to the ATR-72 and of the B747-100B. It's has to be noted that, as explained in the first paragraph, the maximum range condition is actually related to a low speed and also that, with a penalty of -1% in range, the specific range is about the same with a significantly higher speed; for example, in figure 3.15, the cruising Mach number, related to the maximum range condition of the B747-100B, varies, with the aircraft weight, between 0.74 and 0.80 while the long range one varies between 0.80 and 0.82, being more similar to the real cruising Mach number. Moreover, the specific fuel consumption, from figures 3.10 and 3.11, grows with the Mach number, as expected, due to the major thrust given by engines; while the efficiency, from figures 3.12 and 3.13, decreases rapidly in the B747-100B case due to the increasing wave drag, not present in the ATR-72 case.

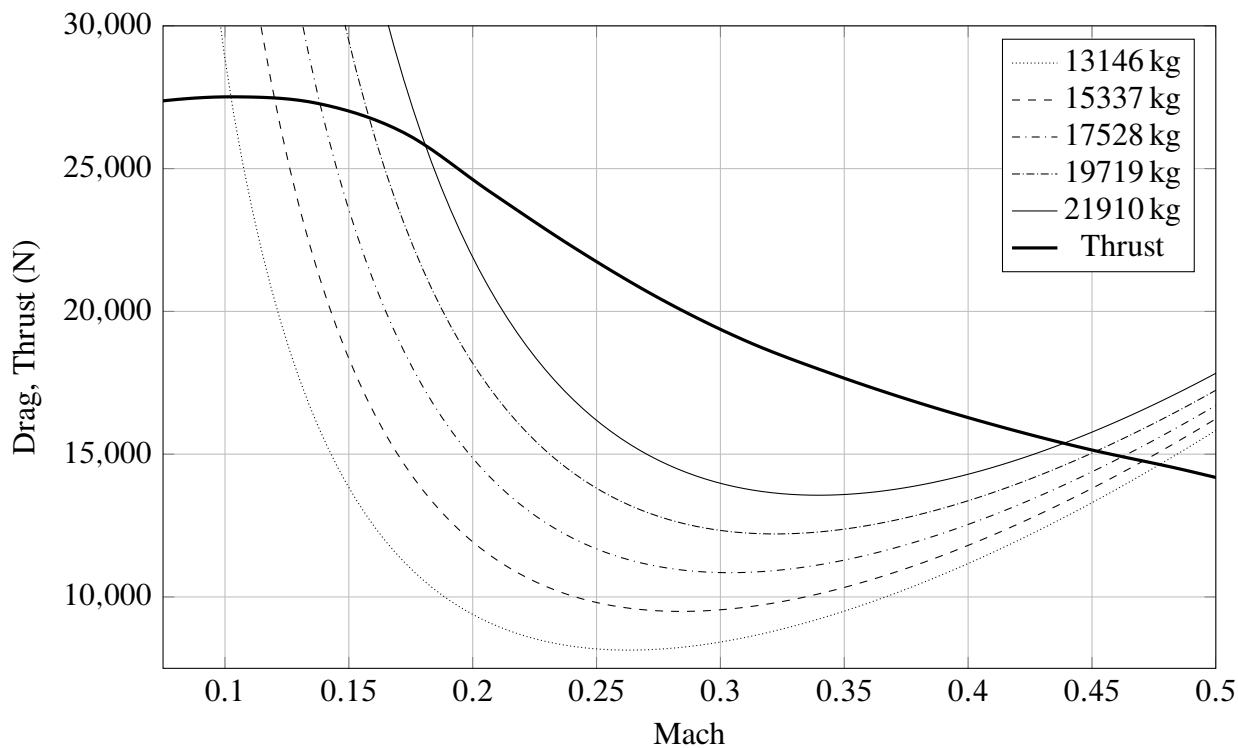


Figure 3.8 Intersection of drag and thrust curves at 6000m - ATR-72

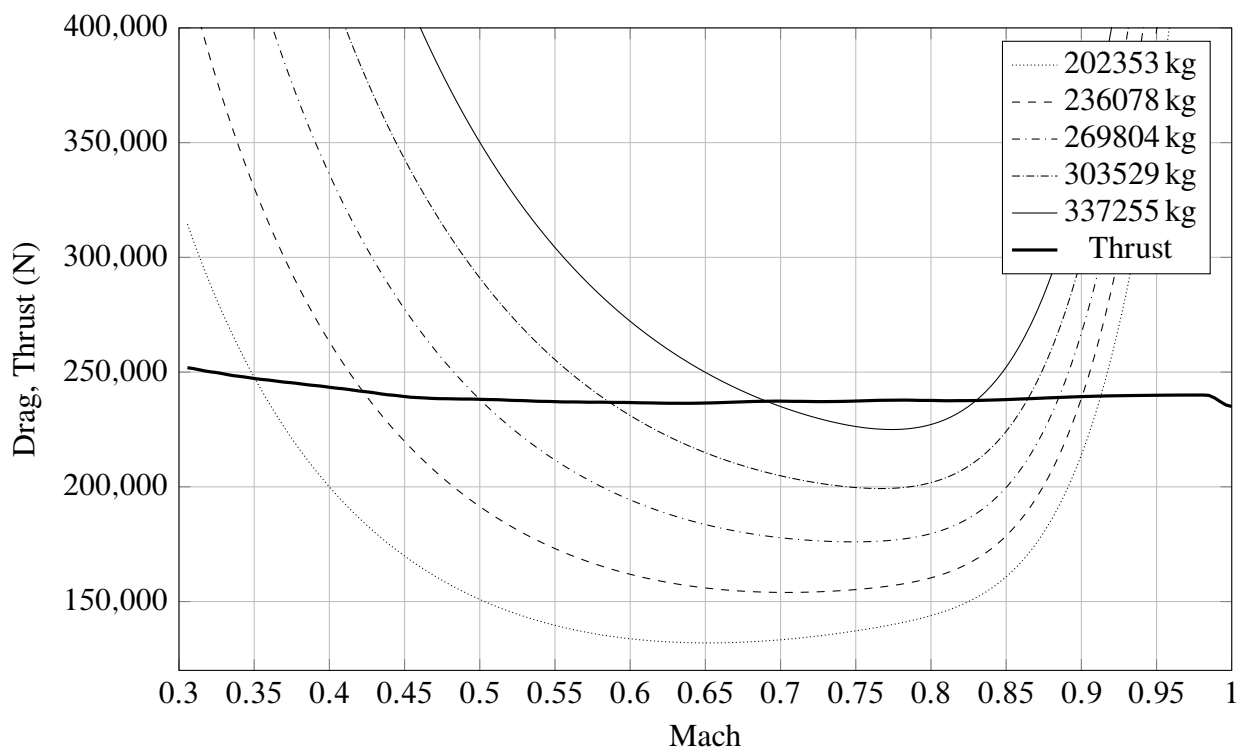


Figure 3.9 Intersection of drag and thrust curves at 10000m - B747-100B

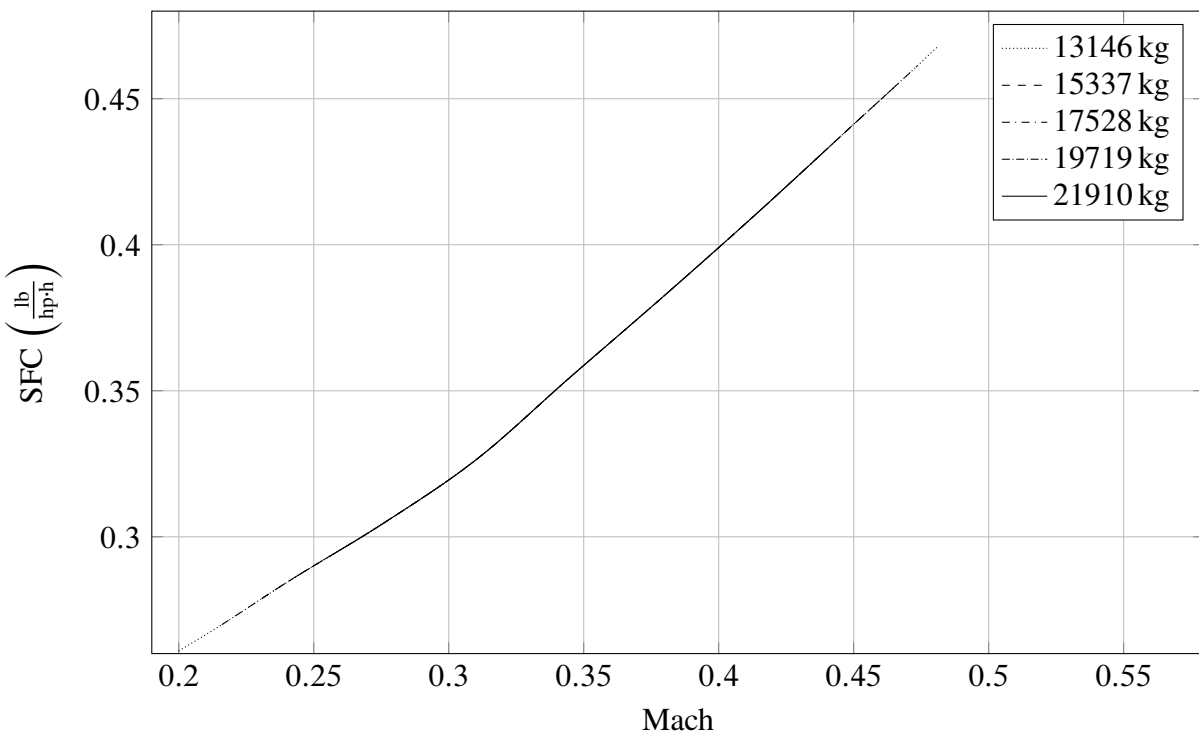


Figure 3.10 ATR-72 specific fuel consumption against Mach number at 6000m

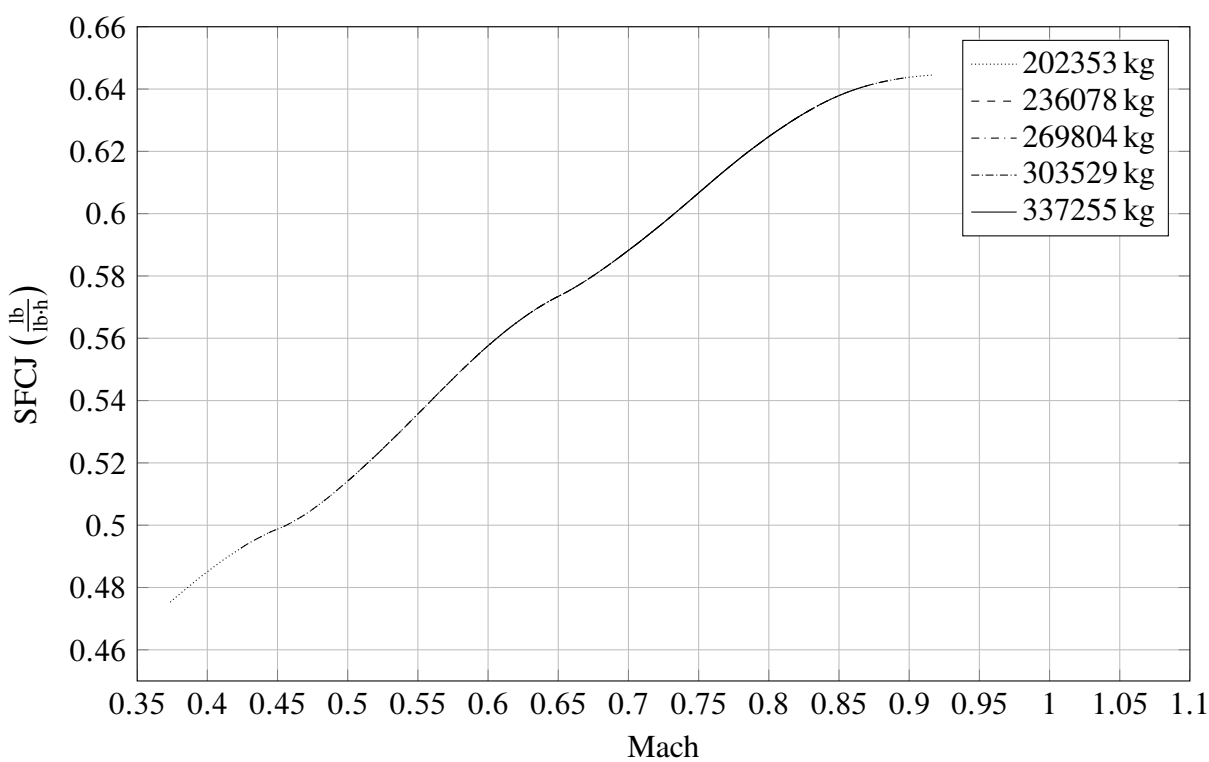


Figure 3.11 B747-100B specific fuel consumption against Mach number at 10000m

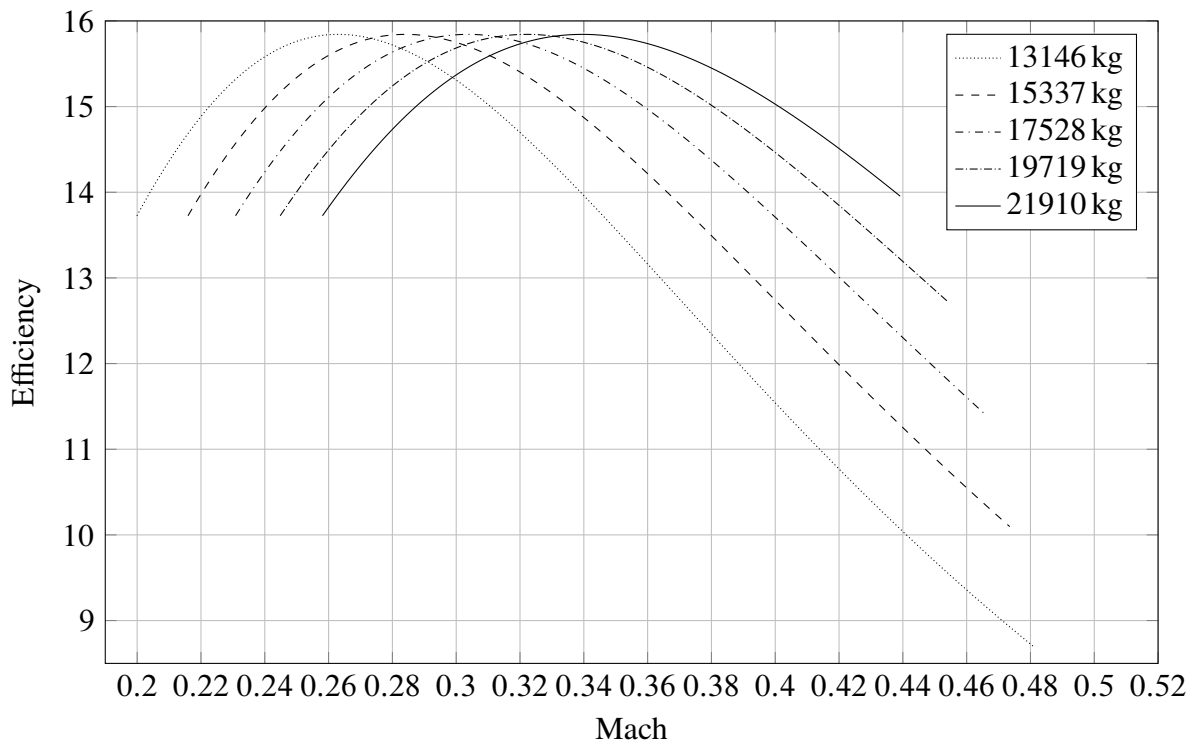


Figure 3.12 ATR-72 efficiency against Mach number at 6000m

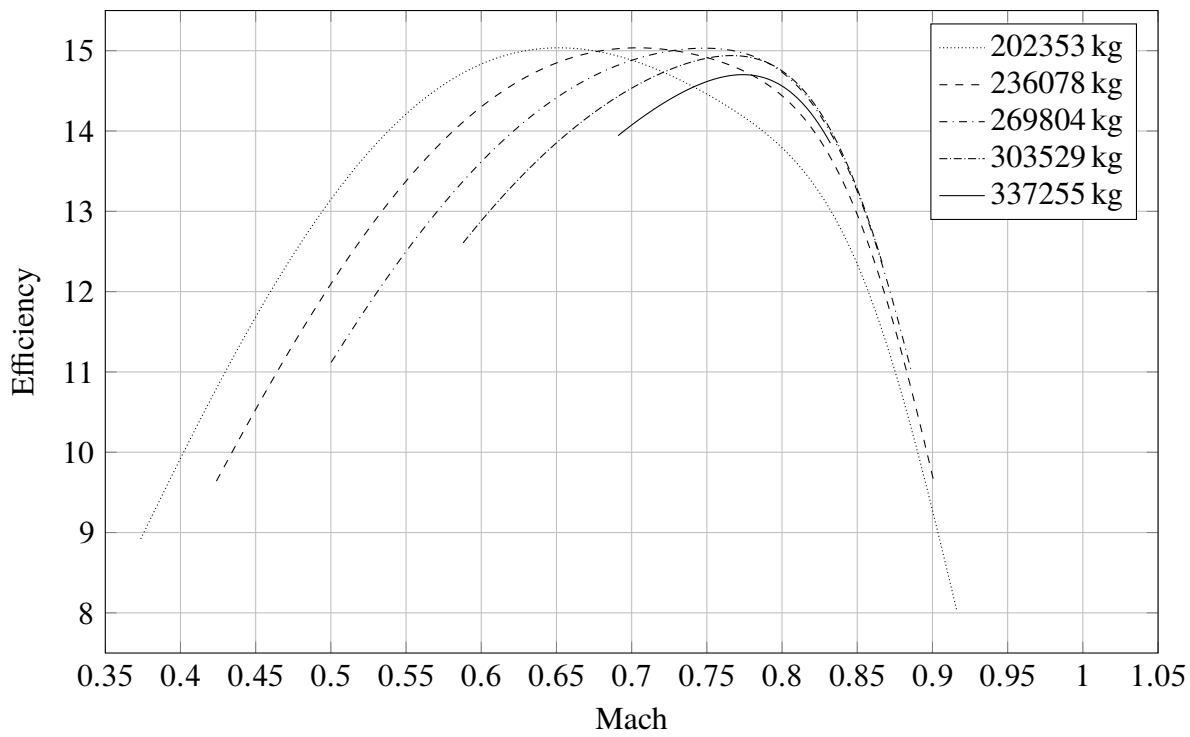
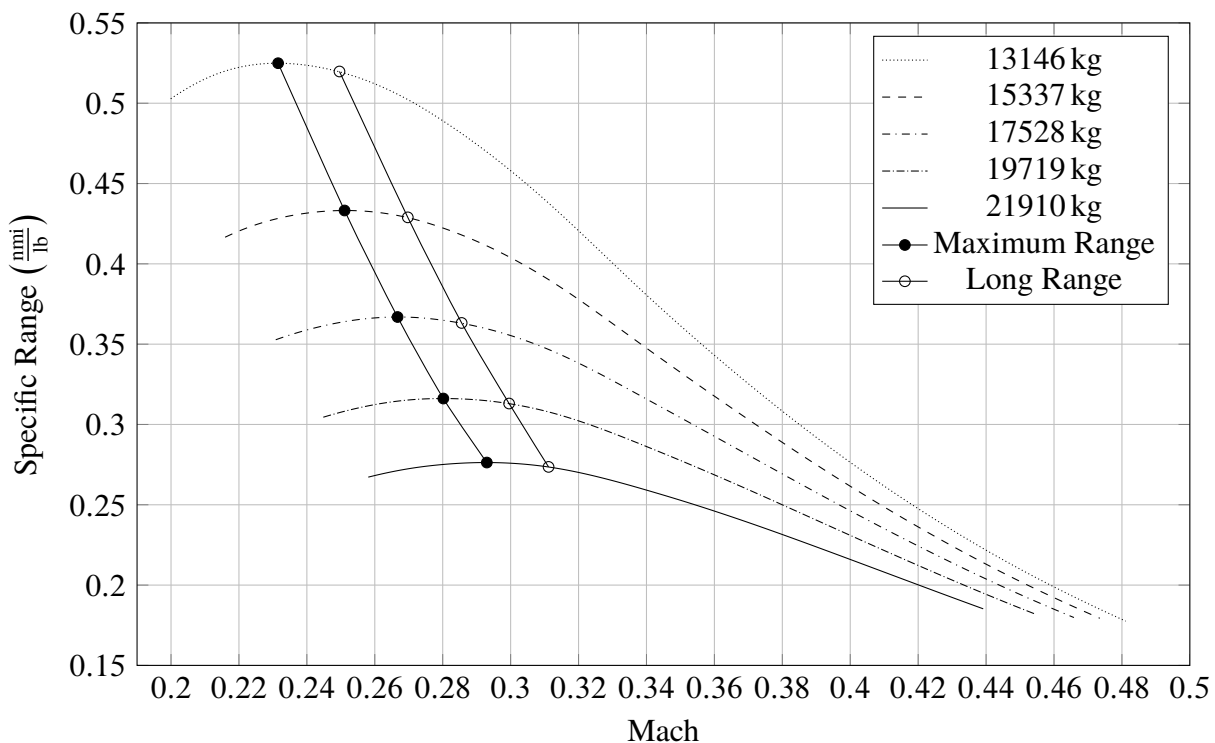
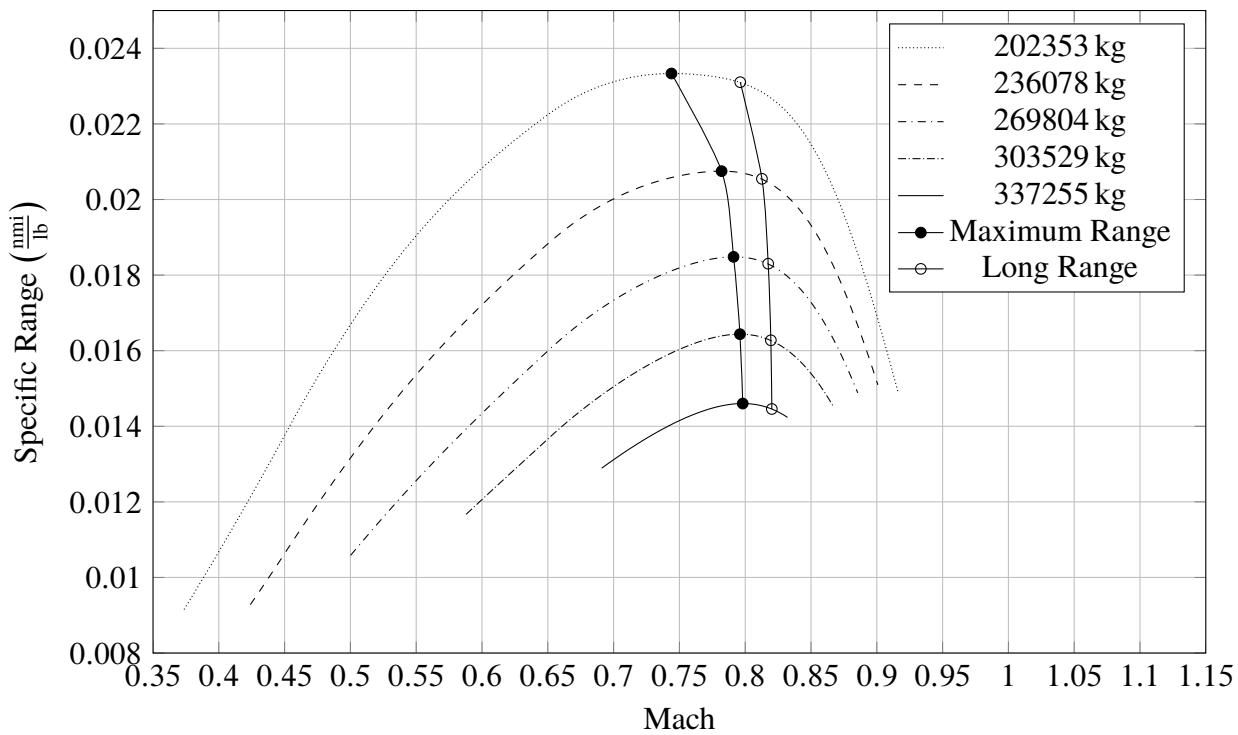


Figure 3.13 B747-100B efficiency against Mach number at 10000m

**Figure 3.14** ATR-72 cruise grid chart at 6000m**Figure 3.15** B747-100B cruise grid chart at 10000m

Chapter 4

HIGH LIFT DEVICES EFFECTS

In the preliminary design of the wing a large number of requirements have to be fulfilled as exemplified in table 4.1; but, as many of them are in conflict, it is hardly ever possible to check them all, so that a compromise has to be found.

Wing design requirements

- Low drag
 - High lift
 - Satisfactory maximum lift coefficient
 - Satisfactory stall quality
 - High value of the critical Mach number
 - Low weight
 - Ensure satisfactory performance in all flight phases
-

Table 4.1 Some wing design requirements

With respect of the last shown requirement, the wing is usually equipped with high-lift devices, which change its shape, in order to make it performant both in cruise both in take-off and landing phases. In fact, as can be seen from table 4.2, these phases show conflicting objectives which can only be mediated through the introduction of these devices.

Cruise requirements

- Small wing surface and high wing loading W/S
 - Small camber
 - Low drag
 - High speed
 - Lift generated using low c_L
-

Take-Off and Landing requirements

- Big wing surface, or high c_{Lmax} , in order to have an high equivalent wing loading $m = W/(S \cdot c_{Lmax})$
 - High drag value in landing
 - Lift generated using high c_L due to the low speed
-

Table 4.2 Comparison between cruise and take-off/landing design requirements

4.1 Theoretical background

In this paragraph, a general overview of the different type of high-lift devices is provided as well as the semi-empirical steps used to predict their effects on aerodynamic performance of the wing.

The designer may choose from a large collection of feasible high-lift systems, although in the case of a specific project this freedom will be limited, since incremental drag, mechanical complexity, development and maintenance costs and structural weight are all factors to be considered [31].

All high-lift devices can be divided in two main groups of which only the first one will be analyzed in this discussion:

- Systems for passive lift increase, such as *leading-edge devices* or *trailing-edge devices*, which modify the wing shape.
- Systems for active lift increase, such as *blown flaps* or *jet flaps*, which acts directly on the flow in order to control it.

Generally speaking, *trailing-edge devices* are used to increase the wing maximum lift coefficient, while *leading-edge devices* are used to increase the stalling angle of attack. A more in depth analysis shows that *trailing-edge devices* increase the camber and improve the flow at the trailing edge, but tend to promote leading edge stall on thin sections and may cause a reduction in the stalling angle of attack; on the other hand *leading-edge devices* postpone or eliminate leading edge stall, but they have little effects on the airfoil camber as a whole, although locally the camber is increased [31].

About *trailing-edge devices*, their effects can be resumed in:

- Higher c_L at a given angle of attack and higher $c_{L_{max}}$
- Lower stalling angle of attack
- Lower zero-lift angle due to increasing camber

while *leading-edge devices* provide the followings:

- Extension of the linear trait of the lift curve with an increase of the maximum angle of attack and of the $c_{L_{max}}$
- Higher zero-lift angle due to translation of the lift curve on the right caused by leading edge deflection which reduce the actual angle of attack
- Higher slope of the linear trait of the lift curve, for those devices which extend airfoils chords with the effect of increase the wing surface and, with constant wing span, the aspect ratio

Among the variety of different devices, only the followings will be taken into account as they represents the most used ones.

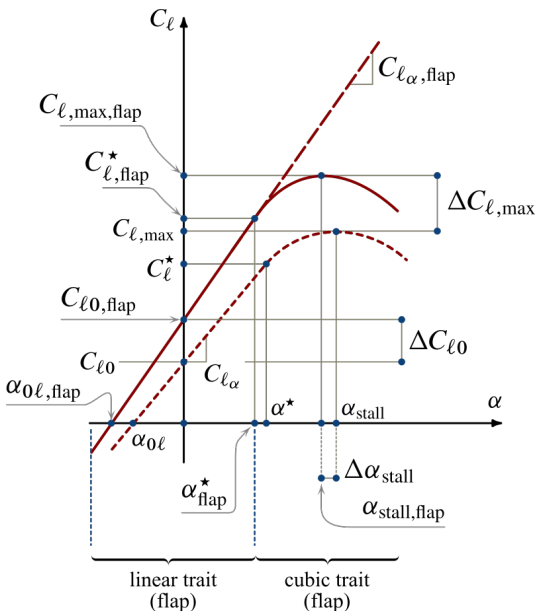


Figure 4.1 Trailing-edge devices effects

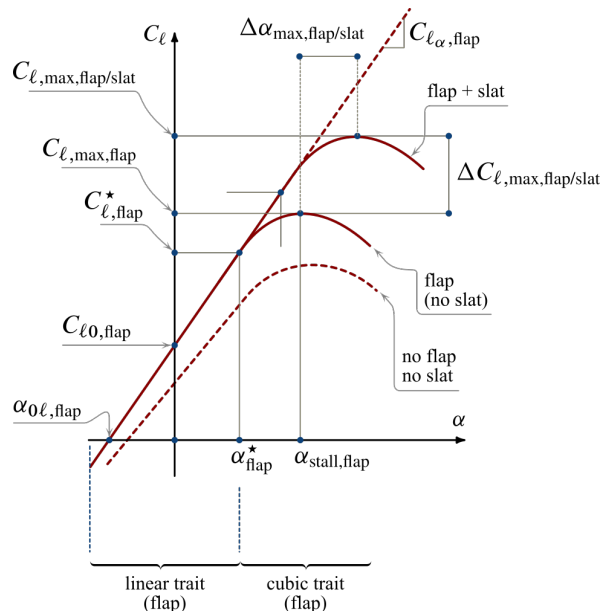


Figure 4.2 Leading-edge devices effects

Plain flap This device is most used on small aircraft or ones equipped of a thin wing because it doesn't support a complex mechanism of retraction. Typical deflections are about 20° for take-off and 60° for landing.

Single slotted flap It can be seen as a plain flap with a gap between the two elements composing the airfoil. The single slotted flap has very little flap overlap with the fixed trailing edge and hence develops only little Fowler motion, that is the aft travel of the flap that increases the section chord. Its typical deflections are about 20° for take-off and 45° for landing. The effects of a single slotted flap show an increment in all the aerodynamic coefficients, but it must be said that the increment in drag is lower than that for plain flaps. The slotted flap chord usually ranges from the 25% up to the 30% of the section chord. Moreover the slot influences boundary layer control, in fact it introduces a blowing that energizes the boundary layer delaying separation, so an increase in lift is generated.

Double slotted flap This device is superior to the previous type at large deflections, because separation of the flow over the flap is postponed by the more favourable pressure distribution. Its typical deflections are about 20° for take-off and 50° for landing; in particular, in order to avoid an increasing twisting moment due the deflection, this devices are usually combined with leading edge slats deflected of the same quantity.

Triple slotted flap This device is used on several transport aircraft with very high wing loadings. In combination with leading edge devices, this system represents almost the ultimate achievement in passive high-lift technology, but its shape shows that complicated flap supports and controls are required. Its typical deflections are about 20° for take-off and 50° for landing.

Fowler flap It is theoretically a single slotted flap that adds to the downward deflection also a backward motion that allows the increment of the effective chord and camber. Due to the

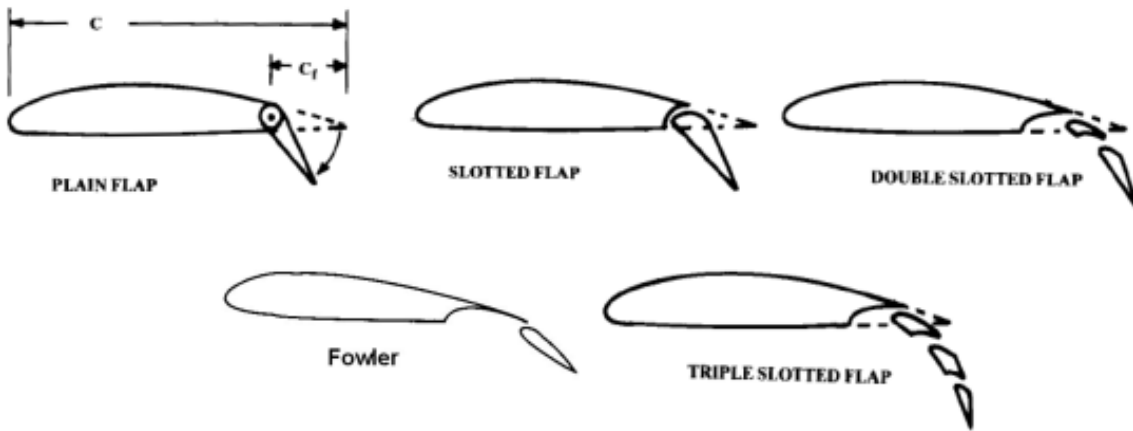


Figure 4.3 Analyzed trailing edge devices types

necessity of keeping the rear part of the wing section extended out the main element its implementation system is usually more complicated than the single slotted flaps but its weight and costs are largely justified by its high lift effectiveness. Its typical deflection are about 40° for landing and 15° for take-off, smaller than other types because the chord extension provides a bigger lift increment due to the bigger wing surface; this also reduces the drag in take-off wth benefit an the required field length.

Slat It's the most efficient leading edge device; thanks to combined deflection and forward motion, it acts in order to increase airfoil camber, and so the maximum lift coefficient, as well as increase the airfoil chord with the result of a bigger surface which provides a bigger aspect ratio with the effect of increase the lift curve slope of the linear trait. Furthermore, thanks to the slot which provides a boundary layer energization, it also increases the stalling angle of attack.

Krueger flap It acts in the same way as the slat, but it is thinner and more suitable for installation on thin wings. Krueger flaps are very common because of their simple architecture.

Plain leading edge flap Is less effective than slat since it has no slot, it is mechanically simple and rigid and particularly suitable for thin airfoil sections. The leading edge can be hinged in order to move it backward (droop nose) or it has a mechanism inside that changes the curvature of the nose (variable camber flap).

Leading edge fixed slot It has a fixed slot at the leading edge that, at high angle of attack, allows the airflow to pass through energizing the boundary layer; this helps to increase the stalling angle of attack. During the criuse phase, in which the angle of attack is small, the gap is usually sealed.

In order to predict, from the preliminary design phase, the aerodynamic characteristics of the high-lift devices, some useful semi-empirical methods are available; in this particular case the followings formulas and charts are taken from [31] and [27].

The guideline that will be followed provides to analyze separately the trailing edge and the leading edge devices effects; moreover it will start by evaluating the changes in aerodynamic

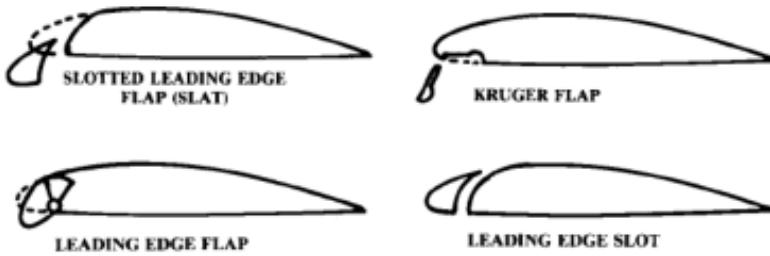


Figure 4.4 Analyzed leading edge devices types

characteristics of airfoils for then extends these to entire wing. From figures 4.1 and 4.2, it's possible to understand that the main changes introduced by trailing edge, or leading edge, devices are related to the evaluation of four quantities:

- ΔC_{l0}
- $\Delta C_{l\max}$
- $C_{l\alpha,\text{flap}}$
- $\Delta\alpha_{\text{stall}}$

4.1.1 ΔC_{l0} and ΔC_{L0} calculation

An empirical method for predicting airfoil lift increments at zero angle of attack for high-lift systems (ΔC_{l0}) comes from the Glauert's linearized theory for thin airfoils with flaps. A result obtained from this theory for the lift due to flap deflection is the following.

$$\alpha_\delta = 1 - \frac{\theta_f - \sin(\theta_f)}{\pi} \quad (4.1)$$

In particular θ_f can be calculated as follows.

$$\theta_f = \cos^{-1} \left(2 \frac{c_f}{c} - 1 \right) \quad (4.2)$$

Known this value, it's possible to evaluate the theoretical Δc_{l0} which can be calculated as proposed in (4.3).

$$\Delta C_{l0} = \alpha_\delta C_{l\alpha} \delta_f \quad (4.3)$$

with $C_{l\alpha}$ equals to the linear slope of the lift curve of the airfoil, and δ_f the flap angular deflection. For large flap deflections and for the separation at large flap angles due to viscosity, linear theory is in error when compared with exact one, for this reason we assume the effectiveness factor η_δ , so the formulation becomes the following.

$$\Delta C_{l0} = \alpha_\delta C_{l\alpha} \delta_f \eta_\delta \quad (4.4)$$

More in detail, η_δ can be evaluated from the charts provided in figures 4.5 and 4.6. In case of flaps which extend the airfoil chord, this effects also contributes to the lift increase and can be taken into account by referring the section lift to the extended chord and then converting the

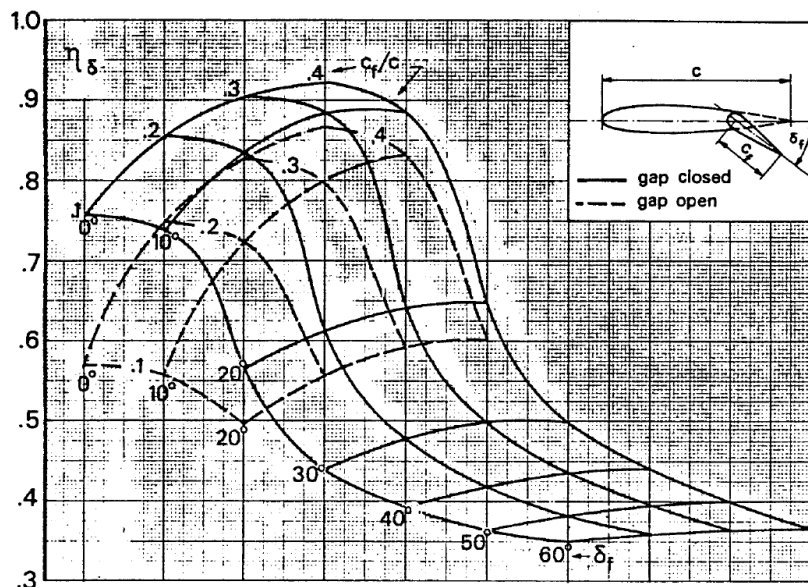


Figure 4.5 η_δ for plain flap

result to the original chord. As a result of this, the section lift coefficient can be evaluated as shown in (4.5).

$$C_l = (C'_{l0} + \Delta C'_{l0}) \frac{c'}{c} \quad (4.5)$$

Here the variables with superscript are referred to the extended chord. Assuming that for the basic section $C'_{l0} = C_{l0}$, it's possible to derive the ΔC_{l0} as follows.

$$\Delta C_{l0} = \Delta C'_{l0} \frac{c'}{c} + C_{l0} \left(\frac{c'}{c} - 1 \right) \quad (4.6)$$

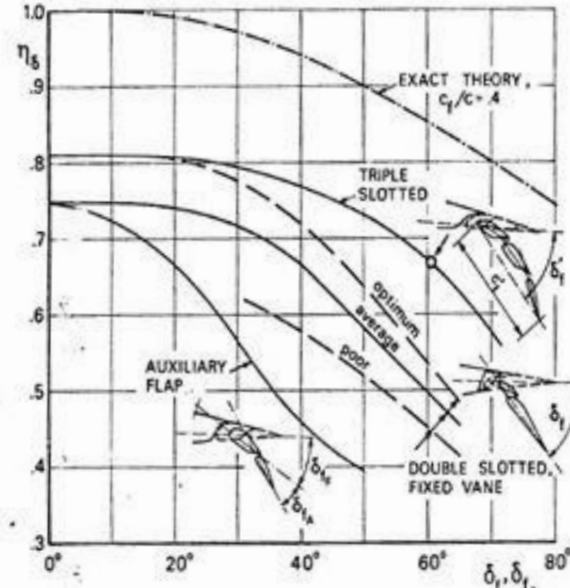
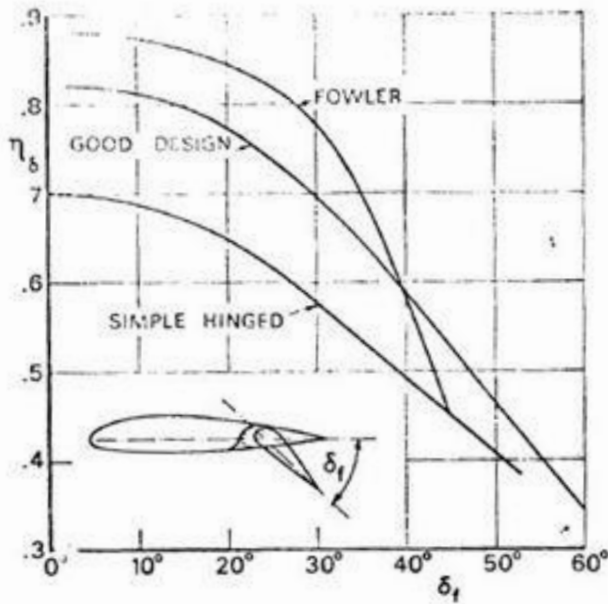


Figure 4.6 η_δ for other type of flaps

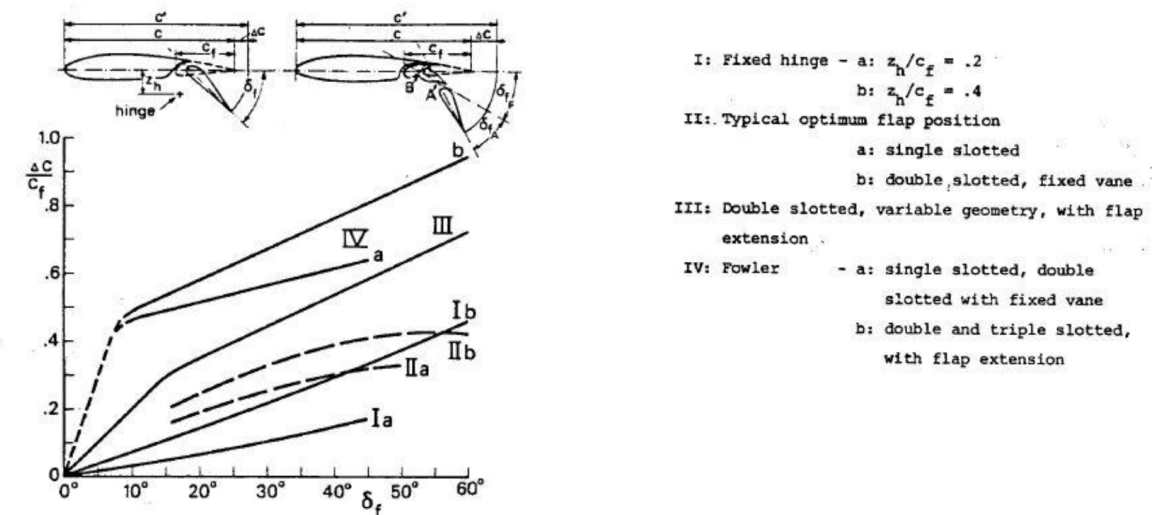


Figure 4.7 $\frac{\Delta c}{c_f}$ for different type of flaps as function of flap deflection

In particular C_{l0} is known, $\Delta C'_{l0}$ is calculated as in (4.4) and $\frac{c'}{c}$ is equal to the following expression.

$$\frac{c'}{c} = 1 + \frac{\Delta c}{c_f} \frac{c_f}{c} \quad (4.7)$$

In particular $\frac{\Delta c}{c_f}$ can be derived from the charts of figure 4.7. The ΔC_{l0} so calculated has now to be extended to the entire wing; this can be through the following formula.

$$\Delta C_{L0} = \Delta C_{l0} \left(\frac{C_{L\alpha}}{C_{l\alpha}} \right) \left[\frac{(\alpha_\delta)_{C_L}}{(\alpha_\delta)_{C_l}} \right] K_b \quad (4.8)$$

where $C_{L\alpha}$ and $C_{l\alpha}$ are respectively the lift curve slopes of the wing and the airfoil, $[(\alpha_\delta)_{C_L} / (\alpha_\delta)_{C_l}] = K_c$ is the ratio of the three-dimensional flap effectiveness parameter to the two dimensional flap effectiveness one, which can be derived from the figure 4.8, and K_b is a flap span effectiveness factor, which is function of the flap span-wise extension, that can be read from 4.9.

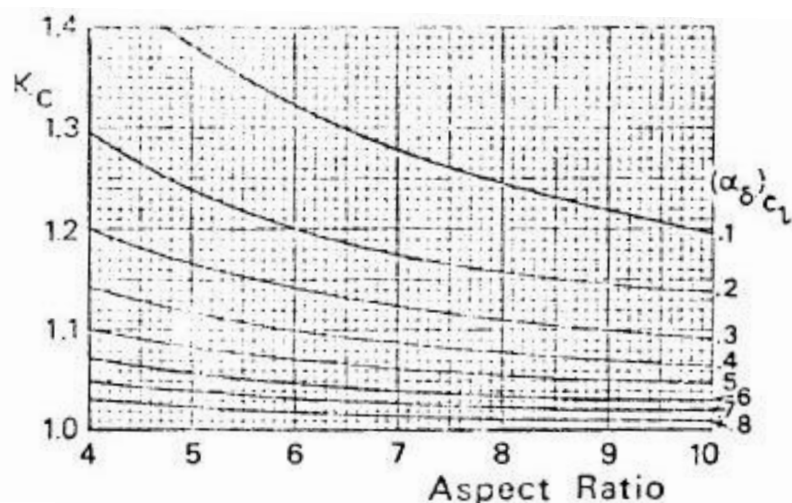


Figure 4.8 K_c for different $(\alpha_\delta)_{C_L}$ as function of wing aspect ratio

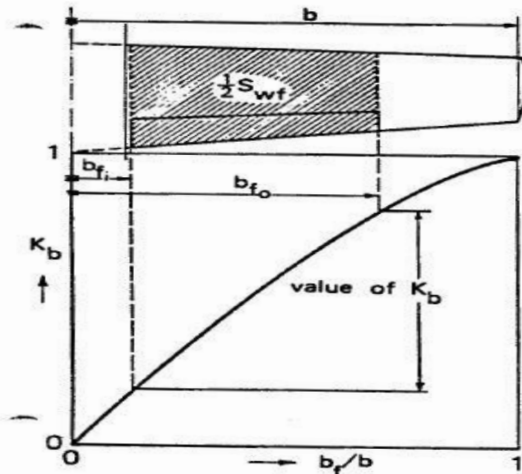


Figure 4.9 K_b as function of flap span to wing span ratio ($\frac{b_f}{b}$)

4.1.2 $\Delta C_{l\max}$ and $\Delta C_{L\max}$ calculation for trailing edge and leading edge devices

An empirical method for predicting airfoil maximum lift increments for plain and slotted flaps is presented in DATCOM and will be followed from [27]. The maximum lift increment provided to an airfoil by the deflection of a trailing edge flap is given by the (4.9).

$$\Delta C_{l\max} = k_1 k_2 k_3 (\Delta C_{l\max})_{\text{base}} \quad (4.9)$$

Here $(\Delta C_{l\max})_{\text{base}}$ is the section maximum lift increment for 25 percent-chord flaps at the reference flap-deflection angle and is shown in figure 4.10 for different flap systems. The quantity k_1 is a factor accounting for flap-chord-to-airfoil chord ratios, $\frac{c_f}{c}$, other than 0.25 and is shown in figure 4.11. The quantity k_2 is a factor accounting for flap deflections other than the reference value and is shown in figure 4.12. Finally, k_3 is a factor accounting for flap motion as a function of flap deflection and is shown in figure 4.13.



Figure 4.10 $(\Delta C_{l\max})_{\text{base}}$ DATCOM chart

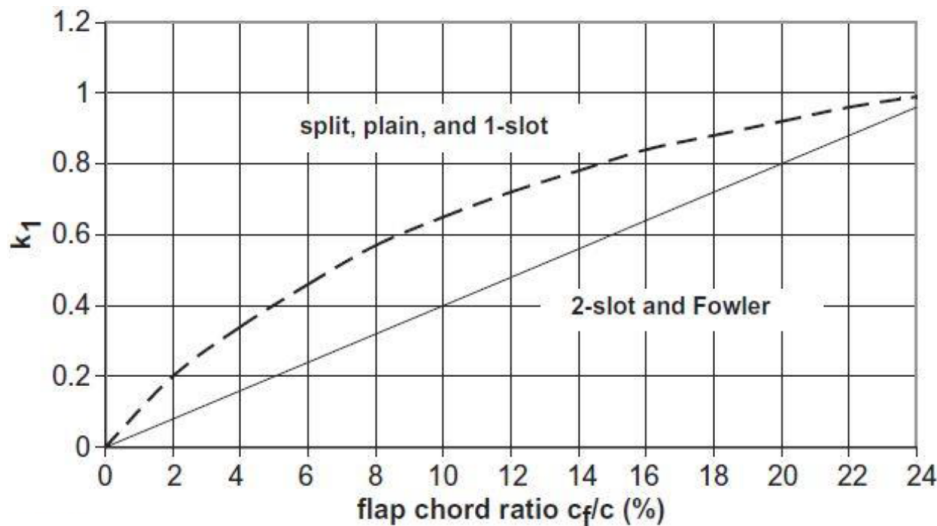


Figure 4.11 k_1 correction factor for trailing edge flap chord to airfoil-chord ratios, $\frac{c_f}{c}$, other than 0.25

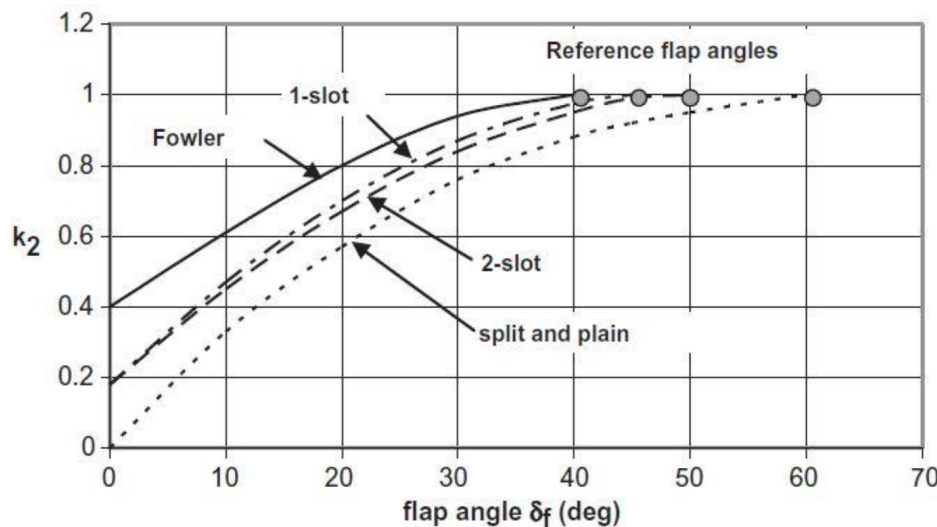


Figure 4.12 Flap angle correction factor k_2 . The reference flap angle for each type of flap is shown as a solid symbol at $k_2 = 1$

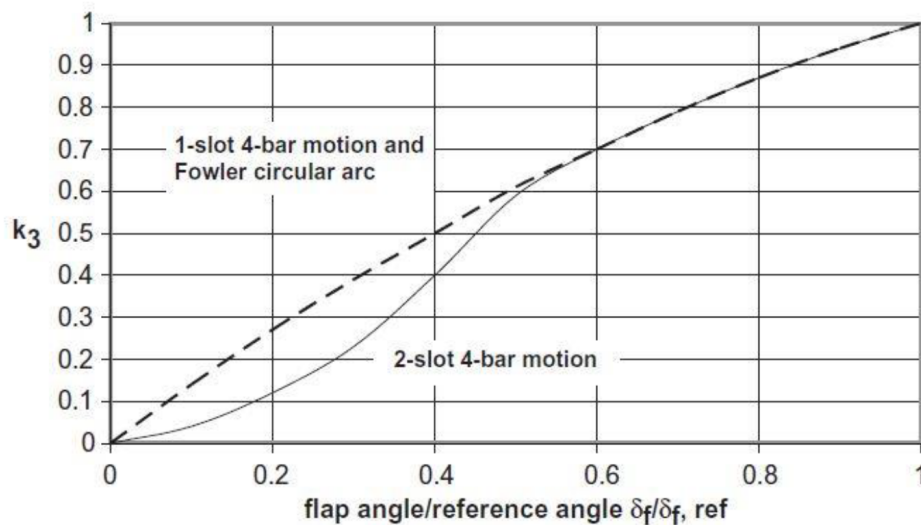


Figure 4.13 Flap motion correction factor k_3

Regarding leading edge devices, the leading edge slats are the most common ones; as explained previously, the latter increase the maximum lift coefficient of the airfoil along with the stall angle. As a result, they are commonly used, particularly in landing, though they are also useful on takeoff because the lift increment they develop comes with little drag penalty. The **DATCOM** method for leading edge flaps and slats proposes that the maximum lift increment for leading edge flaps or slats may be approximated by the following empirical relation.

$$\Delta C_{l\max} = \left(\frac{\partial C_l}{\partial \delta} \right)_{\max} \eta_{\max} \eta_{\delta} \delta_s \frac{c'}{c} \quad (4.10)$$

The first term in the previous equation is the theoretical lift effectiveness which gives the rate of change of the lift coefficient with change in deflection angle; it is shown in figure 4.14 as a function of the leading edge flap, or slat, chord to airfoil-chord ratio $\frac{c_s}{c}$. The second term, η_{\max} , is an empirical factor which accounts for the effects of airfoil leading edge radius and maximum thickness. A graph of this factor is presented in figure 4.15; the discontinuity in the curve for slats is said to be due to a lack of data in the region of the discontinuity, but an *ad hoc* correction is also proposed in order to provide more accurate results. The third term, η_{δ} , is another empirical factor which corrects for flap, or slat, deflections different from the optimum flap angle. This parameter is shown in figure 4.16 as a function of the flap, or slat, deflection angle δ_s . To understand the angle δ_s one may first imagine drawing a chord line on the slat-airfoil combination when the slat is stowed; then when the slat is deflected, the segment of the chord line that was drawn on the slat in the stowed position has now rotated through the deflection angle δ_s . This is the standard used in the **DATCOM** method and is not necessarily used throughout the literature as a definition of slat deflection angle. Finally, the ratio $\frac{c'}{c}$ accounts for the apparent increase in chord length when the slat is deflected and a slot is formed between the two airfoil elements; this dimension, along with the deflection angle δ_s , is illustrated in figure 4.17.

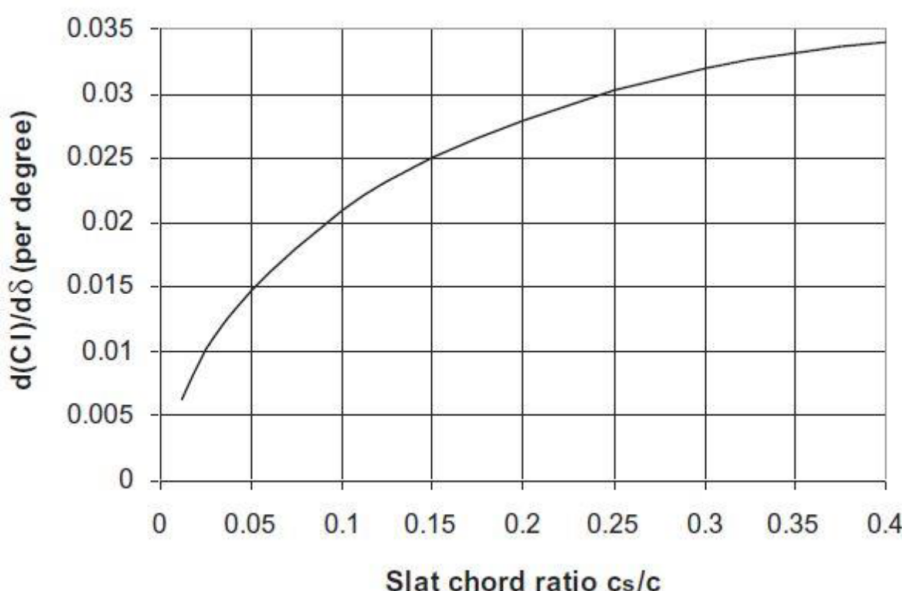


Figure 4.14 Rate of change of airfoil lift coefficient with slat deflection (per degree)

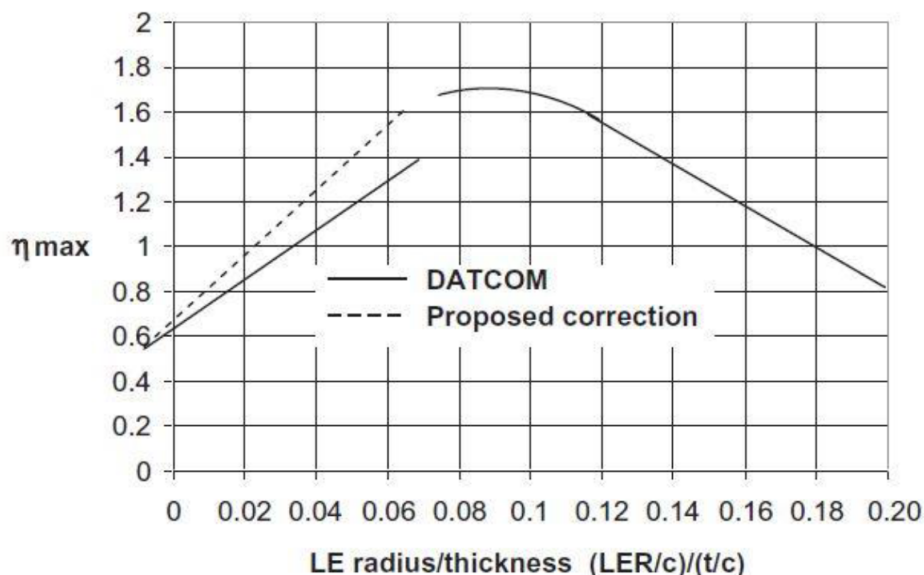


Figure 4.15 Correction factor for leading edge radius and airfoil thickness ratio

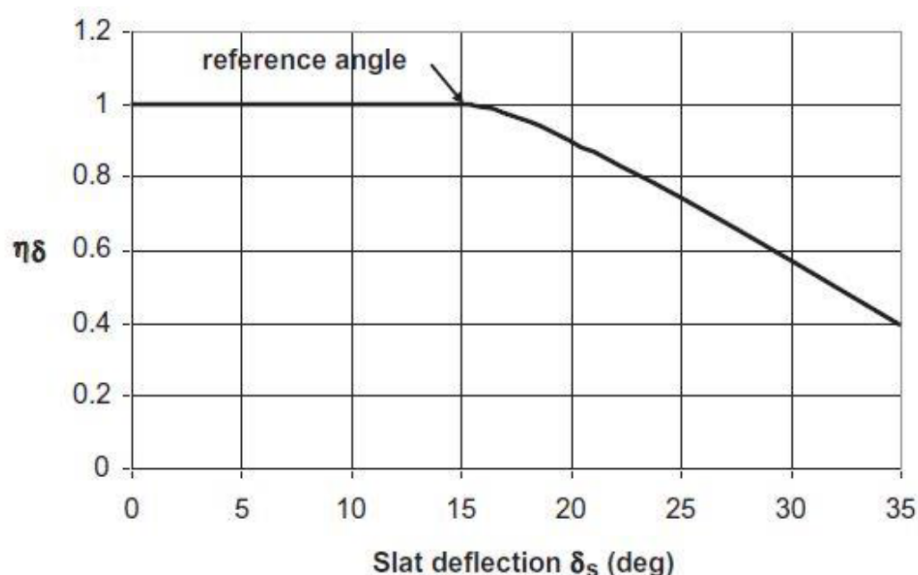


Figure 4.16 Slat deflection correction factor as a function of deflection angle

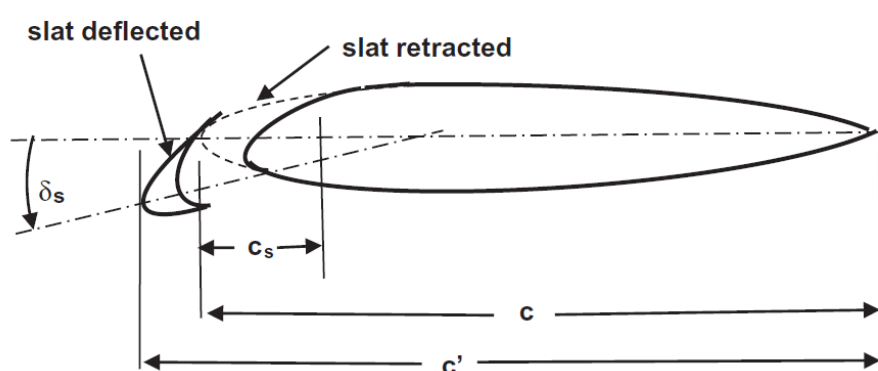


Figure 4.17 Geometry of the leading edge as used in the DATCOM method

Now that all increments related to the airfoil have been explained, the next step is to extend these two-dimensional quantities to the entire three-dimensional wing. Regarding trailing edge devices, the DATCOM method provides the following equation to compute the increment in maximum lift coefficient for the wing.

$$\Delta C_{L\max} = \Delta C_{l\max} \frac{S_{w,f}}{S} K_A \quad (4.11)$$

Here $\Delta C_{l\max}$ is the increment in lift coefficient due to flap deflection as defined in (4.9) while the quantity $\frac{S_{w,f}}{S}$ is the ratio of wing area affected by the trailing edge flap deflection (including both port and starboard wings) to the total wing area, as shown in figure 4.18; the wing area affected by the flap may be written as in (4.12).

$$S_{w,f} = \left(\frac{b}{2} \right) c_r [2 - (1 - \lambda) (\eta_i - \eta_o)] (\eta_i - \eta_o) \quad (4.12)$$

In the (4.12) the quantity $\lambda = \frac{c_t}{c_r}$ is the taper ratio, b is the wingspan while η_i and η_o are, respectively, the non-dimensional inboard location and the outboard location of the flap. If the flaps do not extend continuously along the trailing edge then the affected area for each may be calculated independently and added together.

Finally the correction factor for sweepback wings is given by the following equation.

$$K_A = (1 - 0.08 \cos^2 \Lambda_{c/4}) \cos^{3/4} \Lambda_{c/4} \quad (4.13)$$

The same calculations provided for trailing edge devices can be used for leading edge devices as well with the difference that the $\Delta C_{l\max}$ has to be calculated with the (4.10).

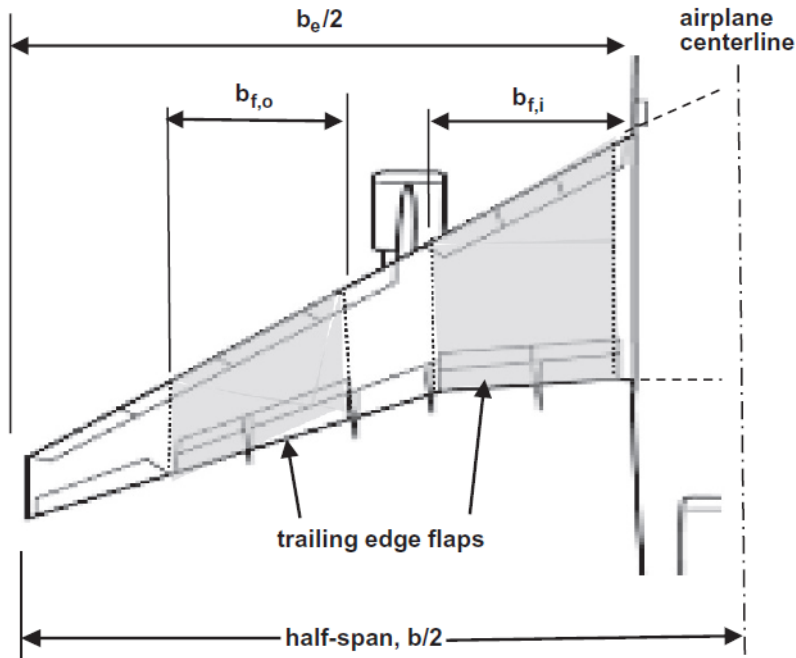


Figure 4.18 Plan view of wing where shaded area, including both the starboard and port wing, is the rated area for the flaps, that is, the portion of the wing planform area affected by the flaps

4.1.3 $C_{l\alpha,\text{flap}}$ and $C_{L\alpha,\text{flap}}$ calculation

The lift gradient is affected by flap deflection in three ways:

- The chord extension increases $C_{l\alpha}$. This effect depends on the multiplicative factor $\frac{c'}{c}$
- The potential flow effect of flap deflection on the lift curve slope is reduced with increasing α . The result is a nonlinearity in the lift curve which is particularly pronounced for large flap angles.
- The effect of viscosity on the lift effectiveness of a flap increases with the angle of attack, thus reducing $(\Delta C_l)_{\text{flap}}$ with increasing α

In order to evaluate the variation in $C_{l\alpha}$ due to flap deflection, references to [31] have been made. In particular, Torenbeek provides the following equation which approximates the results of the exact theory fairly accurately and is in qualitative agreement with experimental data.

$$C_{l\alpha(\text{flap down})} = C_{l\alpha} \left[\frac{c'}{c} \left(1 - \frac{c_f}{c'} \sin^2 \delta_f \right) \right] \quad (4.14)$$

This equation is then corrected for the three-dimensional wing as follows.

$$C_{L\alpha(\text{flap down})} = C_{L\alpha} \left\{ 1 + \frac{\Delta C_{L0}}{\Delta C_{l0}} \left[\left(\frac{c'}{c} \left(1 - \frac{c_f}{c'} \sin^2 \delta_f \right) - 1 \right) \right] \right\} \quad (4.15)$$

4.1.4 $\Delta\alpha_{\text{stall}}$ calculation for trailing edge and leading edge devices

As explained previously, trailing edge devices contribute to lower the stalling angle of attack, while leading edge devices do the opposite providing a higher α_{stall} . In order to compute these two effects, a reference to [21] has been done. In particular, for trailing edge devices, data from [1] suggest the following curve where the $\Delta\alpha_{\text{stall}}$ is negative and is function of flap deflection.

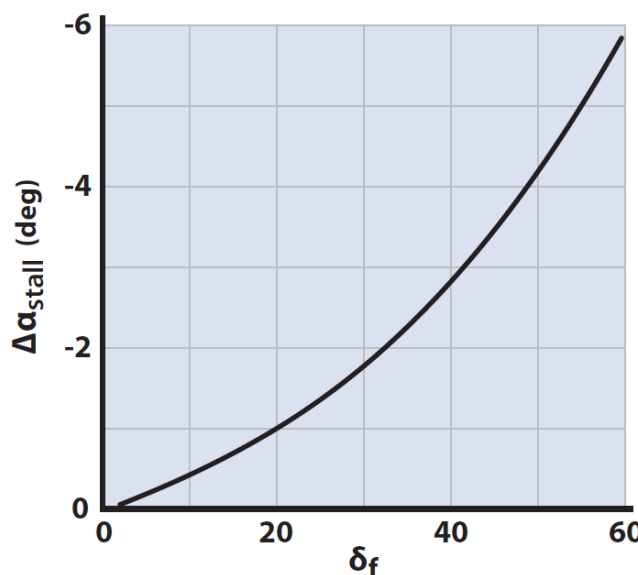


Figure 4.19 Decrease in stall angle with flap deflection

Since there are no precise methods for predicting leading edge devices effects on α_{stall} , references to experimental data are the only way to follow. In order to build the lift curve with flaps and slats effects, this value of $\Delta\alpha_{\text{stall}}$ is taken as the same used in the construction of the clean wing lift curve; the latter shown in figure A.2.

4.1.5 Further effects calculations

High-lift devices influence not only the lift curve but also the wing drag polar, in particular the C_{D0} , and the wing pitching moment. Further calculations are, therefore, necessary to predict these latter.

Regarding the ΔC_{D0} provided by high-lift devices, the reader can refer to [32]. Proceeding on much the same lines as in the analysis of lift coefficient increments, Young and Hufton assumed that $\Delta C_D 0$ can be calculated as follows for a full-span flap.

$$\Delta C_{D0} = \delta_1 (c_f/c) \cdot \delta_2 (\delta_f) \quad (4.16)$$

where δ_1 and δ_2 are functions that were determined from experimental data. Their related curves are shown in figure 4.20 and 4.22, for plain flap, and, in figure 4.21 and 4.23, for slotted flaps.

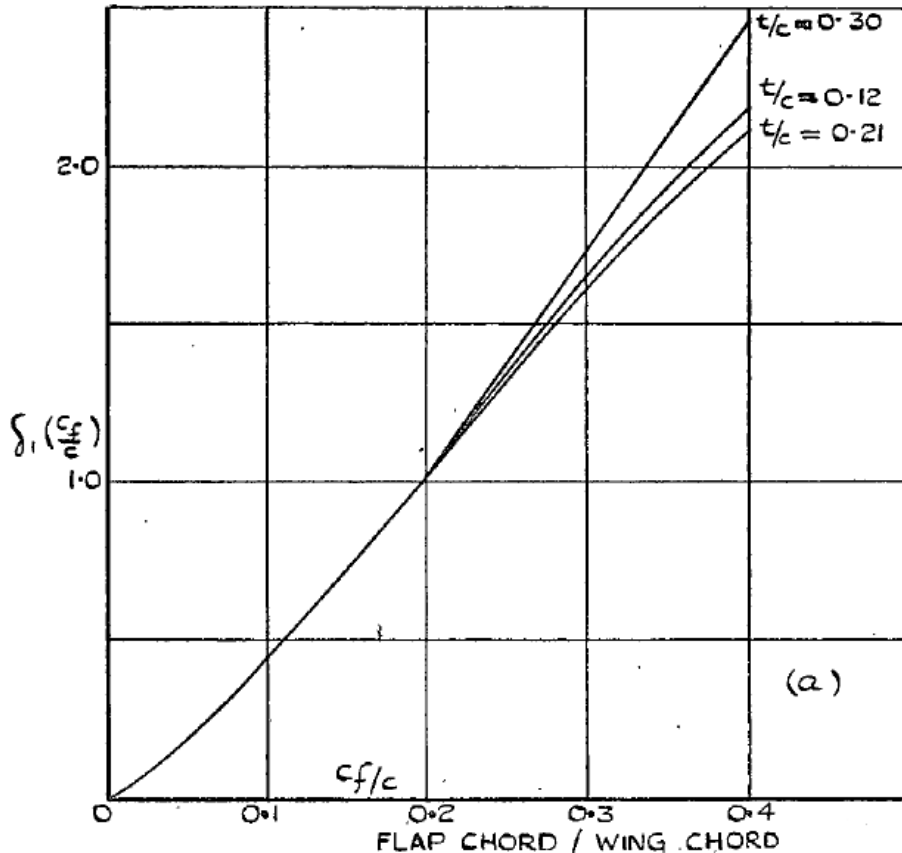


Figure 4.20 The functions $\delta_1 (c_f/c)$ for split and plain flaps

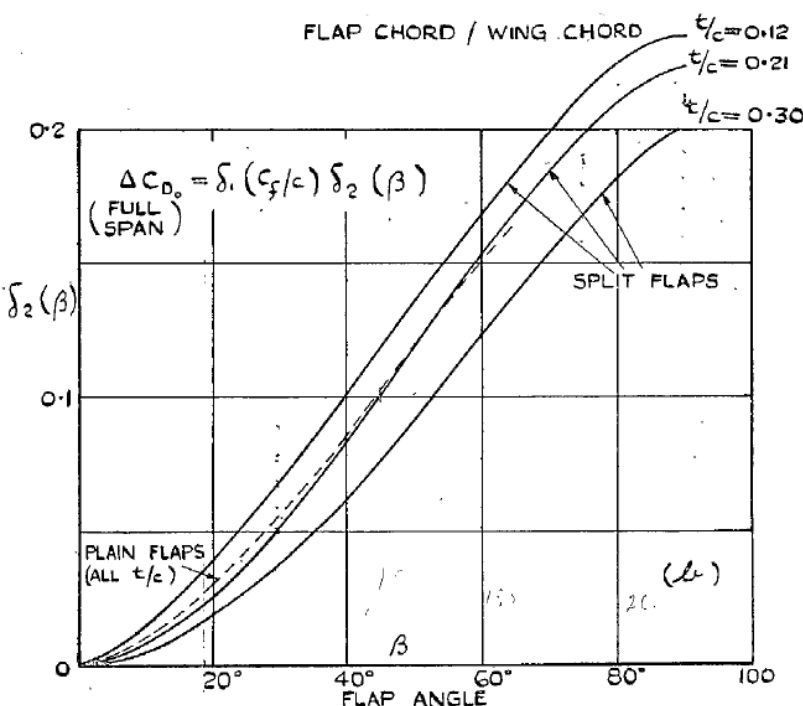


Figure 4.21 The functions $\delta_2 (\delta_f)$ for plain flaps

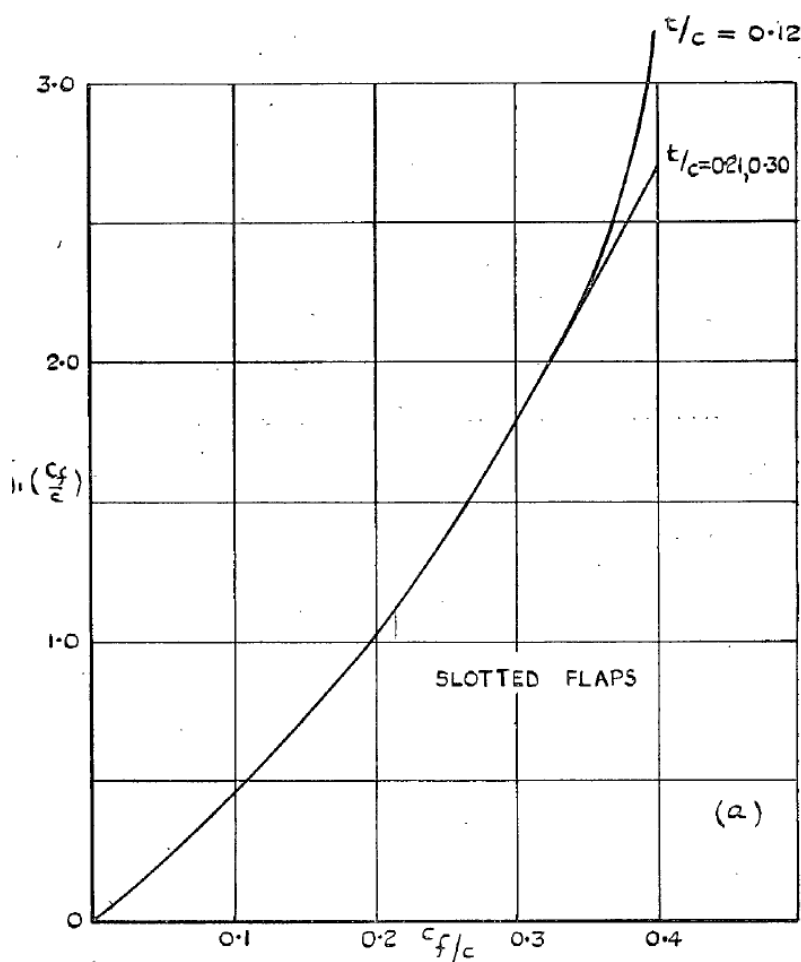


Figure 4.22 The functions $\delta_1 (c_f/c)$ for split and slotted flaps

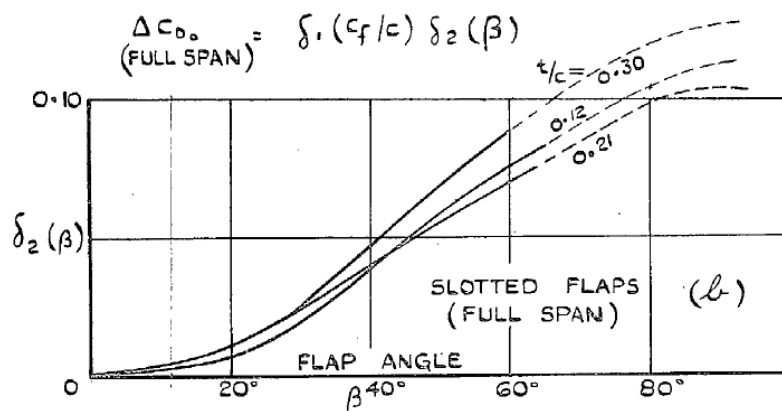


Figure 4.23 The functions $\delta_2(\delta_f)$ for slotted flaps

General considerations, confirmed by experimental data, led Young and Hufton to conclude that the drag increment of a part-span flap of any type is proportional to the area of the flapped part of the wing. Hence, to determine the increment for a part-span flap it's necessary to multiply the increment for a full-span flap by the ratio of the flapped wing area to the total wing area. The latter ratio, denoted by δ_3 , is shown in figure 4.24 as a function of flap span for wings of various taper ratios. Thus the ΔC_{D0} equation becomes the following.

$$\Delta C_{D0} = \delta_1(c_f/c) \cdot \delta_2(\delta_f) \cdot \delta_3(b_f/b) \quad (4.17)$$

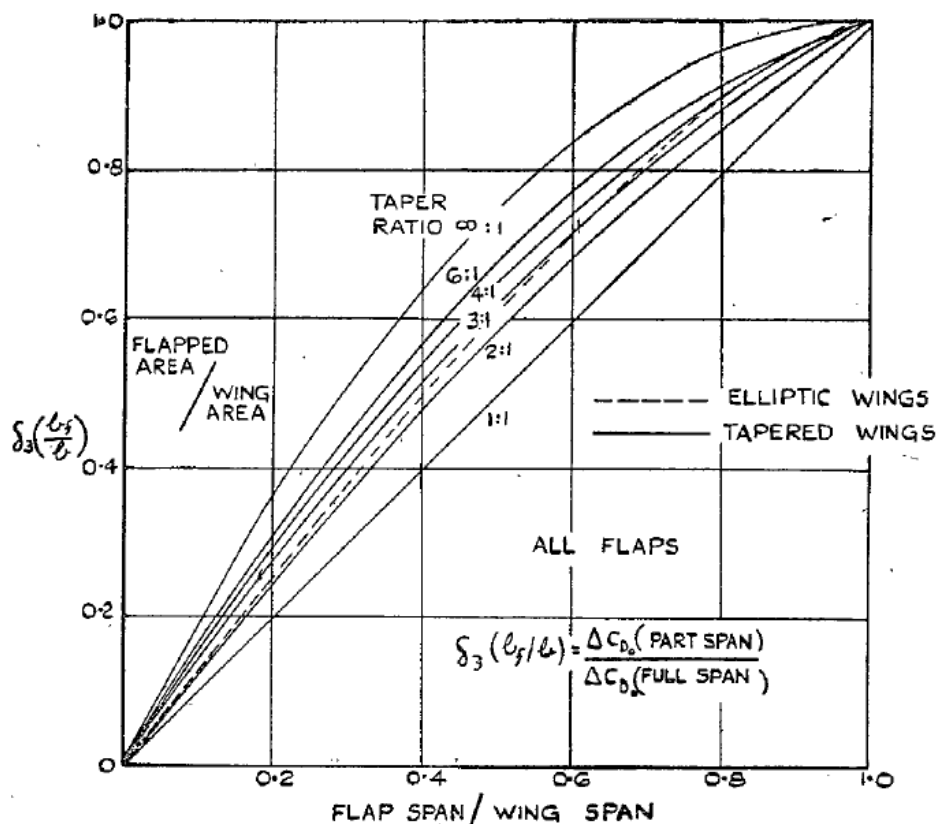


Figure 4.24 The functions $\delta_3(b_f/b)$ for slotted flaps

The last, but not least, effect to be predict refers to the pitching moment of the airfoil and of the wing. Following the guideline proposed in [31], the generalized expression, for airfoils, in (4.18) represents a useful starting point when experimental data are not available.

$$\Delta C_{m_{\frac{c}{4}}} = -\mu_1 \Delta C_{l_{\max}} \left(\frac{c'}{c} \right)^2 - \frac{C_l}{4} \frac{c'}{c} \left(\frac{c'}{c} - 1 \right) + \left(C_{m_{\frac{c}{4}}} \right)_{\delta_f=0} \left[\left(\frac{c'}{c} \right)^2 - 1 \right] \quad (4.18)$$

where extended chord c' , shown in figure 4.7, allows for the effects of the backward movement of the flap while it is being extended. In equation this equation, the first contribution is due to the increased section camber and the factor μ_1 is defined as follows according to Glauert's linear theory for small flap deflections.

$$\mu_1 = \frac{1}{2} \left(1 - \frac{c_f}{c} \right) \frac{\sin \theta_f}{\pi - (\theta_f - \sin \theta_f)} \quad (4.19)$$

where θ_f is the one from equation (4.2). This theoretical value of μ_1 generally underpredicts the pitching moment coefficient; in fact it has been found that, for slotted flaps with, or without, Fowler movement, most data are on a single line, provided the second term of the equation (4.19), representing the theoretical rearward shift of the airfoil aerodynamic center, is halved. Furthermore, in the case of split and plain flaps, the flap angle is observed to exert a pronounced influence on μ_1 as shown in figure 4.25. The last term of the (4.19) is generally of a low order and can be ignored. This, together with the halving of the second term of the previous equation, leads to the following practical expression of $\Delta C_{m_{\frac{c}{4}}}$.

$$\Delta C_{m_{\frac{c}{4}}} = -\mu_1 \Delta C_{l_{\max}} \left(\frac{c'}{c} \right) - \frac{C_l}{8} \frac{c'}{c} \left(\frac{c'}{c} - 1 \right) \quad (4.20)$$

The obtained two-dimensional equation can, then, be converted into a three-dimensional one,

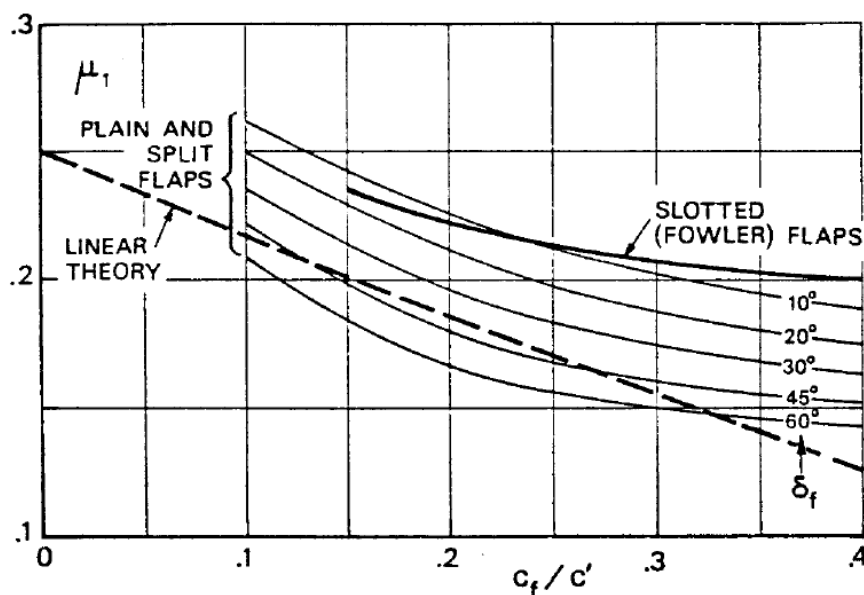


Figure 4.25 The pitching moment function μ_1

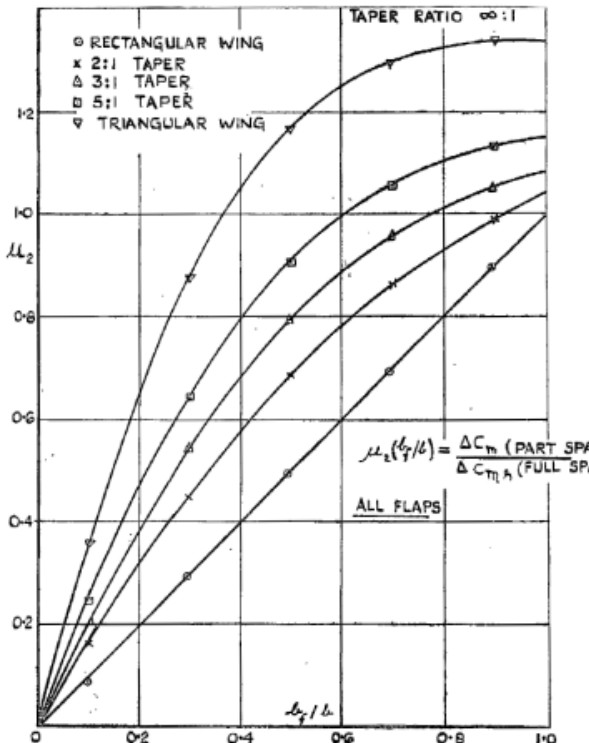


Figure 4.26 The pitching moment function μ_2

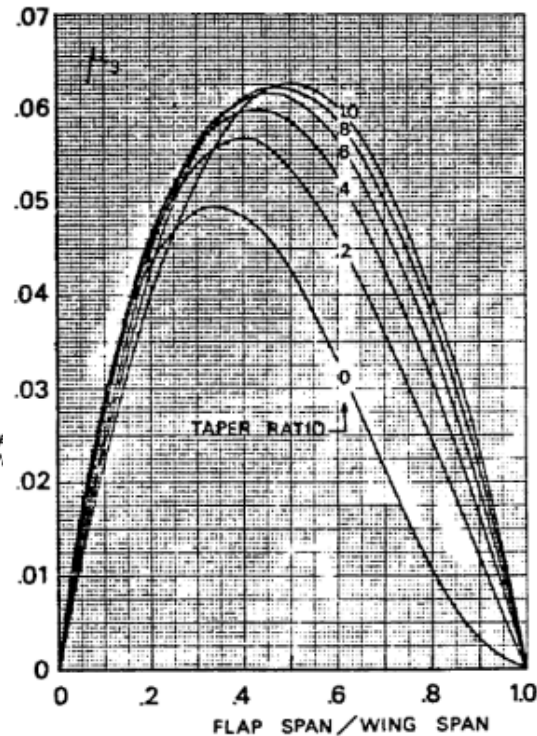


Figure 4.27 The pitching moment function μ_3

which computes the pitching moment change on the entire wing, as follows.

$$\Delta C_{M_{\frac{c}{4}}} = \mu_2 \Delta C_{m_{\frac{c}{4}}} + 0.7 \frac{\mathcal{R}}{1 + \frac{2}{\mathcal{R}}} \mu_3 \Delta C_{l_{\max}} \tan \Lambda_{\frac{c}{4}} \quad (4.21)$$

where $\Delta C_{m_{\frac{c}{4}}}$ is the one from (4.20), provide that $C_l = C_L + \Delta C_{l_{\max}} \left(1 - \frac{S_{w,f}}{S}\right)$, and the correction factors μ_2 and μ_3 are the one shown in figures 4.26 and 4.27. Making the appropriate substitutions, the following operational formula is, finally, obtained.

$$\begin{aligned} \Delta C_{M_{\frac{c}{4}}} = & \mu_2 \left\{ -\mu_1 \Delta C_{L_{\max}} \frac{c'}{c} - \left[C_L + \Delta C_{l_{\max}} \left(1 - \frac{S_{w,f}}{S}\right) \right] \frac{1}{8} \frac{c'}{c} \left(\frac{c'}{c} - 1 \right) \right\} \\ & + 0.7 \frac{\mathcal{R}}{1 + \frac{2}{\mathcal{R}}} \mu_3 \Delta C_{l_{\max}} \tan \Lambda_{\frac{c}{4}} \end{aligned} \quad (4.22)$$

4.2 Java class architecture

The main purpose of this paragraph is to provide a comprehensive description of how all semi-empirical methods, presented previously, are implemented and used inside the Java class created to manage high-lift devices effects upon wings. Because of the great number of charts from which some important data have to be derived, an external database, containing all the digitized curves shown in previous paragraph figures, has been created following the procedure explained in appendix A.1.

This database, named `HighLiftDatabase`, is then read by a dedicated class created inside the database package of `JPADCore` which name is `HighLiftDatabaseReader`; the latter, in particular,

Available Flaps	Typical maximum deflection	Database index
Single slotted	45°	1.0
Double slotted	50°	2.0
Plain	60°	3.0
Fowler	40°	4.0
Triple slotted	50°	5.0

Table 4.3 Summary of available flaps types with thier related properties

has been built up following the giudeline of appendix A.2.

Having now a powerful tool to bypass the charts reading, it's now possible to create the Java class dedicated to the management of high-lift devices effects. Since this class, named `CalcHighLiftDevices`, has to evaluate these effects on a wing, the philosophy followed in its creation suggests to relate it to the class in charge of all analysis upon a lifting surface; in particular, this class is named `LSAerodynamicsManager` and `CalcHighLiftDevices` is an inner class of it.

The first component of `CalcHighLiftDevices` that has to analyzed is the constructor; the latter, used whenever an object of this class has to be created, has three main purposes:

1. Assign user's inputs to their related class fields
2. Recognize flaps types from a `List` of `FlapTypeEnum` objects and link them to their typical maximum deflection value; moreover it gives them an appropriate index to be used inside `HighLiftDatabaseReader` in order to access to the specific flap type curve of the database when needed
3. Perform the preliminary calculation of the wing clean maximum lift coefficient, and of the related stalling angle of attack, using the method named `calcAlphaAndCLMax`, of the `LSAerodynamicsManager`, which accepts as input the wing mean airfoil calculated by the constructor using the method `calculateMeanAirfoil`, of a `LSAerodynamicsManager` inner class named `MeanAirfoil`, which performs the calculation of the required characteristics using influence areas method based on the three main wing airfoils (Root, Kink, Tip).

In particular `FlapTypeEnum` is an [Enumeration](#)[7] of possible flaps types created inside the `JPADConfigs` package to manage in a smart and intuitive way this parameter. Furthermore it has to be noted that having the clean maximum lift coefficient, and its stalling angle of attack, calculated in the constructor allows to reduce computational cost because these heavy calculations are performed only once when the object is created; this is very useful when the user wants to calculate the lift coefficient, at a specific angle of attack on the flapped lift curve, many time, for example, during iterations.

`CalcHighLiftDevices` class is also made up of three main methods each of which in charge of a specific task. The first one is `calculateHighLiftDevicesEffects` which implements all formulas explained in paragraph 4.1 using input data derived from the constructor, and shown in table 4.4. This method is defined `void` so that it returns nothing as output; in fact, the latter

theWing	A <code>LiftingSurface</code> object representing an aircraft wing
theConditons	An <code>OperatingConditions</code> object representing aircraft flight conditions
deltaFlap	A <code>List</code> of <code>Double</code> arrays containing each flap deflections
flapType	A <code>List</code> of <code>FlapTypeEnum</code> values for each flap
deltaSlat	A <code>List</code> of <code>Double</code> values containing each slat deflections; to be set to null if there aren't slats
etaInFlap	A <code>List</code> of <code>Double</code> values containing each flap inner adimensional position
etaOutFlap	A <code>List</code> of <code>Double</code> values containing each flap outer adimensional position
etaInSlat	A <code>List</code> of <code>Double</code> values containing each slat inner adimensional position, to be set to null if there aren't slats
etaInSlat	A <code>List</code> of <code>Double</code> values containing each slat outer adimensional position, to be set to null if there aren't slats
cfc	A <code>List</code> of <code>Double</code> values containing flap chord to airfoil chord ratios for each flap
csc	A <code>List</code> of <code>Double</code> values containing slat chord to airfoil chord ratios for each slat, to be set to null if there aren't slats
leRadiusRatioSlat	A <code>List</code> of <code>Double</code> values containing Leading Edge Radius (LER) to airfoil thickness ratios ($LER/t = LER/c \cdot t/c$) for each slat, to be set to null if there aren't slats
cExtcSlat	A <code>List</code> of <code>Double</code> arrays containing extended chord to airfoil chord ratios for each slat

Table 4.4 `CalcHighLiftDevices` constructor input

has only to provide the required calculations leaving to the user the output data retrieval using the appropriate *getter* methods of which the class is provided.

The second one is `calcCLatAlphaHighLiftDevice`, which requires firstly to perform the analysis of `calculateHighLiftDevicesEffects`; it calculates the lift coefficient at a given angle of attack for a wing with high-lift devices deflected. This method calculates both linear trait and non-linear trait of the curve using the NASA Blackwell method for the slope of the linear trait and a cubic interpolation for the non-linear one. In particular it sums up the effect of ΔC_{L0} to the clean wing C_{L0} in order to obtain the new value with deflected high-lift devices, then it replaces the clean wing $C_{L\alpha}$ with the new one calculated with the previous method; assuming also that the angle of attack at the end of the linear trait is taken as the mean of the old one, realted to the mean airfoil, and the one calculated at the same C_L^* but on the new curve, the new C_L^* can be evaluated completing the calculations of the linear trait parameters. From this point on, $\Delta C_{L\max}$ and $\Delta\alpha_{stall}$ are summed to the clean curve $C_{L\max}$ and α_{stall} calculated into the constructor; then a cubic interpolation, starting from the end of linear trait, allows to build the non-linear one. The method accept as input an angle of attack which is then compared with α^* calculated previously for the flapped curve; if this is lower the methods calculates the required lift coefficient using the linear trait, otherwise it uses the non-linear one.

The third, and last, method is `plotHighLiftCurve`. It is used to plot both the clean wing lift curve, both the flapped one; the first task is done by an `LSAerodynamicsManager` method named `PlotCLvsAlphaCurve`, while the second one follows the same philosophy of the previous method to calculate the lift coefficient for 30 angles of attack starting from -10° and ending at $(\alpha_{stall})_{flap} + 2^\circ$.

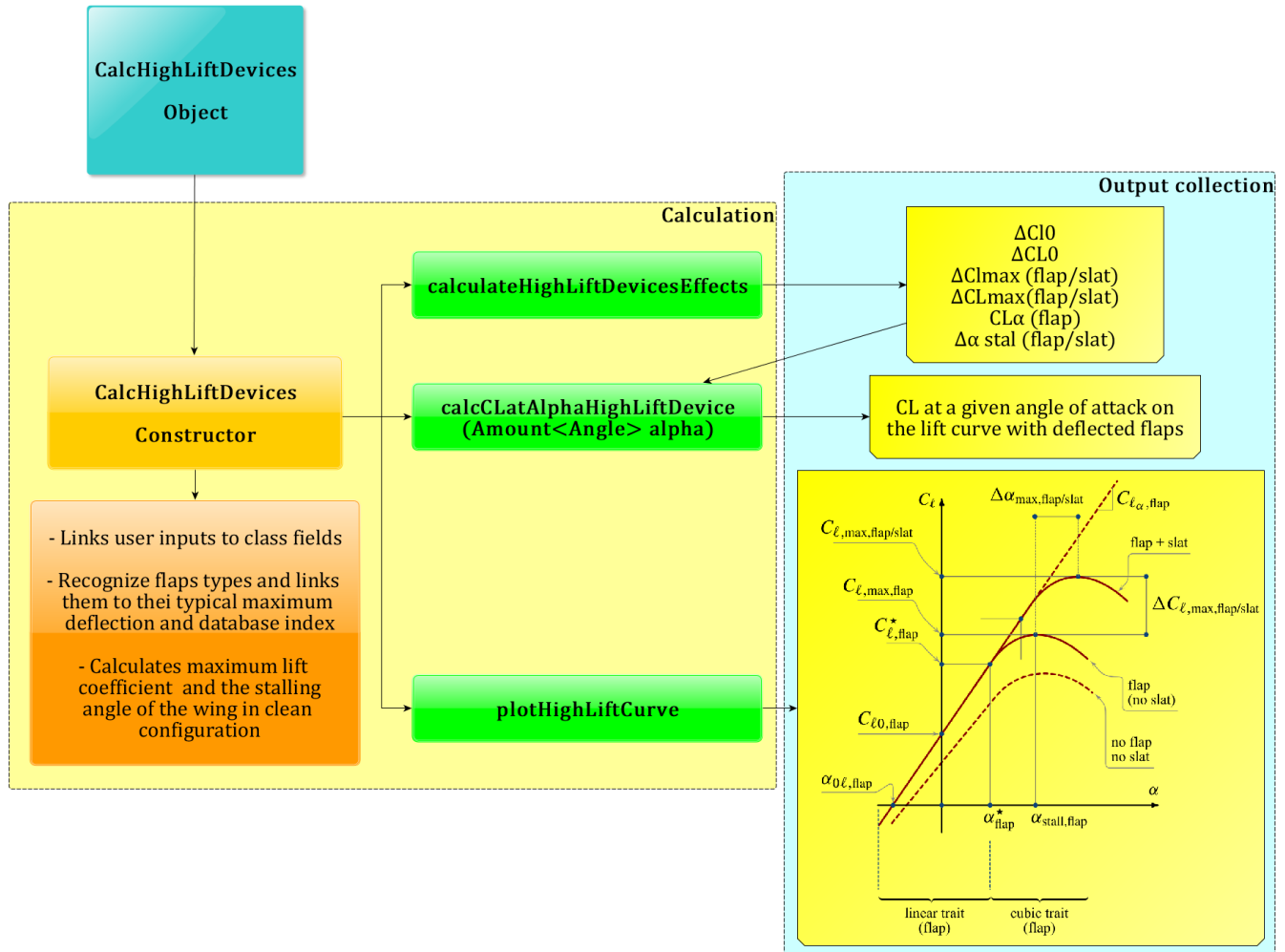


Figure 4.28 `CalcHighLiftDevices` class flowchart

4.3 Case study: ATR-72 and B747-100B

The last task to be done is to show an application of the `CalcHighLiftDevices` class in order to validate the calculation performed as well as to give a useful example to a potential user developer. As in previous chapters the test will be performed using ATR-72 and B747-100B aircraft models, built up as explained in paragraph 1.4. These aircraft models doesn't have high-lift devices input data embedded, so that they have to be assigned from an external .xml file; this choice has been taken because the user may want to try different high-lift devices setups without changing the aircraft model on which these latter will be applied. The input .xml file[5] has to provide all data from 4.4, except for the lifting surface model and the operating condition, and it is modeled as follows.

```

1 <input>
2     <B747>
3         <Flap_Number unit="">2</Flap_Number>
4         <Flap1>
5             <FlapType unit="">DOUBLE_SLOTTED</FlapType>
6             <Cf_C unit="">0.1264</Cf_C>
7             <Delta_Flap1 unit="deg">15</Delta_Flap1>
8             <Delta_Flap1 unit="deg">5</Delta_Flap1>
9             <Flap_inboard>0.0995</Flap_inboard>
10            <Flap_outboard>0.3614</Flap_outboard>
11        </Flap1>
12        <Flap2>
13            <FlapType unit="">DOUBLE_SLOTTED</FlapType>
14            <Cf_C unit="">0.2806</Cf_C>
15            <Delta_Flap2 unit="deg">15</Delta_Flap2>
16            <Delta_Flap2 unit="deg">5</Delta_Flap2>
17            <Flap_inboard unit="">0.4123</Flap_inboard>
18            <Flap_outboard unit="">0.6624</Flap_outboard>
19        </Flap2>
20        <Slat1>
21            <Delta_Slat unit="deg">15</Delta_Slat>
22            <Cs_C unit="">0.15</Cs_C>
23            <cExt_c unit="">1.1</cExt_c>
24            <LEradius_c_ratio unit="">0.0097</LEradius_c_ratio>
25            <Slat_inboard unit="">0.14</Slat_inboard>
26            <Slat_outboard unit="">0.37</Slat_outboard>
27        </Slat1>
28        <Slat2>
29            <Delta_Slat unit="deg">15</Delta_Slat>
30            <Cs_C unit="">0.193</Cs_C>
31            <cExt_c unit="">1.1</cExt_c>
32            <LEradius_c_ratio unit="">0.0097</LEradius_c_ratio>
33            <Slat_inboard unit="">0.42</Slat_inboard>
34            <Slat_outboard unit="">0.9</Slat_outboard>
35        </Slat2>
36    </B747>
37 </input>

```

Listing 4.1 Example of high-lift devices .xml input file for the B747-100B in take-off configuration

```

1 <input>
2     <ATR72>
3         <Flap_Number unit="">2</Flap_Number>
4         <Flap1>
5             <FlapType unit="">SINGLE_SLOTTED</FlapType>
6             <Cf_c unit="">0.35</Cf_c>
7             <Delta_Flap1 unit="deg">20</Delta_Flap1>
8             <Flap_inboard>0.0884</Flap_inboard>
9             <Flap_outboard>0.34575</Flap_outboard>
10            </Flap1>
11            <Flap2>
12                <FlapType unit="">SINGLE_SLOTTED</FlapType>

```

```

13          <Cf_c unit="">0.35</Cf_c>
14          <Delta_Flap2 unit="deg">20</Delta_Flap2>
15          <Flap_inboard>0.34575</Flap_inboard>
16          <Flap_outboard>0.82063</Flap_outboard>
17      </Flap2>
18  </ATR72>
19 </input>
```

Listing 4.2 Example of high-lift devices .xml input file for the ATR-72 in take-off configuration

The first thing to do in order to read these data is use the Java library `args4j`; the latter allows the user to make the **parsing** of the input file in order to make it available for reading inside the test class. For more information regarding this library the reader can consult [17]. After the input file has been parsed correctly, the reading process can start. The user now has to create a **List** for each input data of table 4.4 and then an object of the class `JPADXmlReader`, of the `JPADCore standaloneutils` package, in order to manage the scan of the .xml file through its methods.

```

1 // High Lift Devices Input
2 List<Double[]> deltaFlap = new ArrayList<Double[]>();
3 List<FlapTypeEnum> flapType = new ArrayList<FlapTypeEnum>();
4 List<Double> etaInFlap = new ArrayList<Double>();
5 List<Double> etaOutFlap = new ArrayList<Double>();
6 List<Double> cfc = new ArrayList<Double>();
7 List<Double> deltaSlat = new ArrayList<Double>();
8 List<Double> etaInSlat = new ArrayList<Double>();
9 List<Double> etaOutSlat = new ArrayList<Double>();
10 List<Double> csc = new ArrayList<Double>();
11 List<Double> cExtcSlat = new ArrayList<Double>();
12 List<Double> leRadiusSlatRatio = new ArrayList<Double>();
13
14 // XML reading phase:
15 // Arguments check
16 if (args.length == 0){
17     System.err.println("NO INPUT FILE GIVEN --> TERMINATING");
18     return;
19 }
20
21 // Input file parsing
22 main.theCmdLineParser.parseArgument(args);
23 // Creation of the reader object
24 String path = main.get_inputFile().getAbsolutePath();
25 JPADXmlReader reader = new JPADXmlReader(path);
26 // XML file scan through JPADXmlReader methods
27 List<String> flapNumberProperty = reader.getXMLPropertiesByPath("//Flap_Number");
28 int flapNumber = Integer.valueOf(flapNumberProperty.get(0));
29 List<String> flapTypeProperty = reader.getXMLPropertiesByPath("//FlapType");
30 List<String> cfcProperty = reader.getXMLPropertiesByPath("//Cf_C");
31 List<String> deltaFlap1Property = reader.getXMLPropertiesByPath("//Delta_Flap1");
32 List<String> deltaFlap2Property = reader.getXMLPropertiesByPath("//Delta_Flap2");
33 List<String> etaInFlaProperty = reader.getXMLPropertiesByPath("//Flap_inboard");
```

```

34 List<String> etaOutFlapProperty =
35         reader.getXMLPropertiesByPath("//Flap_outboard");
36 List<String> deltaSlatProperty = reader.getXMLPropertiesByPath("//Delta_Slat");
37 List<String> cscProperty = reader.getXMLPropertiesByPath("//Cs_C");
38 List<String> cExtcSlatProperty = reader.getXMLPropertiesByPath("//cExt_c");
39 List<String> leRadiusSlatRatioProperty =
40         reader.getXMLPropertiesByPath("//LEradius_c_ratio");
41 List<String> etaInSlatProperty = reader.getXMLPropertiesByPath("//Slat_inboard");
42 List<String> etaOutSlatProperty =
43         reader.getXMLPropertiesByPath("//Slat_outboard");
44 // Management of the Lists of String in order to populate the previous Lists
45 // Recognizing flap type
46 for(int i=0; i<flapTypeProperty.size(); i++) {
47     if(flapTypeProperty.get(i).equals("SINGLE_SLOTTED"))
48         flapType.add(FlapTypeEnum.SINGLE_SLOTTED);
49     else if(flapTypeProperty.get(i).equals("DOUBLE_SLOTTED"))
50         flapType.add(FlapTypeEnum.DOUBLE_SLOTTED);
51     else if(flapTypeProperty.get(i).equals("PLAIN"))
52         flapType.add(FlapTypeEnum.PLAIN);
53     else if(flapTypeProperty.get(i).equals("FOWLER"))
54         flapType.add(FlapTypeEnum.FOWLER);
55     else if(flapTypeProperty.get(i).equals("TRIPLE_SLOTTED"))
56         flapType.add(FlapTypeEnum.TRIPLE_SLOTTED);
57     else {
58         System.err.println("NO VALID FLAP TYPE!!!");
59         return;
60     }
61 }
62 Double[] deltaFlap1Array = new Double[delta_flap1_property.size()];
63 for(int i=0; i<deltaFlap1Array.length; i++)
64     deltaFlap1Array[i] = Double.valueOf(deltaFlap1Property.get(i));
65 Double[] deltaFlap2Array = new Double[deltaFlap2Property.size()];
66 for(int i=0; i<deltaFlap1Array.length; i++)
67     deltaFlap2Array[i] = Double.valueOf(deltaFlap2Property.get(i));
68 deltaFlap.add(deltaFlap1Array);
69 deltaFlap.add(deltaFlap2Array);
70 for(int i=0; i<cfcProperty.size(); i++)
71     cfc.add(Double.valueOf(cfcProperty.get(i)));
72 for(int i=0; i<etaInFlapProperty.size(); i++)
73     etaInFlap.add(Double.valueOf(etaInFlapProperty.get(i)));
74 for(int i=0; i<etaOutFlapProperty.size(); i++)
75     etaOutFlap.add(Double.valueOf(etaOutFlapProperty.get(i)));
76 for(int i=0; i<deltaSlatProperty.size(); i++)
77     deltaSlat.add(Double.valueOf(deltaSlatProperty.get(i)));
78 for(int i=0; i<cscProperty.size(); i++)
79     csc.add(Double.valueOf(cscProperty.get(i)));
80 for(int i=0; i<cExtcSlatProperty.size(); i++)
81     cExtcSlat.add(Double.valueOf(cExtcSlatProperty.get(i)));
82 for(int i=0; i<leRadiusSlatRatioProperty.size(); i++)
83     leRadiusSlatRatio.add(Double.valueOf(leRadiusSlatRatioProperty.get(i)));
84 for(int i=0; i<etaInSlatProperty.size(); i++)
85     etaInSlat.add(Double.valueOf(etaInSlatProperty.get(i)));
86 for(int i=0; i<etaOutSlatProperty.size(); i++)

```

```
87     etaOutSlat.add(Double.valueOf(etaOutSlatProperty.get(i)));
```

Listing 4.3 Excerpt of B747-100B test - Input data reading

It's important to highlight that `JPADXmlReader` methods can return an `Amount`[9] or a `String` for each data read this way so that a post-reading management is necessary in order to have data in correct types.

At this point all the required data are ready for use; now the user just have to create the object of the class `CalcHighLiftDevices` and call its methods as described in figure 4.28. It has to be noted that, since `CalcHighLiftDevices` is a class nested into `LSAerodynamicsManager`, the creation of the required object is a little bit different from the usual; in particular an object of `LSAerodynamicsManager`, named `theLSAnalysis` in the example below, has to be created first and then the `CalcHighLiftDevices` one can be created as follows.

```
1 LSAerodynamicsManager.CalcHighLiftDevices highLiftCalculator = theLSAnalysis
2     .new CalcHighLiftDevices(
3         aircraft.get_wing(),
4         theCondition,
5         deltaFlap,
6         flapType,
7         deltaSlat,
8         eta_in_flap,
9         eta_out_flap,
10        eta_in_slat,
11        eta_out_slat,
12        cf_c,
13        cs_c,
14        leRadius_c_slat,
15        cExt_c_slat
16    );
```

Listing 4.4 Excerpt of B747-100B test - calculator object creation

In conclusion, the following pages show the numerical and graphical results of the described tests, applied to the two aircraft, mentioned at the beginning of paragraph, in take-off configuration.

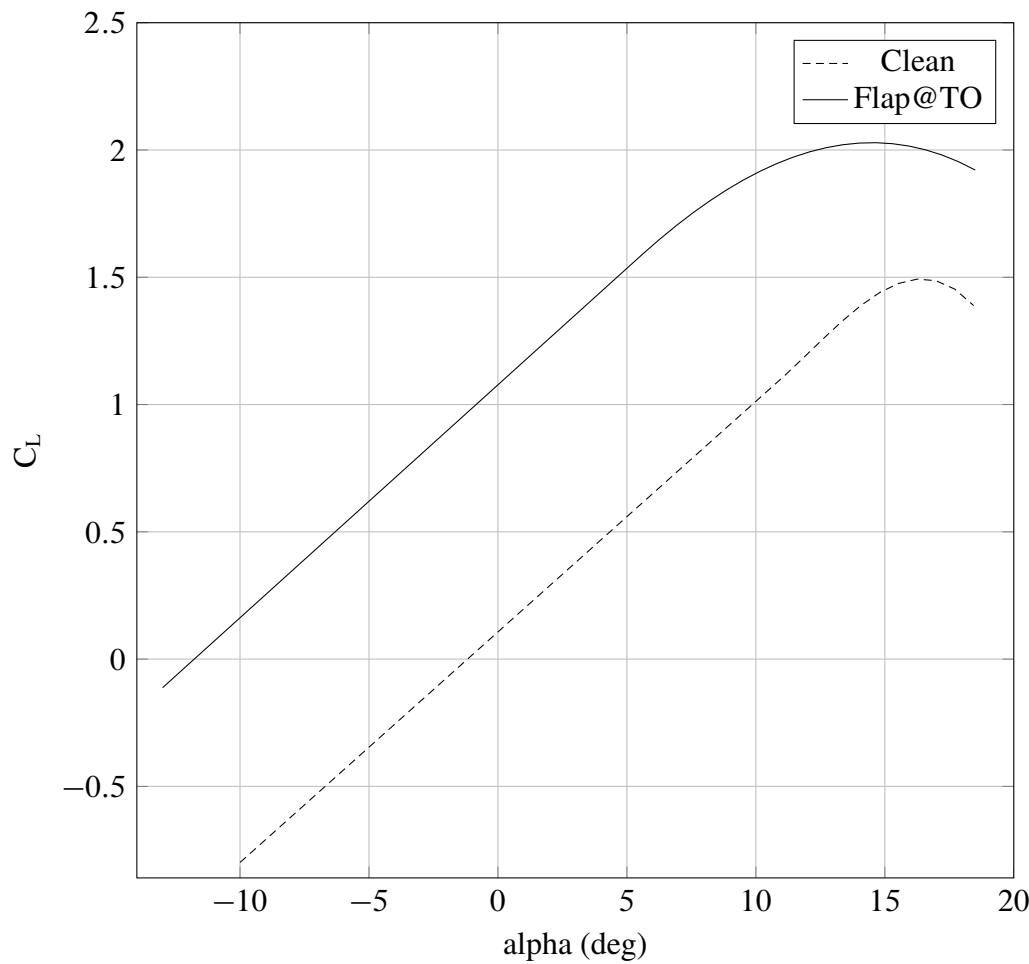


Figure 4.29 ATR-72 lift curve with and without flaps in take-off configuration

```

1 deltaCl0_flap = 2.3939974237661317
2 deltaCL0_flap = 0.9707980864918362
3 deltaClmax_flap = 1.2122379635109801
4 deltaCLmax_flap = 0.5352640320770878
5 cLalpha_new = 0.09150912423296985 (1/deg)
6 deltaAlphaMax = -1.9369466185196893 (deg)
7 deltaCD = 0.01518722606307197
8 deltaCMc_4 = -0.12338582743821447
9
10 -----CLEAN-----
11 alpha max 16.44529532754857 (deg)
12 alpha star 10.918671750781748 (deg)
13 cL max 1.4934954072726092
14 cL star 1.0956477082461238
15 cL alpha 5.189644003702159 (1/rad)
16 -----HIGH LIFT-----
17 alpha max 14.50713741489647 (deg)
18 alpha star 5.55824828132392 (deg)
19 cl max 2.028759439349697
20 cl star 1.5861753654540678
21 cl alpha 5.243472818549172 (1/rad)

```

Listing 4.5 ATR-72 test results

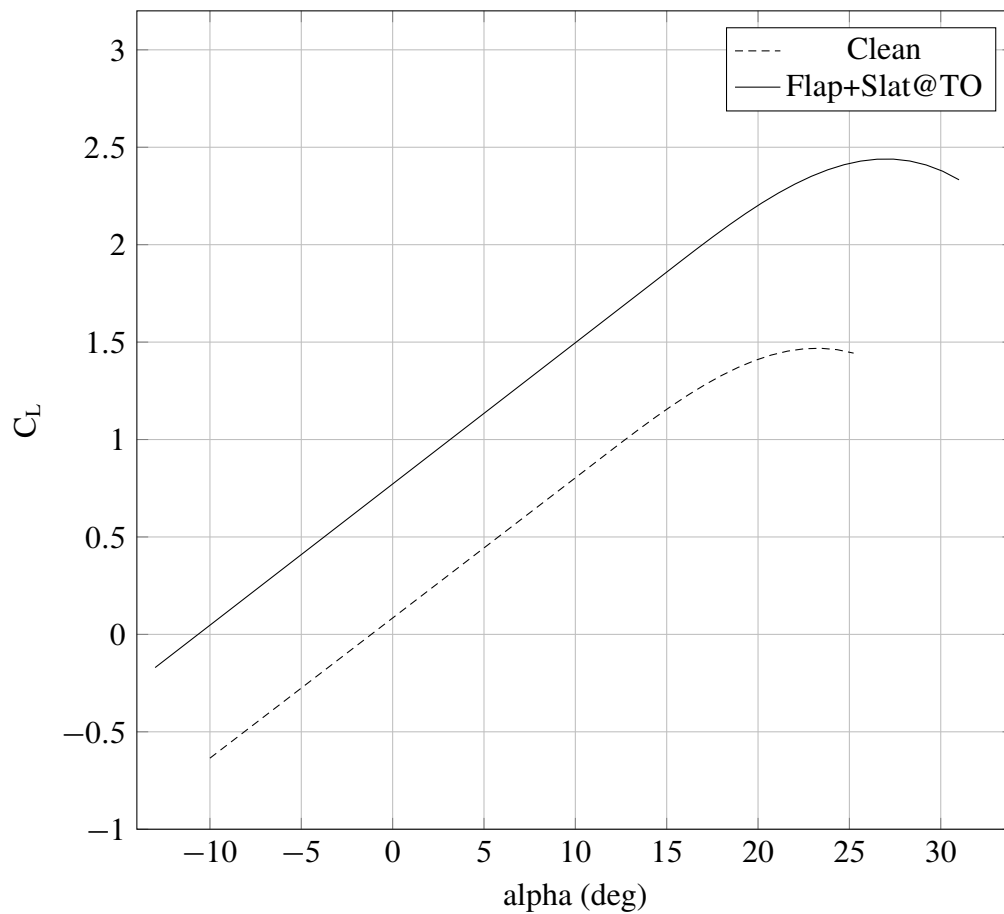


Figure 4.30 B747-100B lift curve with and without flaps in take-off configuration

```

1 deltaCl0_flap = 2.275544332733731
2 deltaCL0_flap = 0.687810914469225
3 deltaClmax_flap = 0.6867057564174156
4 deltaCLmax_flap = 0.24074371285515445
5 deltaClmax_slat = 1.3986165535139938
6 deltaCLmax_slat = 0.7307256446849437
7 cLalpha_new = 0.07247171535879046 (1/deg)
8 deltaAlphaMaxFlap = -1.9369466185196893 (deg)
9 deltaCD = 0.006456897617521261
10
11 -----CLEAN-----
12 alpha max 23.232964070877248 (deg)
13 alpha star 10.32038751072542 (deg)
14 cL max 1.4686492856382116
15 cL star 0.8263686942120971
16 cL alpha 4.121408852511741 (1/rad)
17 -----HIGH LIFT-----
18 alpha max 27.00200178515614 (deg)
19 alpha star 14.091414230062869 (deg)
20 cl max 2.4401186431783097
21 cl star 1.7930955427485755
22 cl alpha 4.152629290058694 (1/rad)

```

Listing 4.6 B747-100B test results

Chapter 5

TAKE-OFF PERFORMANCE

Although the take-off field length may seem like a performance characteristic of secondary importance, it is very often one of the critical design constraints. If the required runway length is too long, the aircraft cannot take-off with full fuel or full payload and its economics are compromised. So take-off performance play a significant role in the preliminary design of an aircraft because they are both design requirements, specified by the FAR and by the customer, to be fulfilled, both driving parameters in the definition of the design point.

5.1 Theoretical background

The take-off may be considered as made up of two parts: a ground run and an air run, as shown schematically in figure 5.1. The simplest description of the take-off process is that the engine thrust is increased to the take-off level at $x = 0$ and the brakes are released to begin acceleration down the runway. At some point, the pilot commands rotation of the aircraft which lifts the nose wheel from the ground and allows to achieve the take-off angle of attack;

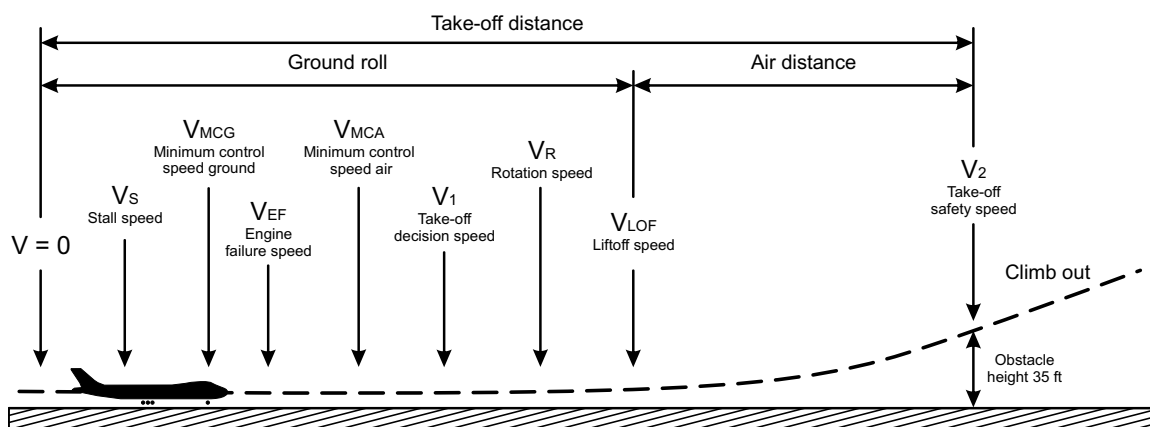


Figure 5.1 Scheme of an aircraft take-off run

in this way the aircraft lift can grows faster and, when it is equal to the aircraft maximum take-off weight, the aircraft can lifts completely from the ground and begins climbing. The point at which it reaches an altitude of 35 ft (10.7 m), is considered, for an aircraft which refers to the FAR-25, the end of the take-off run. This is the usual situation for take-off; subsequently, the modifications to safely deal with a take-off emergency, such as an engine failure, will be discussed.

5.1.1 AOE take-off run

In order to deal with the calculation of the take-off run distance, a smart strategy is to find out all the foundamentals variables, which describes completely the aircraft state in this phase, and so, to study the dynamic system in exam in a state-space representation. To find out these state variables it is necessary to analyze aircraft equations of motion during take-off phases, these latter described as follows.

- **Ground roll phase:** starting from standstill with brakes released and at maximum power output, the aircraft accelerates on the runway, with constant angle of attack, until it reaches a speed equals to the rotation speed V_{Rot} ; after that the following subphase begin.
 - **Rotation phase:** a short phase in which the pilot gives an assigned pitching law to lift the aircraft nose and, as a result, increasing the angle of attack. This phase ends when the load factor is equal to 1, meaning that the lift has reached the value of the maximum take-off weight, and the relative lift-off speed is indicated with V_{LO} .
- **Airborne phase:** is the phases in which the aircraft, once it has lifted from the ground, gains altitude until it reaches the obstacle height of 35 ft (10.7 m) imposed by the FAR-25. This phase begin at V_{LO} and ends at the speed related to the obstacle overcoming, indicated with V_2 ; furthermore it can be divided into the followngs two subphases:
 - **Transition phase:** in which the aircraft rotates in order to increase the climb angle (γ) with the result of increasing the angle of attack and the relative lift coefficient, which should not surpass a safety value of the 90% of the maximumlift coefficient in take-off configuration. This sub-phase ends when the desidered climb speed is reached.
 - **Climb-out to the obstacle phase:** in which the aircraft climbs at constant climb angle until the obstacle is surpassed.

For more information regarding take-off equations of motion during each of the previously described phases, the reader can refer to [20].

The set of Ordinary Differential Equations (ODE) that models the take-off run is written in the following form:

$$\begin{Bmatrix} \dot{s} \\ \dot{V} \\ \dot{\gamma} \\ \dot{h} \end{Bmatrix} = \begin{Bmatrix} f_1(s, V, \gamma, h; \alpha) \\ f_2(s, V, \gamma, h; \alpha) \\ f_3(s, V, \gamma, h; \alpha) \\ f_4(s, V, \gamma, h; \alpha) \end{Bmatrix} \quad \text{with} \quad \begin{Bmatrix} x_1 = s \\ x_2 = V \\ x_3 = \gamma \\ x_4 = h \end{Bmatrix} \quad \text{and} \quad u = \alpha \quad (5.1)$$

These equations can be also written in a more concise way as shown below.

$$\dot{x} = f(x; u) \quad (5.2)$$

The unknown $x = [x_1, x_2, x_3, x_4]^T$ is the vector of state variables. The input $u(t)$ is a given function of time, for $0 \leq t \leq t_{\text{final}}$, that corresponds to an assumed time history of the angle of attack during take-off. The right-hand sides of system (5.1) are defined by the following functions:

$$f_1(x, u) = x_2 \quad (5.3a)$$

$$f_2(x, u) = \frac{g}{W} \begin{cases} T(x_2) - D(x_2, u) - \mu[W - L(x_2, u)] & \text{if } \delta(x_2, u) < 1 \\ T(x_2) \cos u - D(x_2, u) - W \sin x_3 & \text{if } \delta(x_2, u) \geq 1 \end{cases} \quad (5.3b)$$

$$f_3(x, u) = \frac{g}{W x_2} \begin{cases} 0 & \text{if } \delta(x_2, u) < 1 \\ L(x_2, u) + T(x_2) \sin u - W \cos x_3 & \text{if } \delta(x_2, u) \geq 1 \end{cases} \quad (5.3c)$$

$$f_4(x, u) = x_2 \sin x_3 \quad (5.3d)$$

The thrust $T(x_2)$ is calculated by means of the interpolating function $T_{\text{tab}}(V_a)$ based on a table lookup algorithm, where $V_a = V + V_w$ is the airspeed and V_w is the wind speed (horizontal component, positive if opposite to the aircraft motion). The drag D and lift L , as functions of airspeed V_a and angle of attack, are given by the following conventional formulas.

$$D(x_2, u) = \frac{1}{2} \rho (x_2 + V_w \cos x_3)^2 S C_D(u) \quad (5.3e)$$

$$L(x_2, u) = \frac{1}{2} \rho (x_2 + V_w \cos x_3)^2 S C_L(u) \quad (5.3f)$$

The switching function δ of aircraft velocity and angle of attack is defined as follows:

$$\delta(x_2, u) = \frac{L(x_2, u)}{W \cos x_3} \quad (5.3g)$$

The formulas (5.3) make the system (5.2) a closed set of ODEs. When the function $u(t)$ is assigned and the system is associated to a set of initial conditions, in this particular case equal to $x_0 = [0, 0, 0, 0]^T$, a well-posed **Initial Value Problem (IVP)** is formed, which can be solved numerically. In table 5.1 are reported the take-off characteristic speeds and their corresponding requirements as defined by FAR 25.

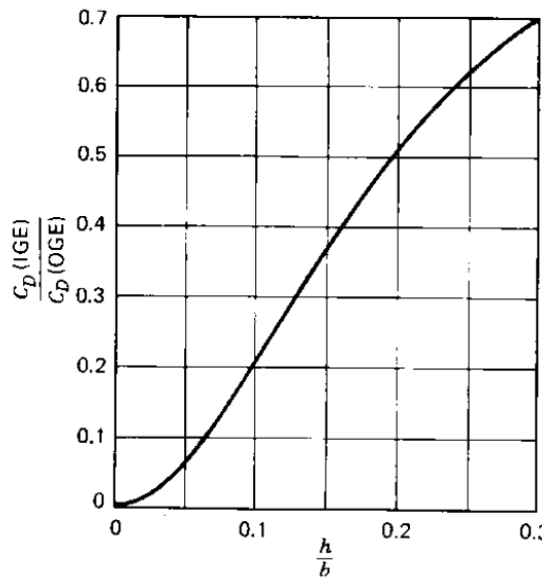
Speed	Description	Requirement
V_S	aircraft stalling speed in take-off configuration	—
V_{MC}	minimum control speed with one engine inoperative (OEI)	—
V_1	OEI decision speed	$\geq V_{mc}$
V_{Rot}	rotation speed	$> 1.05 V_{MC}$
V_{MU}	minimum unstick speed for safe flight	$\geq V_S$
V_{LO}	lift-off speed	$> 1.10 V_{MU}$ $> 1.05 V_{MU}$ (OEI)
V_2	take-off climb speed at 35 ft	$> 1.20 V_S$ $> 1.10 V_{MC}$

Table 5.1 Take-off speeds and FAR 25 requirements

It has to be highlighted that the drag coefficient C_D that appears in (5.3f) can be modelled as:

$$C_D = C_{D0} + (\Delta C_{D0})_{flap+lg} + K_g \frac{C_L^2}{\pi A Re} \quad (5.4)$$

with $(\Delta C_{D0})_{flap+lg}$ due to flap, as shown in subparagraph 4.1.5, and landing gears, which contribution is usually about $0.010 \div 0.015$; moreover C_L is the one from the lift curve with flaps, and eventually slats, deflected. The term K_g in (5.4) incorporates the ground effect and it is calculated from [20] using the (5.5) which is a fifth order interpolating function of the graph in figure 5.2, where the ratio h_W/b is obtained dividing the height of wing above the ground by the wing span, usually between 0.1 and 0.2 when the aircraft is on the ground and assumed as $h_W \approx h$ during the airborne.

**Figure 5.2** Ground effect parameter K_g as function of the h_W/b ratio

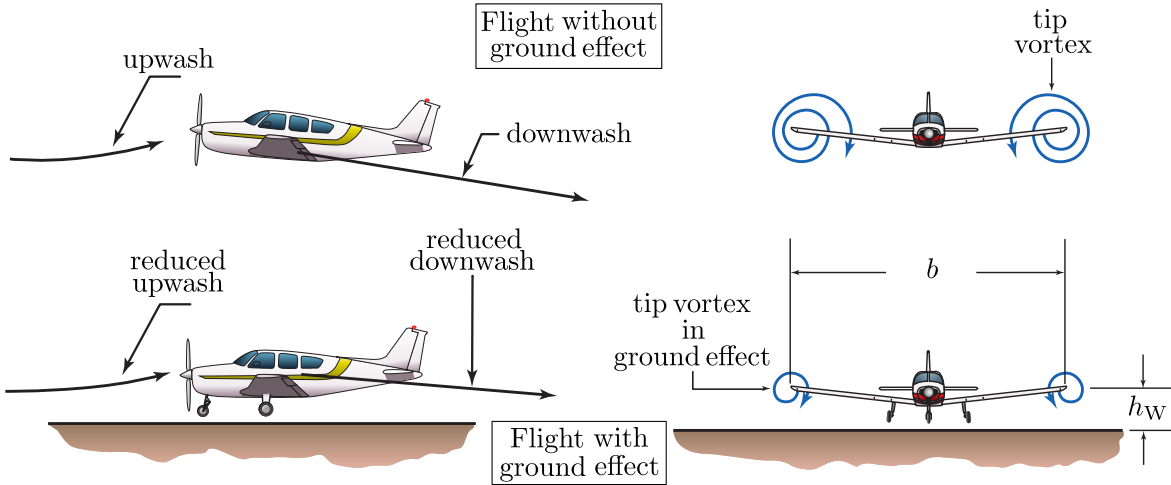


Figure 5.3 Comparison between flight with and without ground effect

$$K_g = -622.44x^5 + 624.46x^4 - 255.24x^3 + 47.105x^2 - 0.6378x + 0.0055 \quad (5.5)$$

This polynomial equation has a coefficient of determination R^2 of 0.9999 which justifies the approximation.

In order to better understand the nature of the ground effect it is convenient to refer to [21], where the ground effect is explained as follows. As the aircraft flies close to the ground, the ground interferes with the horseshoe vortex system trailing behind the wing. Ground effect is often analyzed by putting an image horseshoe vortex system of equal but opposite strength at the same distance h_W below the ground. This image vortex system induces velocities at the wing aerodynamic center, which decreases the strength of the downwash at that point, thereby decreasing the induced angle of attack, α_i . Thus, the wing C_L is increased (or more correctly, the lift curve slope increases, giving an increase in C_L for the same geometric angle of attack, α) and the induced drag is decreased. This influence of the ground effect is a function of how close the aircraft is to the ground and of the size of the wing.

Speaking of the C_D , it has also to be noted that, at high C_L , the parabolic drag polar it's no longer accurate in describing the drag characteristics of the aircraft so that two correction factors have to be added to the (5.4). These latter triggers only when the C_L is higher than 1.2 as can be seen from the following equation in which $K_1 = 0.079$ and $K_2 = 0.365$.

$$C_D = C_{D0} + (\Delta C_{D0})_{flap+lg} + K_g \frac{C_L^2}{\pi A Re} + K_1 (C_L - 1.2) + K_2 (C_L - 1.2)^2 \quad (5.6)$$

Focusing, now, on the input law of the angle of attack, the function u can be constructed by picking the time t_{Rot} when the rotation speed V_{Rot} is reached along the ground roll; thus the $u(t)$ function can be defined as follows.

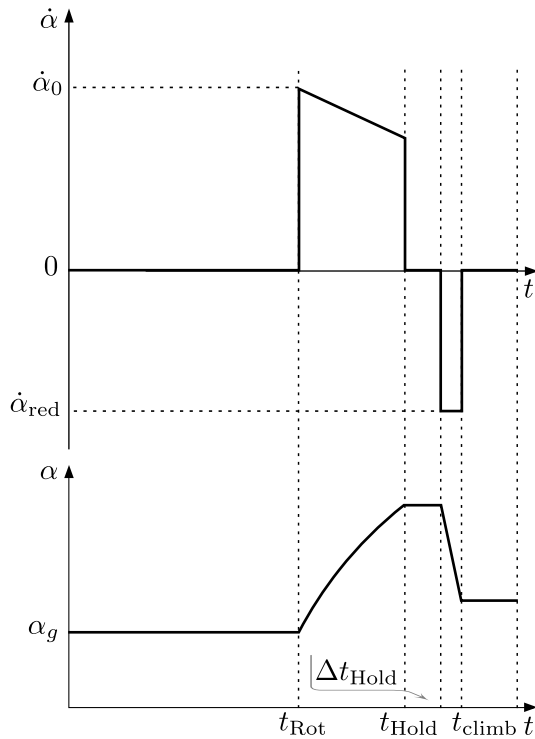


Figure 5.4 Qualitative representation of the angle of attack input law

$$u(t) = \begin{cases} \alpha_g & \text{if } t < t_{\text{Rot}} \\ \alpha_1(t) & \text{if } t \geq t_{\text{Rot}} \end{cases} \quad (5.7)$$

with a constant α_g during the ground run up to the rotation speed, and a given non-zero law $\alpha_1(t)$ for the post-rotation angle of attack time history. Figure 5.4 shows a qualitative representation of the $\alpha_1(t)$ law. As can be seen, after t_{Rot} the pilot applies an initial angular velocity $\dot{\alpha}_0$, which decreases with time, according to the law written in (5.8) as function of α , until the time t_{Hold} has been reached; this particular instant is related to the achievement of the maximum admitted lift coefficient in take-off, which is set at 90% of the $C_{L_{\max,TO}}$.

$$\dot{\alpha} = \dot{\alpha}_0 (1 - k_\alpha \alpha) \quad (5.8)$$

In equation (5.8), the k_α slope is assigned (a good value could be 0.07 ($1/\text{°}$)), while the initial angular velocity $\dot{\alpha}_0$ is calculated as follows.

$$\dot{\alpha}_0 = \frac{\Delta\alpha}{\Delta t_{\text{Rot}}} = \frac{\alpha_{\text{LO}} - \alpha_g}{\Delta t_{\text{Rot}}} \quad (5.9)$$

where α_{LO} can be obtained from the lift curve of the wing, with flaps deflected in take-off configuration, by assigning the $C_{L_{\text{LO}}}$; this can be derived from the $C_{L_{\max,TO}}$ dividing it by the parameter K_{LO}^2 , which represents the quantity that has to be multiplied by V_S in order to obtain V_{LO} (for example 1.1 with reference to table 5.1).

From this point on the pilot stops the pitching manouver and keeps the angle of attack constant for an assigned Δt_{Hold} . During this time interval, the lift coefficient is high and, as a result, also the induced drag is high so that aircraft acceleration will reduce. After this short time

interval the pilot has to reduce the angle of attack in order to avoid the acceleration to decrease too much and so an assigned negative angular velocity $\dot{\alpha}_{\text{red}}$ is applied; the latter assumed to be constant for simplicity. Finally, since the decrease of α determines also a reduction in C_L , the time t_{climb} will be reached when the load factor is reduced to 1; this means that a balance of the forces, perpendicular to the flight path, has been achieved and so the climb phase, at constant γ , can begin, leaving α constant and equal to last value reached.

5.1.2 OEI take-off run and balanced field length

A good description of the take-off with one engine failure is proposed in [27]. Here it is explained that in the event of an engine failure during the take-off roll the pilot must decide whether to continue the take-off or, instead, abort the take-off and decelerate to a stop on the runway. Obviously, if the engine failure occurs when the aircraft is traveling very slowly, the aircraft should be kept on the ground and brought to a stop at some safe location off the runway. Conversely, if the engine failure occurs when the aircraft is close to the take-off speed the take-off should be continued. The designer must provide a means for deciding whether it is safer to abort the take-off or continue it. The critical velocity, denoted as V_{act} , is the velocity at which action is taken, not that at which the decision to act is taken. The time between the recognition of an engine failure, which occurs at V_{ef} , and the critical velocity V_{act} , when action is taken is required to be more than one second. Generally this time period, which is set by the reaction time of the pilot, is taken to be about 3 s. If the pilot's decision is to continue the take-off with one engine inoperative, the distance to the lift-off speed V_{LO} and to the subsequent climb-out to 35 ft height above the runway, will obviously be longer than with all engines operating.

The calculation of the take-off distance in this situation is quite the same as the one explained previously, with the difference that now there is a discontinuity in thrust due to the broken engine. In particular, the thrust, $T(x_2)$, will still be read from the database but considering a number of engines reduced by one from the time t_{ef} at which the engine failure occurs.

On the other hand, in the case of the aborted take-off the pilot will apply the necessary braking procedures in order to get the maximum permissible deceleration while maintaining adequate control of the airplane's motion. The portion of the aborted take-off run up to the engine failure velocity V_{ef} is calculated in the same way as that for the continued take-off, so that the distance is the same in both cases. From this point on, until the pilot reacts by activating brakes, there is only a discontinuity in thrust due to the failed engine; while, after the time interval in which the pilot decides to abort the take-off, the thrust is set to minimum (ideally zero) and the brakes action provides an higher friction coefficient. During this last phase, the equation (5.3b) changes in the following.

$$f_2(x, u) = \frac{g}{W} \left\{ -D(x_2, u) - \mu_{\text{brakes}} [W - L(x_2, u)] \right\} \quad (5.10)$$

where μ_{brakes} is bigger than μ and it is usually about 0.3. Furthermore, it has to be noted that, even if the aircraft in exam is supplied with a reverse thrust device, this effect has not to be taken into account for a more conservative result.

Instead of considering the limiting cases of aborting take-off at low V_{act} and continued take-off at high V_{act} , it is useful determine the critical velocity for which the distance required to continue the take-off is equal to the distance required to safely abort it. This velocity is the one from table 5.1 and it's called *decision speed* V_1 , while the related distance is called the *balanced field length*. The latter, in particular, plays an important role in the sizing of the runway since is the maximal distance the aircraft can cover both in continued take-off, both in aborted take-off. In order to calculate this distance, and the related velocity, it's possible to evaluate, at different V_{act} , both the continued take-off distance with one inoperative engine, both the aborted take-off distance. Each couple of speed and distance can then be plotted with the result of building the curves of figure 5.5. The intersection of these latter, at which the two distances are the same, defines the *balanced field length* and the V_1 .

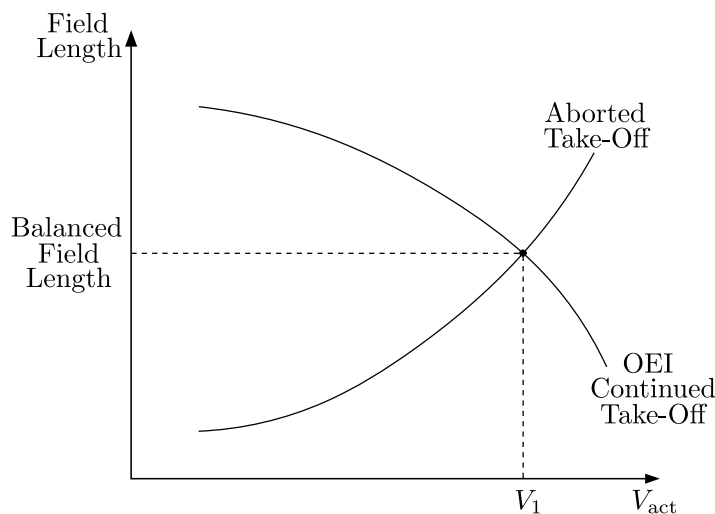


Figure 5.5 Qualitative representation of the field distances required to continue a takeoff or to abort it when one engine fails as a function of critical velocity.

As expected, the take-off distance on the curve related to the continued take-off with one inoperative engine decreases with the failure speed, tending to the AOE condition; while the take-off distance on the other curve grows with the failure speed because the deceleration to stop the aircraft begins from an higher speed, requiring more distance to be dissipated.

5.2 Java class architecture

5.3 Case study: ATR-72

Appendices

Appendix

A

HDF DATABASE CREATION AND READING

A.1 Creation of a database using MATLAB

Creation and mangment of an HDF Dataset are very important to handle because they allow to generate resources which are required by a lot of analysis; for example by using this datasets it's possible to implement a new engine type allowing the analysis of the preformance of a new aircraft. This feature has not been implemented inside JPAD with the purpose of being able to generate the required resources independently. For more information regarding the **HDF**, the reader can refer to [11].

First of all it's necessary to have curves of the database that has to be digitized; then, with the use of sotware like *PlotDigitizer*, it's possible to acquire them using a finite number of points chosen by the user. The output of this procedure is a .csv file containing all the copule of points which have been used to digitize the specific curve. Now the matlab code comes in play to manage these data and to generate the digitized curves and the HDF dataset. In the example reported there are four curves defined by points through *PlotDigitizer* which have, firstly, been imported in MATLAB generating four .mat files; at this point the code interpolates curves points with cubic splines in order to have more points to plot for each curve. Finally curves are plotted and the HDF Dataset is populated by using *h5create* and *h5write*; in particular curves points, abscissas and parameterization values are attached to the h5 file through these commands.

Listing A.1 MATLAB script for creating the HDF Database

```
1 clc; close all; clear all;
2
3 %% Import data
4 DeltaAlphaCLmax_vs_LambdaLE_dy1p2 =
    importdata('DeltaAlphaCLmax_vs_LambdaLE_dy1p2.mat');
5 DeltaAlphaCLmax_vs_LambdaLE_dy2p0 =
    importdata('DeltaAlphaCLmax_vs_LambdaLE_dy2p0.mat');
```

```

6 DeltaAlphaCLmax_vs_LambdaLE_dy3p0 =
    importdata('DeltaAlphaCLmax_vs_LambdaLE_dy3p0.mat');
7 DeltaAlphaCLmax_vs_LambdaLE_dy4p0 =
    importdata('DeltaAlphaCLmax_vs_LambdaLE_dy4p0.mat');
8
9 nPoints = 30;
10 lambdaLEVector_deg = transpose(linspace(0, 40, nPoints));
11
12 %% dy/c = 1.2
13 smoothingParameter = 0.999999;
14 DAlphaVsLambdaLESplineStatic_Dy1p2 = csaps( ...
15     DeltaAlphaCLmax_vs_LambdaLE_dy1p2(:,1), ...
16     DeltaAlphaCLmax_vs_LambdaLE_dy1p2(:,2), ...
17     smoothingParameter);
18 DAlphaVsLambdaLEStatic_Dy1p2 = ppval( ...
19     DAlphaVsLambdaLESplineStatic_Dy1p2, ...
20     lambdaLEVector_deg);
21 %% dy/c = 2.0
22 smoothingParameter = 0.999999;
23 DAlphaVsLambdaLESplineStatic_Dy2p0 = csaps( ...
24     DeltaAlphaCLmax_vs_LambdaLE_dy2p0(:,1), ...
25     DeltaAlphaCLmax_vs_LambdaLE_dy2p0(:,2), ...
26     smoothingParameter);
27 DAlphaVsLambdaLEStatic_Dy2p0 = ppval( ...
28     DAlphaVsLambdaLESplineStatic_Dy2p0, ...
29     lambdaLEVector_deg);
30 %% dy/c = 3.0
31 smoothingParameter = 0.999999;
32 DAlphaVsLambdaLESplineStatic_Dy3p0 = csaps( ...
33     DeltaAlphaCLmax_vs_LambdaLE_dy3p0(:,1), ...
34     DeltaAlphaCLmax_vs_LambdaLE_dy3p0(:,2), ...
35     smoothingParameter);
36 DAlphaVsLambdaLEStatic_Dy3p0 = ppval( ...
37     DAlphaVsLambdaLESplineStatic_Dy3p0, ...
38     lambdaLEVector_deg);
39 %% dy/c = 4.0
40 smoothingParameter = 0.999999;
41 DAlphaVsLambdaLESplineStatic_Dy4p0 = csaps( ...
42     DeltaAlphaCLmax_vs_LambdaLE_dy4p0(:,1), ...
43     DeltaAlphaCLmax_vs_LambdaLE_dy4p0(:,2), ...
44     smoothingParameter);
45 DAlphaVsLambdaLEStatic_Dy4p0 = ppval( ...
46     DAlphaVsLambdaLESplineStatic_Dy4p0, ...
47     lambdaLEVector_deg);
48
49 %% Plots
50 figure(1)
51 plot(lambdaLEVector_deg, DAlphaVsLambdaLEStatic_Dy1p2, '-*b' ... , ...);
52 hold on;
53 plot(lambdaLEVector_deg, DAlphaVsLambdaLEStatic_Dy2p0, '-b' ... , ...);
54 plot(lambdaLEVector_deg, DAlphaVsLambdaLEStatic_Dy3p0, '*b' ... , ...);
55 plot(lambdaLEVector_deg, DAlphaVsLambdaLEStatic_Dy4p0, 'b' ... , ...);
56 xlabel('\Lambda_{le} (deg)'); ylabel('\Delta\alpha_{C_{L,max}}');
```

```

57 title('Angle of attack increment for wing maximum lift in subsonic flight');
58 legend('\Delta y/c = 1.2', '\Delta y/c = 2.0', '\Delta y/c = 3.0', '\Delta y/c =
      4.0');
59 axis([0 50 0 9]);
60 grid on;
61
62 %% preparing output to HDF
63 % dy/c
64 dyVector = [1.2;2.0;3.0;4.0];
65 %columns --> curves
66 myData = [ ...
67     DALphaVsLambdaLEStatic_Dy1p2, ...
68     DALphaVsLambdaLEStatic_Dy2p0, ...
69     DALphaVsLambdaLEStatic_Dy3p0, ...
70     DALphaVsLambdaLEStatic_Dy4p0];
71
72 hdfFileName = 'DALphaVsLambdaLEVsDy.h5';
73 if ( exist(hdfFileName, 'file') )
74     fprintf('file %s exists, deleting and creating a new one\n', hdfFileName);
75     delete(hdfFileName)
76 else
77     fprintf('Creating new file %s\n', hdfFileName);
78 end
79 % Dataset: data
80 h5create(hdfFileName, '/DALphaVsLambdaLEVsDy/data', size(myData));
81 h5write(hdfFileName, '/DALphaVsLambdaLEVsDy/data', myData);
82 % Dataset: var_0
83 h5create(hdfFileName, '/DALphaVsLambdaLEVsDy/var_0', size(dyVector));
84 h5write(hdfFileName, '/DALphaVsLambdaLEVsDy/var_0', dyVector);
85 % Dataset: var_1
86 h5create(hdfFileName, '/DALphaVsLambdaLEVsDy/var_1', size(lambdaLEVector_deg));
87 h5write(hdfFileName, '/DALphaVsLambdaLEVsDy/var_1', lambdaLEVector_deg);

```

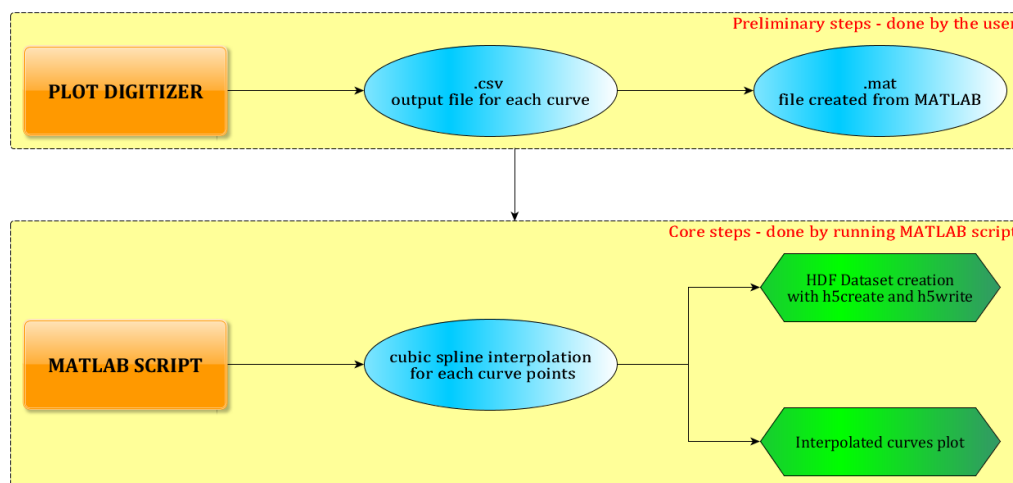


Figure A.1 Flowchart of an HDF Database creation

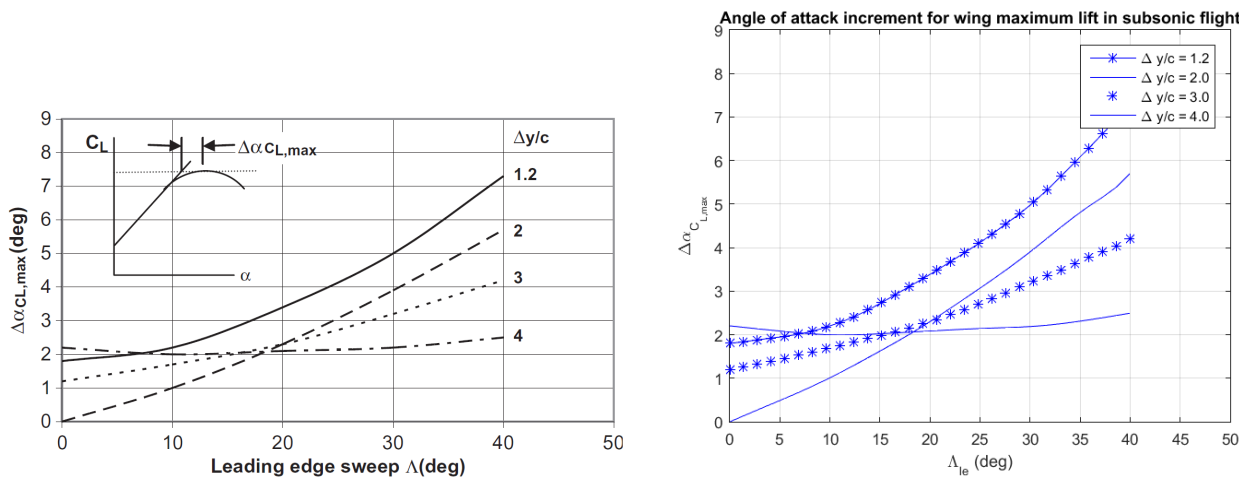


Figure A.2 Comparison between the initial graph and the digitized one

A.2 Reading data from an HDF database in JPAD

After creating the database, this has to be read in order to obtain the required data; inside JPAD this operation can be done defining a specific class, which extends the abstract class `DatabaseReader` that is designed for HDF dataset reading. This son class has a specific structure which main key points can be summarized in the following ones:

1. Creation of variables, in number equal to the function to be interpolated, using the type `MyInterpolatingFunction`
2. Creation of variables for all values that are wanted to be read from the interpolating functions
3. Creation of a constructor that accepts the folder path string and the file name string of the database. This constructor has to launch the interpolating method for all functions contained into the database by using `MyInterpolatingFunction` methods.
4. Creation of a getter method for each of the variables allocated at point 2 in order to obtain values from interpolated functions by giving in input the required parameters

In particular the class `MyInterpolatingFunction` implements methods for a spline, bicubic and tricubic data interpolation as well as three methods for extracting a specific value from each of the previous interpolated curve.

The following listing describes, with an example upon the aerodynamic database, how the reader class should be built up following the previous steps.

Listing A.2 DatabaseReader son class creation

```

1 public class AerodynamicDatabaseReader extends DatabaseReader {
2 // STEP 1:
3     private MyInterpolatingFunction
4         c_m0_b_k2_minus_k1_vs_FFR,
5         ar_v_eff_c2_vs_Z_h_over_b_v_x_ac_h_v_over_c_bar_v;
6 // STEP 2:

```

```

7   double cM0_b_k2_minus_k1, ar_v_eff_c2;
8 // STEP 3:
9   public AerodynamicDatabaseReader(String databaseFolderPath, String
10    databaseFileName) {
11     super(databaseFolderPath, databaseFileName);
12     c_m0_b_k2_minus_k1_vs_FFR =
13       database.interpolate1DFromDatasetFunction(
14         "(C_m0_b)_k2_minus_k1_vs_FFR"
15       );
16     ar_v_eff_c2_vs_Z_h_over_b_v_x_ac_h_v_over_c_bar_v =
17       database.interpolate2DFromDatasetFunction(
18         "(AR_v_eff)_c2_vs_Z_h_over_b_v_(x_ac_h--v_over_c_bar_v)"
19       );
20   }
21 // STEP 4:
22   public double get_C_m0_b_k2_minus_k1_vs_FFR(double length, double diameter) {
23     return c_m0_b_k2_minus_k1_vs_FFR.value(length/diameter);
24   }
25 // STEP 4:
26   public double get_AR_v_eff_c2_vs_Z_h_over_b_v_x_ac_h_v_over_c_bar_v(double zH,
27     double bV, double xACHV, double cV) {
28     return ar_v_eff_c2_vs_Z_h_over_b_v_x_ac_h_v_over_c_bar_v.value(zH/bV, xACHV/cV);
29   }

```

Once the class is created, is possible to create an object of it in any test class in order to have access to all its methods; in particular the user needs to invoke the getter related to the quantity he wants to read from the interpolating function.

BIBLIOGRAPHY

- [1] H.I. Abbott and E.A. Von Doenhoff. *Theory Of Wing Sections*. Dover Publications, Inc., 1949.
- [2] L. Attanasio. «Development of a Java Application for Parametric Aircraft Design». Master thesis. University of Naples "Federico II", 2014.
- [3] Various Authors. *ATR 72*. URL: https://en.wikipedia.org/wiki/ATR_72.
- [4] Various Authors. *Boeing 747*. URL: https://en.wikipedia.org/wiki/Boeing_747.
- [5] Various Authors. *eXtensible Markup Language (XML)*. URL: <https://en.wikipedia.org/wiki/XML>.
- [6] S. Ciornei. *Mach number, relative thickness, sweep and lift coefficient of the wing - An empirical investigation of parameters and equations*. Paper. 31.05.2005.
- [7] Oracle Corporation. *Enumeration*. URL: <https://docs.oracle.com/javase/8/docs/api/java/util/Enumeration.html>.
- [8] Oracle Corporation. *List*. URL: <https://docs.oracle.com/javase/8/docs/api/java/util/List.html>.
- [9] Jean-Marie Dautelle. *Jscience*. URL: <http://jscience.org/api/org/jscience/physics/amount/Amount.html>.
- [10] D. et al Gilbert. *JFreeChart*. URL: <http://www.jfree.org/jfreechart/>.
- [11] The HDF Group. *HDF*. URL: <https://www.hdfgroup.org/products/java/hdf-javadoc/nccsa/hdf/hdf5lib/H5.html>.
- [12] W.F. Hilton. *High-speed Aerodynamics*. Longmans, Green, 1951.
- [13] D. Howe. *Aircraft conceptual design synthesis*. Aerospace Series. Professional Engineering Publishing, 2000.
- [14] J. Huwaldt. *1976 Standard Atmosphere Program*. URL: <http://thehuwaldtfamily.org/java/Applications/StdAtmosphere/StdAtmosphere.html>.
- [15] P. Jackson and FRAeS. *Jane's All the World's Aircraft*. Jane's All the World's Aircraft. Jane's Information Group, 2004-2005.
- [16] L.R. Jenkinson, D. Rhodes, and P. Simpkin. *Civil jet aircraft design*. AIAA education series. Arnold, 1999.
- [17] K. Kawaguchi. *Args4j*. URL: <http://args4j.kohsuke.org/>.

-
- [18] I. Kroo and R. Shevell. *Aircraft Design: Synthesis and Analysis*. 1999.
 - [19] A. Lausetti. *Decollo e atterramento di aeroplani, idrovolanti trasportati*. Levrotto & Bella Editrice S.a.s., 1992.
 - [20] B. W. McCormick. *Aerodynamics, Aeronautics, and Flight Mechanics*. John Wiley & Sons, 1979.
 - [21] L.M. Nicolai and G. Carichner. *Fundamentals of Aircraft and Airship Design*. AIAA education series v. 1. American Institute of Aeronautics and Astronautics, 2010.
 - [22] F. Nicolosi and G. Paduano. *Behind ADAS*. 2011.
 - [23] E. Obert. *Aerodynamic Design of Transport Aircraft*. IOS Press, 2009.
 - [24] D.P. Raymer. *Aircraft Design: A Conceptual Approach*. 1992.
 - [25] D.P. Raymer. *Aircraft Design / RDS-Student: A Conceptual Approach*. AIAA Education Series. Amer Inst of Aeronautics &, 2013.
 - [26] M.H. Sadraey. *Aircraft Design: A Systems Engineering Approach*. Aerospace Series. Wiley, 2012.
 - [27] P.M. Sforza. *Commercial Airplane Design Principles*. Elsevier Science, 2014.
 - [28] E. Torenbeek. *Advanced Aircraft Design: Conceptual Design, Technology and Optimization of Subsonic Civil Airplanes*. Aerospace Series. Wiley, 2013.
 - [29] E. Torenbeek. *Optimum Cruise Performance of Subsonic Transport Aircraft*. Delft University Press, 1998.
 - [30] E. Torenbeek. *Synthesis of Subsonic Aircraft Design*. 1976.
 - [31] E. Torenbeek. *Synthesis of Subsonic Airplane Design: An Introduction to the Preliminary Design of Subsonic General Aviation and Transport Aircraft, with Emphasis on Layout, Aerodynamic Design, Propulsion and Performance*. Springer, 1982.
 - [32] A.D. Young. *The Aerodynamic Characteristics of Flaps*. Technical Report. 1947.

GLOSSARY

Autonomy Factor Is the combination of three main efficiency: the propulsive efficiency represented by SFC, the propeller efficiency η_p or the jet efficiency represented by V and, finally, the aerodynamic efficinecy $\frac{L}{D}$.

DATCOM Digital Datcom is a computer program which calculates static stability, high lift and control, and dynamic derivative characteristics using the methods contained in the USAF Stability and Control Datcom (Data Compendium). Configuration geometry, attitude, and Mach range capabilities are consistent with those accommodated by the Datcom. The program contains a trim option that computes control deflections and aerodynamic increments for vehicle trim at subsonic Mach numbers.

Direct Operative Cost The totality of aircraft costs directly connected to the aircraft flight. It can be seen as the amount of money necessary to carry 1 ton of payload upon 1 km.

Enumeration The `java.util Enumeration` interface represents a special data type that enables for a variable to be a set of predefined constants. The variable must be equal to one of the values that have been predefined for it. Because they are constants, the names of an enum type's fields are in uppercase letters..

Hierarchical Data Format A set of file formats (HDF4, HDF5) designed to store and organize large amounts of data.

Java Program toolchain for Aircraft Design Collection of libraries and classes with the aim of providing complete aircraft preliminary design analyses through the use of several semi-empirical formulas tested against experimental data.

List The `java.util.List` interface is a subtype of the `java.util.Collection` interface. It represents an ordered list of objects, meaning you can access the elements of a List in a specific order, and by an index too. You can also add the same element more than once to a List.

Map The `java.util.Map` interface represents a mapping between a key and a value. The Map interface is not a subtype of the Collection interface. Therefore it behaves a bit different from the rest of the collection types.

parsing Parsing or syntactic analysis is the process of analysing a string of symbols, either in natural language or in computer languages, conforming to the rules of a formal grammar.

Portable Network Graphics A raster graphics file format that supports lossless data compression. PNG was created as an improved, non-patented replacement for Graphics Interchange Format (GIF), and is the most used lossless image compression format on the Internet.

static method The term static means that the method is available at the Class level, and so does not require that an object is instantiated before it's called.

TikZ Is a set of higher-level macros that use PGF.

True AirSpeed Is the speed of the aircraft relative to the airmass in which it is flying; TAS is the true measure of aircraft performance in cruise, thus it is the speed listed in aircraft specifications, manuals, performance comparisons, pilot reports, and every situation when cruise or endurance performance needs to be measured. It is the speed normally listed on the flight plan, also used in flight planning, before considering the effects of wind.

user developer The term refers to the developer which will use a method without being interested in how the method performs the required action. This is the case of a utility method: the developer is the one who writes the method, while the user developer is who uses that method to accomplish some action which requires the functionality provided by the utility method. It has to be noticed that the user developer and the developer can be the same person.

ACRONYMS

A.F. Autonomy Factor.

AOE All Operative Engines.

D.O.C. Direct Operative Cost.

HDF Hierarchical Data Format.

IVP Initial Value Problem.

JPAD Java Program toolchain for Aircraft Design.

LER Leading Edge Radius.

MZFW Maximum Zero Fuel Weight.

ODE Ordinary Differential Equations.

OEI One Inoperative Engine.

png Portable Network Graphics.

SFC Specific Fuel Consumption.

SFCJ Jet Specific Fuel Consumption.

TAS True AirSpeed.

UAV Unmanned Aerial Vehicles.

LIST OF SYMBOLS

\mathcal{A} aspect ratio.

()_{cruise} quantity related to cruise condition.

η_p propeller efficiency.

()_f quantity related to flaps.

()_{LG} quantity related to the landing gear.

b span.

C_D aerodynamic drag coefficient.

C_L aerodynamic lift coefficient.

C_{D0} aerodynamic parasite drag coefficient.

D aerodynamic drag.

g gravitational acceleration.

i_W the angle between the wing root chord and the ACRF x-axis.

L aerodynamic lift.

M Mach number.

M_{ff} Fuel fraction over entire mission.

c chord.

Λ sweep.

λ taper ratio.

t thickness.

n load factor.

R range in nmi or km.

S surface.

T thrust.

V scalar velocity.

W_{OE} Operating Empty Weight.

W_{TO} Take Off Weight.

W_{fuel} Fuel Weight.

$W_{Payload}$ Payload Weight.

W weight, in N or lbf.

α_W angle of attack referred to wing root chord.

ρ air density.